Feary, D.A., Hine, A.C., Malone, M.J., et al., 2000
Proceedings of the Ocean Drilling Program, Initial Reports Volume 182

9. Site 1131[1]

Shipboard Scientific Party[2]

BACKGROUND AND OBJECTIVES

Site 1131 is located on the uppermost slope, adjacent to the Eucla Shelf, in 332.4 m of water (Fig. F1). Site 1131, together with the shallower Site 1129 and deeper Site 1127, form a depth transect designed to sample an impressive set of prograding sigmoidal clinoforms constituting Sequence 2 as defined by Feary and James (1998, reprinted as Chap. 2) and projected to be of Pliocene–Pleistocene age (Fig. F2). This seismic sequence forms a thin succession over the outer shelf (70–90 m), reaches peak thickness at the present shelf edge (350–550 m), and thins as a wedge farther seaward beneath the modern slope. The sequence occurs over the entire width of the Eucla Basin (~350 km) and reaches its thickest extent in the vicinity of Site 1131. This site, together with adjacent sites on this transect (Sites 1127 and 1129), offers the opportunity to develop an in-depth understanding of shelf edge and upper slope depositional and progradational processes. Complex reflection onlap and erosional truncation patterns within the clinoform package reflect hiatus or erosional episodes. Site 1131 was located to intersect an expanded record of the middle part of this clinoform sequence, as compared to Sites 1127 (younger part) and 1129 (older part).

In addition, seismic data indicated the presence of mounded seismic facies that have been interpreted as possible deep-water biogenic features (Feary and James, 1995, 1998 [reprinted as Chap. 2]). Site 1131 was designed to intersect a laterally restricted zone of mounds possessing distinct bathymetric and subsurface seismic expression to determine the extent of biogenic contribution and the factors controlling mound development.

The principal objective at these sites was to collect a transect of detailed high-resolution profiles through an upper Neogene shelf edge (high energy) to upper slope (low energy) succession deposited within a cool-water carbonate environment and to determine the response of

F1. Map showing Site 1131 in relation to other Leg 182 sites and the AGSO169 seismic lines, p. 28.

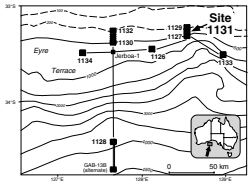

F2. Portion of seismic Line AGSO169/05a showing seismic stratigraphic sequences at Site 1131, p. 29.

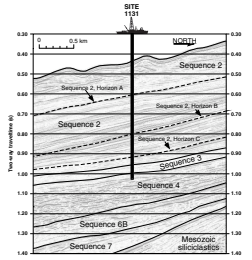

[1]Examples of how to reference the whole or part of this volume.
[2]Shipboard Scientific Party addresses.

Ms 182IR-109

such a depositional system to Pliocene–Pleistocene sea-level fluctuations.

Additional objectives were to

1. Obtain a high-resolution record of upper Neogene paleoceanographic variation within an upper slope setting as a component of the shelf-to-basin paleoceanographic transect;
2. Evaluate the diagenetic history of calcitic sediments that have accumulated in an environment at or near wave base; and
3. Characterize fluid circulation and the heat-flow regime within uppermost slope/shelf edge sediments.

In addition to providing a detailed understanding of seismic Sequence 2 depositional dynamics at Site 1131, we also sought to recover an incomplete Sequence 3 record before reaching the target depth in Sequence 4.

OPERATIONS

Transit to Site 1131

Because of long-period swell (~3 m high) and the resulting heave, which averaged 1.5 m with excursions over 2.0 m, operations in water depths less than 300 m were precluded. Thus, we proceeded to alternate proposed site GAB-08A. The 46-nmi transit required 4.6 hr at an average speed of 10.0 kt. A beacon was launched at 1338 hr on 16 November, initiating Site 1131. A second beacon was deployed, as required for shallow-water operations.

Hole 1131A

The ship was stabilized on position, and an advanced hydraulic piston corer/extended core barrel (APC/XCB) bottom-hole assembly (BHA) was run to the seafloor. Hole 1131A was spudded at 1605 hr on 16 November. The bit was positioned at 339 meters below rig floor (mbrf), and Core 1H recovered 3.39 m, indicating a water depth of 333.4 meters below sea level (mbsl). Advanced hydraulic piston coring advanced to 60.4 meters below seafloor (mbsf) (Table T1). Cores 3H–7H were oriented, and an Adara tool heat-flow measurement was made during Core 4H. A nonmagnetic cutting shoe and a steel 10-finger core catcher were run on Cores 3H, 5H, and 7H (see "Appendix: Magnetics Experiment"). Recovery of Core 7H required 70 kips overpull; therefore, APC coring was terminated in favor of the XCB system. Hydrogen sulfide (H_2S) (86 ppm; headspace analysis) was detected in Core 4H (26.9 mbsf). Hydrogen sulfide alert procedures were implemented, including use of breathing apparatus. Hydrogen sulfide concentrations reached a maximum of 156,600 ppm in a vacutainer sample (359.6 mbsf), but ambient air readings remained below 10 ppm. No H_2S was detected below Core 56X (>511.3 mbsf)

Extended core barrel coring advanced from 60.4 to 616.9 mbsf with 56.3% recovery (Table T1). Recovery was minimal below 540.2 mbsf in presumed mixed chalk and chert, and five XCB hard-formation shoes were destroyed. Hydrocarbon gases up to C_5 were detected beginning with Core 38X (338.3 mbsf), and the coring rate was controlled to allow proper gas monitoring. However, C_{2+} volumes were extremely low and

T1. Site 1131 coring summary, p. 57.

subsequently diminished downhole; C_1/C_2 varied primarily as a function of methane fluctuation (see "Organic Geochemistry," p. 17). Coring was terminated near the depth objective because of poor recovery in cherts.

Hole conditions appeared to be excellent, and the bit was pulled to 102 mbsf without a conditioning trip for logging. Logging tools were run in the following order (depths of penetration are included): (1) triple combination logging tool (triple combo) from 578 mbsf, 39 m off bottom, to the mudline in two passes; (2) Formation MicroScanner (FMS)/sonic from 573 mbsf to the end of pipe; and (3) well seismic tool (WST) tool from 567 mbsf to the end of pipe, recording eight checkshot stations. With an improving forecast and diminishing long-period swell, continued operations at Site 1131 were postponed for a return to Site 1129. After plugging the hole with mud, the drill string was retrieved, both beacons were recovered, and the rig was secured for transit at 1800 hr on 19 November, ending Hole 1131A.

Transit Back to Site 1131 (Hole 1131B)

The ship was moved in dynamic positioning mode from Site 1129 back to Site 1131 to complete a second APC/XCB hole. The 2-nmi transit required 1 hr at 2 kt. A beacon was dropped at 0335 hr on 20 November, and the ship was positioned ~40 m north of Hole 1131A.

Hole 1131B

Hole 1131B was spudded at 0545 hr on 20 November. The bit was positioned at 342.0 mbrf, and Core 1H recovered 8.40 m, which indicated a water depth of 331.4 mbsl. Advanced hydraulic piston coring advanced to 65.4 mbsf with 94.0% recovery (Table T1). Cores 3H–7H were oriented and an Adara tool heat-flow measurement was taken on Core 6H. The nonmagnetic shoe and flapper core catcher with a steel 10-finger core catcher were deployed on Cores 3H, 5H, and 7H (see "Appendix: Magnetics Experiment"). Hydrogen sulfide was detected in Core 5H at 46 mbsf, and H_2S alert procedures were implemented. Extended core barrel coring extended the hole from 65.4 to 105.8 mbsf with 83.3% recovery (Table T1). A Davis-Villinger temperature probe (DVTP) was deployed after Core 12X at 105.8 mbsf. We plugged the hole with mud, recovered the beacon, and secured the rig for transit; the vessel was under way for Site 1132 at 1730 hr, on 20 November.

LITHOSTRATIGRAPHY

Introduction

Site 1131 is located on the upper continental slope of the eastern Eyre Terrace in 332.4 m of water. It is situated immediately seaward of the modern shelf edge, where the seafloor displays an irregular mound-like topography. Underlying the mounds is a thick (>500 m) succession of offshelf-trending prograding clinoforms, which are oblique to sigmoidal and contain high-amplitude parallel reflection surfaces (Feary and James, 1995; see "Seismic Stratigraphy," p. 26, in the "Site 1127" chapter). Seismic data indicate that the ridge-like topography is the surface expression of a series of mounds lying immediately below the seafloor (Feary and James, 1998, reprinted as Chap. 2; see "Seismic

Stratigraphy," p. 26, in the "Site 1127" chapter). Individual mounds are stacked on top of one another, prograding upslope.

Site 1131 intersected the flank of one of the near-surface mounds and continued through the thickest part of the clinoform package, providing a record of relatively rapid and uninterrupted upper Pliocene–Pleistocene sediment production and accumulation (Fig. F3) (see "Biostratigraphy," p. 9). The base of the succession is marked by an unconformity representing a major hiatus. Recovery below this hiatus was extremely poor. Three lithostratigraphic units are recognized on the basis of differences in sediment texture, composition, and packaging.

F3. Site 1131 summary of lithostratigraphy, p. 30.

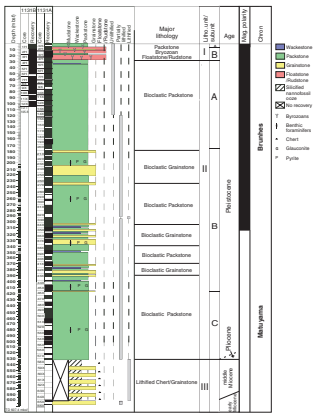

Lithostratigraphic Units

Unit I

Intervals: Sections 182-1131A-1H-1 through 4H-2, 110 cm; Sections 182-1131B-1H-1 through 3H-7, 27 cm
Depth: 0–25.00 mbsf (Hole 1131A); 0–27.17 mbsf (Hole 1131B)
Age: Pleistocene

Unit I consists of a thin succession of neritic carbonate sediments with packstone, floatstone, and rudstone textures and a few decimeter-scale wackestone layers. Unit I is divided into two subunits, based on differences in texture and bioclastic composition.

Subunit IA

Intervals: Sections 182-1131A-1H-1 through 2H-1, 136 cm; Sections 182-1131B-1H-1 through 1H-3, 34 cm
Depth: 0–4.76 mbsf (Hole 1131A); 0–3.34 mbsf (Hole 1131B)
Age: Pleistocene

Subunit IA consists of light gray to olive gray, unlithified bioclastic packstone. It is massive and homogeneous throughout, probably the result of extensive bioturbation, although individual burrows cannot be recognized. Grain size of the >63-µm fraction is fine to very fine sand, composed mainly of bryozoans with benthic and planktonic foraminifers, ostracodes, and echinoderm spines present in subordinate amounts. The mud fraction includes nannofossils, benthic and planktonic foraminifers, and sponge and tunicate spicules (see "Site 1131 Smear Slides," p. 73). The basal contact with Subunit IB is gradational in Hole 1131A. In Hole 1131B it is burrowed, with Subunit IA material incorporated as far as 50 cm down into the top of Subunit IB.

Subunit IB

Intervals: Sections 182-1131A-2H-1, 136 cm, through 4H-2, 110 cm; Sections 182-1131B-1H-3, 34 cm, through 3H-7, 27 cm
Depth: 4.76–25.00 mbsf (Hole 1131A); 3.34–27.17 mbsf (Hole 1131B)
Age: Pleistocene

Subunit IB is a heterogeneous 20-m-thick interval of unlithified bryozoan floatstone and rudstone, punctuated by thin (decimeter scale) layers of wackestone, packstone, and grainstone. The matrix of the floatstone and rudstone is fine grained, giving the interval an overall muddy appearance.

The gravel-sized fraction is mainly bryozoans, with accessory serpulids, whole small infaunal echinoids, infaunal bivalves, and crab claws. The bryozoan assemblage is diverse but dominated by a small number of growth forms, particularly delicate branching, flat robust branching, fenestrate, and nodular-arborescent types (Bone and James, 1993). Diversity is highest within the delicate and flat robust branching forms, with most nodular arborescent types being relatively large centimeter-sized *Celleporaria* sp. Articulated zooidal growth forms are not as obvious, but their remains make up a large proportion of the silt and very fine sand-sized fraction.

The sand-sized fraction is bimodal and includes medium-sized fecal pellets, fine to very fine sand-sized planktonic and benthic foraminiferal tests, serpulid worm tubes, ostracode shells, sponge spicules, infaunal echinoid spines, and bioclasts, with rare pteropod shields. The mud-sized fraction is composed of common nannofossils with accessory benthic and planktonic foraminifers, small sponge and tunicate spicules, and rare dolomite rhombs (see **"Site 1131 Smear Slides,"** p. 73).

Particle preservation is excellent in all size grades, and, although broken, fragile skeletal fragments typically retain even the most delicate surface ornamentation. The sediment appears thoroughly burrowed throughout with an overall patchy, heterogeneous texture resulting partly from the multigeneration filling of *Thalassinoides*-type burrows.

Unit II

Intervals: Sections 182-1131A-4H-2, 110 cm, through 58X-1, 140 cm; Section 182-1131B-3H-7, 27 cm, through Core 12X
Depth: 25.00–532.00 mbsf (Hole 1131A); 27.17–105.80 mbsf (Hole 1131B)
Age: late? Pliocene–Pleistocene

Unit II consists of a succession of massive, homogeneous, light gray to light olive gray bioclastic packstone to grainstone, punctuated by decimeter-scale intervals of wackestone. The contact with the overlying Unit I is gradational and placed at a strong peak in the natural gamma radiation (NGR) (principally uranium) log at 25 mbsf (see **"Downhole Measurements,"** p. 23). Unit II is divided into three subunits, based primarily on textural changes and patterns of sediment interbedding.

Subunit IIA

Intervals: Sections 182-1131A-4H-2, 110 cm, through 20X-5, 110 cm; Section 182-1131B-3H-7, 27 cm, through Core 12X
Depth: 25.00–176.48 mbsf (Hole 1131A); 27.17–105.80 mbsf (Hole 1131B)
Age: Pleistocene

Subunit IIA consists of an interval of light gray to olive gray, unlithified to partially lithified bioclastic packstone ~150 m thick. The entire interval is massive and homogeneous, and interpreted to be completely bioturbated. The grain size ranges from coarse silt to fine sand. The bioclastic fraction seems to reflect a low-diversity fauna; however, this may be a result of poor preservation, which makes individual grains difficult to identify. The identifiable components in the sand-sized (>63-µm) fraction consist of benthic and planktonic foraminifers, sponge spicules, rare ostracodes, and echinoderm spines. The fine (<63-µm) fraction con-

tains nannofossils, planktonic foraminifers, sponge and tunicate spicules, and dolomite rhombs (see **"Site 1131 Smear Slides,"** p. 73). The most distinguishing feature of Subunit IIA is its uniformity and the lack of any indication of variability or interruption in deposition, such as omission surfaces, firmgrounds, or hardgrounds.

Subunit IIB

Interval: Section 182-1131A-20X-5, 110 cm, through Core 46X
Depth: 176.48–424.70 mbsf
Age: Pleistocene

Subunit IIB is a light gray to light olive gray, partially lithified bioclastic packstone and grainstone, locally interrupted by decimeter-scale wackestone intervals. The grain size is very fine to fine sand size, and the entire interval is massive to homogeneous. Subunit IIB is characterized by three 40- to 60-m-thick grainstone-dominated packages separated by two packstone intervals, each 30–70 m thick. The position of the boundaries of the subunit are defined by the first and last occurrences (FO and LO, respectively) of grainstone. Boundary locations are supported by NGR (primarily uranium) peaks, and the upper boundary shows an additional change in the FMS signal from high resistivity above to low resistivity below (see **"Downhole Measurements,"** p. 23).

The packstones are similar to those in the overlying Subunit IIA, with only subtle differences. The bioclastic assemblage is more diverse and includes the appearance of large miliolid foraminifers. Additionally, blackened grains occur immediately below the subunit boundary and maintain a significant presence, primarily in the sand-sized (>63 µm) fraction, throughout the subunit. The origin and mineralogy of blackened grains is not known, but they are commonly associated with pyrite and glauconite grains and form coarse-grained burrow fills. Additional components of the sand-sized (>63 µm) fraction include benthic and planktonic foraminifers, sponge spicules, and rare echinoderm spines, ostracodes, and bryozoans. The fine-grained fraction includes abundant nannofossils, together with benthic and planktonic foraminifers, sponge and tunicate spicules, and dolomite rhombs (see **"Site 1131 Smear Slides,"** p. 73). Grainstone layers exhibit the same grain size and composition as the packstone intervals but lack the fine fraction.

Subunit IIB contains evidence of two possible interruptions in deposition. A possible omission surface occurs at 226 mbsf (Section 182-1131A-26X-1, 125 cm), represented lithologically by a color change from light olive to light gray in a moderately disturbed (biscuited) section of the core. It appears as a peak in the NGR log and as a change in character in the FMS log, from less to more resistant downcore (see **"Downhole Measurements,"** p. 23). Another omission surface occurs at 250 mbsf (Section 182-1131A-28X-4, 140 cm). This omission surface is represented lithologically by a burrowed contact between packstone (above) and grainstone (below) and is reflected as a thin low-resistivity interval in the FMS log (see **"Downhole Measurements,"** p. 23).

Subunit IIC

Interval: Sections 182-1131A-48X-1 through 58X-1, 140 cm
Depth: 424.70–532.00 mbsf
Age: Pleistocene–late? Pliocene

Subunit IIC is a light gray to light olive gray, partially lithified bioclastic packstone. The grain size is very fine to fine sand size, and the entire interval is massive to homogeneous. Sediment is similar to the packstone of the overlying Subunit IIB, with only subtle differences. The bioclastic component appears less diverse and is, therefore, more similar to Subunit IIA, but blackened grains, organic (algal?) filaments, and large miliolid foraminifers (Hole 1131A, below 454 mbsf) are present. Additional components of the sand-sized (>63 µm) fraction include benthic and planktonic foraminifers, sponge spicules, and rare echinoderm spines, ostracodes, and bryozoans. The mud fraction includes abundant nannofossils with accessory benthic and planktonic foraminifers, sponge and tunicate spicules, and dolomite rhombs (see **"Site 1131 Smear Slides,"** p. 73).

A few distinctive units interrupt this apparently continuous packstone succession. A 0.5-cm-thick layer of deformed nannofossil chalk is present at 486 mbsf (Section 182-1131A-53X-3, 56 cm). The significance of this chalk is unknown, but it appears to have been squeezed between biscuits during the drilling process. Also, a thin (few centimeter) layer of celestite-filled cracks occurs at 504 mbsf (interval 182-1131A-55X-3, 1–5 cm, which may be a diagenetic consequence of the high salinities observed in pore waters (see **"Inorganic Geochemistry,"** p. 18). Additionally, a possible omission surface occurs at 463.3 mbsf (Section 182-1131A-51X-1, 13 cm). It is sharp and irregular, but there are no obvious changes in texture or content across the surface. A strong peak on the NGR log at 465–470 mbsf (see **"Downhole Measurements,"** p. 23) may correlate with this surface and seismic surface 2c, which occurs at ~466 mbsf (see **"Seismic Stratigraphy,"** p. 26, in the "Site 1127" chapter). Consequently, the possible omission surface may represent a major boundary and should be scrutinized closely during postcruise studies.

Unit III

Interval: Section 182-1131A-58X-1, 140 cm, through Core 66X
Depth: 532.00–616.90 mbsf
Age: early–middle? Miocene

Unit III is separated from Unit II by an unconformity representing a major hiatus (see **"Biostratigraphy,"** p. 9). Lithologically, the boundary is represented by a sharp contact between the partially lithified packstone of Unit II above and a chert horizon below. It corresponds to the base of seismic Sequence 2, a basinwide unconformity that represents the boundary between the aggradational shelf deposits of seismic Sequence 3 and the progradational outer shelf–upper slope deposits of the overlying seismic Sequence 2 (Feary and James, 1998, reprinted as **Chap. 2**). Recovery is poor below the unconformity. Recovered sediments consist of chert and partially lithified bioclastic grainstone. The chert is dark to very dark gray and consists of a silicified nannofossil ooze. The grainstone is olive gray in color and of fine sand size, consisting of unidentifiable bioclasts with accessory blackened grains and glauconite. A jagged appearance in porosity and density logging data suggests that the chert and grainstone are thinly interbedded (see **"Downhole Measurements,"** p. 23).

Discussion

The cores collected at Site 1131 record a late Pliocene–Quaternary history of rapid and relatively uninterrupted deposition on the outer shelf and upper slope of the eastern Eyre Terrace. An interpretation of lithostratigraphic Unit III is difficult because of poor recovery. Recovered material consists of chert and grainstone, although it is most likely an ooze sequence with horizons that have been preferentially silicified. The age is interpreted as middle Miocene (see **"Biostratigraphy,"** p. 9). The upper boundary corresponds to the sequence boundary between seismic Sequences 2 and 3 and represents a strongly lithified surface as previously suggested by Feary and James (1998, reprinted as **Chap. 2**).

Pliocene–Pleistocene Prograding Upper Slope Wedge

Lithostratigraphic Unit II corresponds to the offshelf-trending prograding clinoform package of seismic Sequence 2 (see **"Seismic Stratigraphy,"** p. 26, in the "Site 1127" chapter), interpreted to have been deposited by the offshelf transport of shallow-water material (James and von der Borch, 1991). This interpretation is corroborated by the dominantly shallow-water carbonate assemblage identified in the bioclastic fraction of these sediments. It appears that deposition was rapid and relatively uninterrupted. This is supported by the relative paucity of indicators of interrupted sedimentation, such as omission surfaces, firmgrounds, or hardgrounds. Sediment accumulation rates are calculated to be ~25 cm/k.y. (see **"Biostratigraphy,"** p. 9), which is high for continental slopes dominated by hemipelagic deposition and higher than most carbonate slopes bordering rimmed platforms (James, 1997). Continuous deposition fed by offshelf transport may be responsible for these high accumulation rates. The timing, mechanisms, and overall controlling factors, such as climate, sea level, and oceanic currents, governing offshelf transport are not known at present. The grainstone/packstone package of Subunit IIB shows some evidence of cyclicity, which may be related to cycles of offshelf transporting activity.

Quaternary Bryozoan Mound Complex

Lithostratigraphic Unit I represents a change in depositional style. The morphology of the bryozoan accumulations of Subunit IB suggest in-place biogenic mounds (e.g., James and Bourque, 1990). There are no skeletons in obvious growth position, but the delicate preservation and abundant mud suggests that the skeletons have not been transported and that bottom currents were weak. Fragmentation of skeletons is probably due to biological processes. The heterogeneous texture argues for some postmortem redistribution of skeletons, probably by burrowing organisms. Following the demise of the bryozoan mounds, it appears that the pre-Holocene depositional style resumed. Pending more accurate age dating, the preferred interpretation of lithostratigraphic Unit I is as follows: the mounds grew during the uppermost sea-level lowstand (~17–22 ka) in water depths of ~200 m and were subsequently buried by the influx of relatively fine-grained sediments, probably by resumed offshelf transport, during the late Pleistocene–Holocene sea-level rise.

BIOSTRATIGRAPHY

Introduction

Site 1131 is the middle site (332.4 m water depth) of a downslope transect from 200 m (Site 1129) to 480 m water depth (Site 1127). The site includes two biostratigraphic units (Fig. F4): (1) an expanded Quaternary interval more than 510 m thick, underlain by a thin and conformable Pliocene? interval and (2) a middle–lower Miocene section that also appears continuous, although poor recovery and poor preservation degraded biostratigraphic resolution of this interval. These units are separated by a disconformity at 532 mbsf that spans ~10 m.y. The disconformity coincides with a prominent change in lithology from bioclastic packstone above to lithified chert and grainstone below, coinciding with the base of seismic Sequence 2 (see "Seismic Stratigraphy," p. 26, in the "Site 1127" chapter). The top and bottom boundaries of an interval of poor nannofossil preservation (at 347.86 and 463.52 mbsf) appear to coincide with seismic Sequence 2 Horizons B and C. Foraminifers throughout the section below ~60 mbsf are strongly affected by calcite reprecipitation, consistent with the high alkalinity reported in pore waters (see "Inorganic Geochemistry," p. 18).

An environmental crisis produced an unusual nannofossil assemblage dominated by *Braarudosphaera bigelowii* near the base of Zone NN19 at ~522 mbsf. A similar event was observed in the same stratigraphic interval at Sites 1127 and 1130.

Benthic foraminifers are relatively abundant and well preserved in the upper part of Hole 1131A (Cores 182-1131A-1H through 11X). However, abundance decreases significantly below Core 182-1131A-11X, where preservation deteriorates markedly with tests being heavily recrystallized. One main Pleistocene upper bathyal assemblage is recognized. This assemblage also contains a large proportion of small neritic tests (63–150 mm), probably redeposited from the shelf. Poor preservation prevented detailed faunal analysis below Core 182-1131A-11X.

Calcareous Nannofossils

At Site 1131, as at Site 1127, an expanded Pleistocene section (~ 532 m) overlies a shorter (~85 m) lower–middle Miocene section. Almost all of the samples are rich in nannofossils, with the exception of those between Samples 182-1131A-58X-CC, 0–3 cm (532.04 mbsf), and 62X-CC, 0–3 cm (568.80 mbsf), which contain rare to few nannofossils. There was no recovery in Core 182-1131A-61X. Preservation of nannofossils is generally good to moderate in the upper 330 mbsf and generally poor over the next ~120 m, with improvement within the lower 120 m of the hole. One hiatus spanning ~10 m.y., indicated by the absence of Zones NN18 through NN6, occurs between Samples 182-1131A-58X-CC, 0–3 cm (532.04 mbsf), and 59X-CC, 19–22 cm (540.39 mbsf).

The upper 195 mbsf of Hole 1131A, as seen in Samples 182-1131A-1H-CC, 16–19 cm (3.36 mbsf), through 22X-CC, 13–16 cm (194.60 mbsf), and all of Hole 1131B (104.64 mbsf total depth), is characterized by common to abundant occurrences of *Gephyrocapsa caribbeanica* and/or *Gephyrocapsa oceanica,* and common small *Gephyrocapsa* spp., *Helicosphaera carteri,* and *Calcidiscus leptoporus* but lacks *Pseudoemiliania lacunosa*. These sections are placed into the combined Zones NN21–NN20. The presence of *P. lacunosa* in Samples 182-1131A-23X-CC, 13–

F4. Calcareous nannofossil and planktonic foraminifer zones and benthic foraminifer assemblages, p. 31.

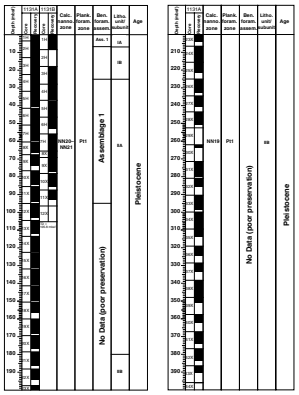

16 cm (204.33 mbsf), through 55X-CC, 30–33 cm (506.14 mbsf), indicates a Zone NN19 assignment. We observed increasing downhole abundances of small *Gephyrocapsa* spp., decreasing abundances of *G. caribbeanica,* and few to common occurrences of *Calcidiscus leptoporus* and *Helicosphaera carteri*. The highest stratigraphic occurrence of *Calcidiscus macintyrei* is in Sample 182-1131A-49X-CC, 33–36 cm (451.62 mbsf). Sample 182-1131A-57X-CC, 43–46 cm (521.97 mbsf), contained dominant *B. bigelowii,* indicating a change in surface-water conditions. This braarudosphaerid chalk was also noted in the lower part of Zone NN19 at Sites 1127 and 1130.

Within Zone NN19, preservation degrades from moderate in Sample 182-1131A-37X-CC, 27–30 cm (333.34 mbsf), to poor in Sample 38X-CC, 20–23 cm (347.86 mbsf), and remains poor to Sample 50X-CC, 42–45 cm (463.52 mbsf), below which preservation improves again to moderate. These levels coincide with prominent seismic stratigraphic reflectors at 336 and 466 mbsf within Sequence 2 but do not seem to coincide with any lithologic contacts or changes (see **"Lithostratigraphy,"** p. 3; also see **"Seismic Stratigraphy,"** p. 26, in the "Site 1127" chapter). The interval of poor preservation does, however, correspond to a drop in the percentage of aragonite in sediments at ~330 mbsf (see **"Inorganic Geochemistry,"** p. 18).

Sample 182-1131A-59X-CC, 19–22 cm (540.39 mbsf), contains *Cyclicargolithus floridanus* and *Calcidiscus macintyrei,* an association that indicates an assignment of Zone NN6. This indicates that Zones NN18–NN7 are missing, which suggests a ~10 m.y. hiatus. Also present in this sample are *Sphenolithus abies, Calcidiscus leptoporus, B. bigelowii, Discoaster variabilis,* and *Cyclicargolithus abisectus*. This hiatus coincides with a change in lithology from a partially lithified bioclastic packstone to lithified chert and grainstones (see **"Lithostratigraphy,"** p. 3).

Samples 182-1131A-63X-CC, 0–3 cm (578.40 mbsf), through 66X-CC, 6–9 cm (607.36 mbsf), contain *Sphenolithus heteromorphus, Helicosphaera euphratis, B. bigelowii, Cyclicargolithus floridanus, C. abisectus,* and *Helicosphaera carteri*. This floral association indicates an assignment to Zones NN5–NN4 for this interval. It is interesting to note that *Cyclicargolithus abisectus* is present in these samples and is found in common abundances associated with the short-ranging *S. heteromorphus*. *Cyclicargolithus abisectus* should not be seen above its extinction in Zone NN1. It is possible that the specimens of *Cyclicargolithus abisectus* were reworked, although there is no direct evidence of reworking, (i.e., overgrowths or fragmentation).

Planktonic Foraminifers

A thick Quaternary to upper? Pliocene section (~532 m) occurs unconformably above a middle–lower Miocene section (~85 m), separated by a major disconformity of ~10 m.y. at 532 mbsf. The biostratigraphic succession at Site 1131 is similar to that at Site 1127, except that the lower Pleistocene section is somewhat expanded. The quality of preservation is also different between these sites. Preservation of planktonic foraminifers is quite poor at Site 1131 because of thick overgrowths, cementation, and recystallization below ~65–100 mbsf. In contrast, preservation is quite good at Site 1127, especially in the upper Neogene section.

Preservation and Abundance

Preservation of planktonic foraminifers declines from the surface to 60–70 mbsf (Sections 182-1131A-7H-CC and 182-1131B-8X-CC) and remains poor throughout the remainder of the section, principally because of calcite overgrowths and cementation on test surfaces and sporadic recrystallization of the tests themselves. This interval of poor preservation coincides with high pore-water alkalinity (see "Inorganic Geochemistry," p. 18), and the depth where overgrowths become prominent coincides with the onset of sediment lithification (see "Lithostratigraphy," p. 3).

Planktonic foraminifers are common in the upper ~40 mbsf but are somewhat diluted in this interval by other sand-sized bioclasts such as bryozoans, gastropods, benthic foraminifers, and ostracodes. Abundance decreases markedly below ~65 mbsf, the depth below which tests are poorly preserved.

Quaternary

The well-preserved samples above 60 and 70 mbsf in Holes 1131A and 1131B, respectively, contain a typical warm temperate Quaternary assemblage comprised of abundant *Globorotalia inflata* and few *Globigerina bulloides, Globigerina falconensis, Globigerina quinqueloba, Globigerinita glutinata, Globigerinoides ruber, Globigerinoides tenellus, Globorotalia hirsuta, Globorotalia scitula, Globorotalia truncatulinoides, Orbulina universa,* and *Neogloboquadrina pachyderma* (dextral). The poorly preserved Quaternary sections below 60 and 70 mbsf in Holes 1131A and 1131B contain a depauperate assemblage of consistently recognizable *Globorotalia inflata, G. ruber, N. pachyderma* (dextral), and *G. truncatulinoides*. Other Quaternary species are recognized sporadically, and many specimens are not recognizable through the cement and recrystallized overgrowths. The section is placed in the subtropical Zone Pt1, based on the presence of *G. truncatulinoides*. The zone could not be divided into Subzones Pt1a and Pt1b because *Globorotalia tosaensis* was recognized in only two samples near the base of the interval (Samples 182-1131A-51X-CC, 35–38 cm [468.54 mbsf], and 56X-CC, 28–31 cm [512.50 mbsf]), ~200 m below the Brunhes/Matuyama boundary, which is older than the true LO of *G. tosaensis*. The base of Zone Pt1 as defined by Berggren et al. (1995) could not be applied because *Globigerinoides fistulosus* and *G. extremus* were not observed. We placed the base at the first appearance of *G. truncatulinoides* (between 512.22 and 521.97 mbsf at Hole 1131A), following the definition of Jenkins (1993) and Chaproniere et al. (1995) for the estimated regional base of the Pleistocene. However, we suspect that the base of this zone in the Great Australian Bight lies in the lower Pleistocene.

Lower? Pleistocene–Upper? Pliocene

The poorly preserved lower? Pleistocene–upper? Pliocene assemblage includes essentially the same species as those of the Quaternary. The upper Pliocene fits the definition of Zone SN13, the *Globorotalia inflata* Zone of Jenkins (1985, 1993) because it contains *Globorotalia inflata* without *G. truncatulinoides*. In this volume, the interval is informally called the *Globorotalia crassaformis* interval, in part because its age and stratigraphic relationships to zones defined in other regions needs clari-

fication. Samples 182-1131A-57X-CC, 43–45 cm, to 58X-1, 89–91 cm (521.97–531.49 mbsf), are placed in this interval.

Miocene

The uppermost sample of this interval (Sample 182-1131A-58X-CC, 0–3 cm; 532.04 mbsf) occurs in a lithified layer that marks the top of lithostratigraphic Unit II (see "Lithostratigraphy," p. 3), corresponding to the top of Sequence 3 (see "Seismic Stratigraphy," p. 26, in the "Site 1127" chapter). The assemblage contains very badly overgrown and recrystallized tests with affinities to *Globorotalia puncticulata,* a species restricted to the Pliocene, and *Globigerina bulloides, Globorotalia conoidea,* and *Globoquadrina dehiscens,* all of which occur together in the upper and middle Miocene. The fossils could be reworked from the middle Miocene unit below the lithified layer or could be a downhole contamination; hence, the sample is tentatively assigned to the Pliocene–Miocene. The underlying samples from 540.39 to 588.00 mbsf (core-catcher samples of Cores 182-1131A-59X to 64X) are assigned to the middle Miocene based on the occurrence of *Fohsella peripheroronda, Globigerinoides sicanus, Globorotaloides suteri, Neogloboquadrina continuosa, Praeorbulina glomerosa, Tenuitella minutissima,* and *Zeaglobigerina druryi*. The bottom two samples are assigned to the lower Miocene based on the occurrence of *Zeaglobigerina connecta*. The fossils in these samples are sparse and badly preserved; therefore, zonal assignments are not possible without further work and good luck.

Benthic Foraminifers

Benthic foraminifers were studied from every core-catcher sample in Cores 182-1131A-1H through 7H and from every fourth core-catcher sample below Core 7H. Benthic foraminifers are relatively abundant and well preserved in the upper part of Hole 1131A (Cores 1H through 11X). However, abundance decreases significantly below Core 182-1131A-11X, where preservation deteriorates markedly because tests are heavily recrystallized. Between 100 and 300 benthic foraminifers were picked from the >63-µm fraction in Samples 182-1131A-1H-CC through 11X-CC. Below Core 182-1131A-11X, benthic foraminifers were picked from the >150-µm fraction. A check of the >63- to 150-µm fraction was also carried out to evaluate the relative proportion of small specimens present in the samples. In the interval below Core 182-1131A-11X, poor preservation impaired taxonomic determination and prevented a detailed faunal analysis. The following benthic foraminifer assemblages are recognized in the Neogene succession of Hole 1131A.

Assemblage 1 (Pleistocene)

Cores 182-1131A-1H through 11X, except Cores 182-1131A-2H and 3H

This Pleistocene assemblage is characterized by the common to abundant occurrence of small (63–150 µm) *Triloculina* spp., *Spiroloculina* spp., *Patellina corrugata, Spirillina* spp., *Palliolatella* spp., and *Rosalina* spp. Also present as rare to frequent constituents of the assemblage are *Hoeglundina elegans, Sphaeroidina bulloides, Cibicides refulgens, Bigenerina nodosaria, Bulimina marginata, Uvigerina hispidocostata, Textularia* spp., *Elphidium* spp., *Cibicidoides* spp., *Loxostomum* spp., *Loxostomoides* spp., and various nodosariids. Upper bathyal paleodepths are suggested by the presence of the depth-indicative species *Hoeglundina elegans, S. bul-*

loides, B. nodosaria, Bulimina marginata, and *U. hispidocostata*. However, the dominance of small shallow-water taxa (*Triloculina* spp., *Spiroloculina* spp., *P. corrugata, Spirillina* spp., *Palliolatella* spp., and *Rosalina* spp.), typically found in shallower neritic depths, suggests grain size sorting and redeposition of a large component of the assemblage in an upper bathyal setting. Sample 182-1131A-6H-CC contains a large proportion (~20%) of dark stained tests, principally miliolids, *Elphidium* spp., and *Cibicidoides* spp., which suggest extensive reworking before deposition.

Site 1131 is situated a few miles away from Site 1127 in a slightly more proximal position and at a slightly shallower water depth (332.4 m at Site 1131 compared to 479.3 m at Site 1127). Sedimentation rates are very high at both sites: 246 m/m.y. at Site 1131 (Fig. **F5**) and 280–350 m/m.y. at Site 1127 (Fig. **F6,** p. 36, in the "Site 1127" chapter). The Pleistocene assemblage at Site 1131 is similar in composition to the coeval assemblage recorded at Site 1127. Both assemblages show similarity to shelf assemblages described from Lakes Entrance in southeastern Australia by Li and McGowran (in press). They include a high proportion of cosmopolitan taxa but also contain more geographically restricted species. Postcruise studies will be necessary to fully document the composition of the benthic foraminifer assemblages at these two sites and to relate faunal changes to climatic, sea level, and/or circulation fluctuations during the Pleistocene.

F5. Sedimentation rate curve from datum levels for Site 1131, **p. 33.**

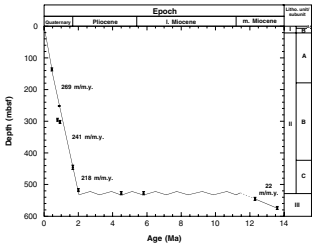

Bryozoan Assemblage (Pleistocene)

Cores 182-1131A-2H and 3H

This striking assemblage was found only in two core-catcher samples that also contained abundant and extremely well-preserved bryozoans. The assemblage includes a few large miliolid and spirillinid tests (>1 mm) and a remarkable proportion of *B. nodosaria* (large) and *Textularia* specimens (>1 mm). Also present are *S. bulloides, Sigmoilina obesa, Cancris auriculus, Hoeglundina elegans, Martinottiella communis, U. hispidocostata, Loxostomum* spp., *Loxostomoides* spp., *Sigmoilina* spp., *Anomalinoides* spp., and some miliolids. The assemblage is extremely well preserved, exhibiting no obvious evidence of sorting or reworking. The presence of *S. bulloides, Hoeglundina elegans,* and numerous *B. nodosaria* indicates upper bathyal paleodepths, providing further evidence that this assemblage was not transported from the shelf. This assemblage appears to have been associated with a flourishing but transitory in situ bryozoan community. No similar benthic foraminifer assemblage was encountered at Site 1127, where only poorly preserved, presumably reworked bryozoan fragments were found in all cores.

Sedimentation Rate

Sediment accumulation rates shown in Figure **F5** were calculated based on preliminary biostratigraphic and paleomagnetic results from Site 1131 (see **"Paleomagnetism,"** p. 14). The biostratigraphic datum levels and relevant paleomagnetic data used to calculate sedimentation rates are listed in Table **T2.**

T2. Datum levels used to calculate the sedimentation rate, **p. 59.**

A very high sedimentation rate averaging 240 m/m.y. is recorded for the Pleistocene to upper? Pliocene section. Interestingly, the paleomagnetic data suggest low sedimentation rates (43 m/m.y.) between the Brunhes/Matuyama boundary and the termination of the Jaramillo, suggesting that short intervals of low rates are likely imbedded amid the long Pleistocene intervals of high rates. The underlying middle Mio-

cene section registered a significantly lower sedimentation rate of ~22 m/m.y. based on poorly constrained datum levels. A hiatus of >10 m.y. occurred at this sharp change in sedimentation rate (Fig. F5).

PALEOMAGNETISM

Shipboard paleomagnetic measurements in Holes 1131A and 1131B consisted of long-core measurements at 5- to 10-cm intervals of the natural remanent magnetization (NRM) and the remanence after alternating field (AF) demagnetization at 20 mT, as described in "Paleomagnetism," p. 12, in the "Explanatory Notes" chapter. Measurements were performed on archive halves of all APC and XCB cores, except for intervals affected by core disturbance. Long-core measurements established a magnetostratigraphy to a depth of ~320 mbsf, which includes the Brunhes and uppermost Matuyama Chrons. Below this, core reorientation by drilling disturbance disrupts the record and interpretation of magnetic polarity is uncertain. In partially lithified materials below 200 mbsf, measurements on discrete samples as well as individual biscuits provide more conclusive polarity determinations than long-core measurements in which remobilized sediment carries a strong spurious magnetization. Discrete samples were also collected from representative core material and were subjected to progressive AF demagnetization up to 30 mT. These samples were also used for anhysteretic remanent magnetization (ARM) and isothermal remanent magnetization (IRM) acquisition and demagnetization experiments.

Long-Core Measurements

The intensity of initial remanence is relatively low with a median of ~2×10^{-4} A/m. High values occur in the uppermost 20 mbsf, and anomalous spikes are observed at the top of several cores. The NRM is of shallow to moderately steep negative inclination with a downhole trend toward positive inclinations (Fig. F6). After partial demagnetization (20 mT), magnetizations above ~280 mbsf are of steeply negative inclination and scatter is reduced significantly, indicating that a magnetization of steeply positive inclination is preferentially removed. In addition, after demagnetization, intensities display a gentle downhole trend to lower values. Superimposed on this trend there are two clear signals. The first is dominated by oscillations with wavelengths of 10–20 m, commonly corresponding to inclination variations. These oscillations may thus be related to geomagnetic field behavior (paleosecular variation). The other signal is a spurious signal associated with anomalies at core ends.

Below 250 mbsf, lower recovery and core disturbance in partially lithified materials results in intervals in which measurements yield lower inclination values than expected for the present latitude. These shallow inclinations are less common in discrete samples, suggesting that they may be caused by contamination by a drilling-induced overprint.

Measurements of discrete samples reveal a characteristic magnetization that is isolated after removing a spurious overprint, which we interpreted as a drilling-induced remanence. Median destructive fields range from 20 to 30 mT. In Sample 182-1131A-31X-1, 27–34 cm (Fig. F7A), a soft component with a steep downward inclination is removed first, isolating a characteristic magnetization of normal polarity that de-

F6. Downhole inclination from NRM long-core measurements and after partial demagnetization, with interpreted magnetostratigraphy, p. 34.

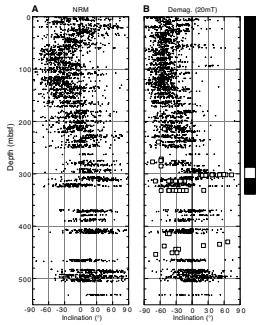

F7. Normalized intensity decay, demagnetization diagrams, and stereoplot of representative samples, p. 35.

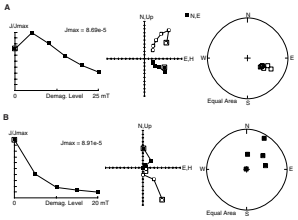

cays to the origin. Sample 182-1131A-48X-1, 45–47 cm, (Fig. F7B) is characteristic of deeper cores. In this sample, a prominent soft steep magnetization is removed with inductions of 5 mT, isolating a characteristic magnetization of lower intensity, although unequivocally of reverse polarity. Line fits were used to define the direction of the characteristic magnetization. These samples yield high maximum angular deviation values.

The magnetic Tensor tool was used in APC Cores 182-1131-3H to 7H in both holes. Within-core declinations at Hole 1131B are relatively well grouped, although between-core declinations are generally scattered. Declinations from Hole 1131A, however, show significant within-core scatter (Fig. F8). After correcting azimuths at Hole 1131B using the Tensor tool, declinations fall near the expected field direction for cores for which a nonmagnetic shoe was used (see "Appendix: Magnetics Experiment"). As with other sites reported in this volume, for XCB cores for which azimuthal orientation is not available, declinations are preferentially along the core fiducial line.

Normal polarity magnetizations are persistent in Cores 182-1131A-1H through 33X (Fig. F6). Within this normal polarity, we observed intensity fluctuations in NRM after 20-mT demagnetization similar to those observed at Sites 1127 and 1130. Once again, although these NRMs have not been normalized, they are of a similar periodicity to variations in the dipole moment of the geomagnetic field (Valet and Meynadier, 1993).

F8. Long-core measurements of declination, inclination, and intensity of remanent magnetization after partial demagnetization, p. 36.

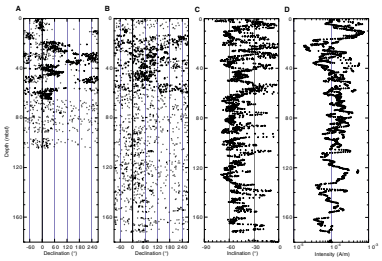

Rock Magnetism

Rock magnetism analysis consisted of measurements of weak-field susceptibility at two frequencies, progressive IRM acquisition, and AF demagnetization of ARM. Rock magnetic properties are rather uniform within the cored interval. Decay of the NRM upon AF demagnetization is typical of a cubic phase, either magnetite or greigite. Representative samples were given a 400-mT IRM and subsequently demagnetized (Fig. F9). Inductions of 400 mT are not sufficient to reach saturation, suggesting that greigite is present and may well be the main remanence carrier in at least some cored intervals. Alternating field decay of the IRM is typical of weakly interacting single-domain grains (Cisowski, 1981). Rapid viscous decay of the saturation IRM was observed in samples from Cores 182-1131A-10X, 13X, and 17X, suggesting that particles near the superparamagnetic-single domain threshold are present. All samples display high ARM:IRM ratios, which suggest a single-domain grain size. Single-domain magnetite may also carry part of the remanence.

F9. Acquisition of IRM and its AF demagnetization, p. 37.

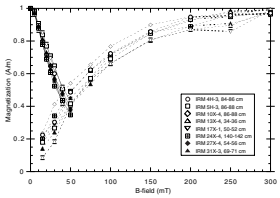

Magnetostratigraphy

Moderately to steeply positive inclinations in Core 182-1131A-33X (at ~290 mbsf) are interpreted as reversed magnetizations. A precise location for the boundary is impossible because of incomplete recovery and core disturbance; discrete samples place the boundary between 280 and 300 mbsf, whereas long-core measurements place it between Sections 182-1131A-32X-2 and 33X-1. After a short interval of reverse polarity, normal polarity magnetizations are observed again in Section 182-1131A-34X-6. This pattern of reversal stratigraphy is interpreted as the uppermost Matuyama and Brunhes epochs, possibly with the top of the Jaramillo Subchron at 308 mbsf. This interpretation implies a lower

sedimentation rate during the upper lower Pleistocene than during the Brunhes epoch. Below this depth, long-core data are of poor quality, although discrete samples from Cores 182-1131A-45X to 48X define normal-reverse-normal transitions between 440 and 420 mbsf. These, however, cannot be uniquely correlated with the geomagnetic polarity time scale.

COMPOSITE DEPTHS

Introduction

Construction of the composite and spliced section from Holes 1131A and 1131B followed the methods outlined in "Composite Depths," p. 14, in the "Explanatory Notes" chapter. Table T3 (also in ASCII format) relates mbsf depth to meters composite depth (mcd) for each core and section at Holes 1131A and 1131B, and provides offset values for the conversion of mbsf depths to mcd. The composite section was constructed to a depth of 104 mcd and indicates that most of the sedimentary section down to this depth was recovered at Site 1131; however, several small gaps are apparent in the record.

T3. Site 1131 core and section depths in mcd and mbsf, p. 60.

Data Input

The primary lithologic parameters used to create the composite section were NGR emission data collected by the multisensor track (MST) on whole-round cores, the 400-nm color reflectance data, and a ratio of the 700- to 400-nm color reflectance data measured on split cores (Fig. F10). For specifics regarding data collection procedures and parameters, see "Physical Properties," p. 21. Because of the high sedimentation rates at Site 1131, biostratigraphic and paleomagnetic datums occurred below the total depth of Hole 1131B and could not be used in the construction of the composite section.

F10. Composite depth section produced using Splicer software, p. 38.

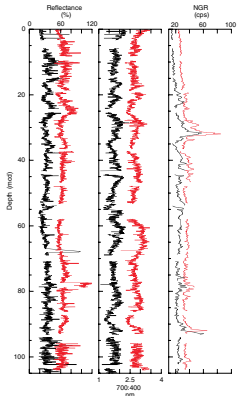

Composite Section Construction

The composite section for Site 1131 is presented in Figure F10. The primary difficulty encountered in the construction of this composite section was the lack of obviously correlative small-scale features (<1 m) throughout much of the section in Holes 1131A and 1131B. This is the result of the general uniformity of the sediments on these scales (uniform wackestones to packstones over much of the section; see "Lithostratigraphy," p. 3). Larger scale (>1 m) distinctive events are also infrequent in the single-band color reflectance data but are more prevalent in the NGR data. The ratio of the 700:400 nm color reflectance data is marginally better than the individual 400- or 700-nm color reflectance data. These ratio data reveal cyclicity in the record in the form of long-wavelength (~10 m), low-amplitude oscillations that were correlated between holes. Core overlap between holes was reduced by significant core disturbance within the first sections of several cores.

The sediments comprising the composite section are entirely of Holocene and Pleistocene age, based upon biostratigraphic data (see "Biostratigraphy," p. 9). The stratigraphic record within the range of the composite section is divided into two primary lithostratigraphic units. The upper unit, lithostratigraphic Unit I (0–32 mcd), is defined by the presence of unlithified bryozoan floatstone and rudstone, interbedded

with wackestone, packstone, and grainstone. The floatstone and rudstone facies exhibit high color reflectance values (60%), which were relatively easy to correlate between holes. Lithostratigraphic Unit II (below 32 mcd) consists of a homogeneous light gray to light olive gray bioclastic packstone to grainstone, which yields a color reflectance data record with few obviously distinctive and correlative features (Fig. F10). Similarly, the characteristics of the NGR and gamma-ray attenuation (GRA) bulk density records are markedly dissimilar between holes, with the exception of some high-amplitude peaks in the NGR record. As a result, the record within lithostratigraphic Unit II was difficult to correlate between holes, and most ties rely upon long-wavelength oscillations apparent in the 700:400 nm color reflectance data.

The composite and spliced sections indicate the existence of at least two unrecovered intervals in the record (Figs. F10, F11). Poor recovery in Cores 182-1131B-6H and 11X resulted in gaps in the record at 53.2–53.9 mcd and 76.9–77.2 mcd, respectively. Furthermore, although core overlap appears to occur between ~42 and 47 mcd (Cores 182-1131B-5H and 182-1131A-6H; Fig. F10), no significant statistical correlation could be found between the records, and the splice was appended at that point (Table T4, also in ASCII format). A similar situation occurs at ~68–69 mcd, between Cores 182-1131A-8X and 182-1131B-8X.

F11. Spliced section of smoothed color reflectance and NGR data produced using Splicer software, p. 39.

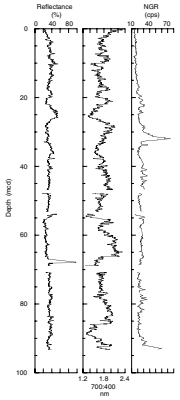

T4. Site 1131 splice tie points, p. 65.

ORGANIC GEOCHEMISTRY

At Site 1131, in addition to routine monitoring of hydrocarbon and H_2S gases for safety, analyses were conducted for inorganic carbon, total carbon, nitrogen, and sulfur. The analytical procedures are described in "Organic Geochemistry," p. 16, in the "Explanatory Notes" chapter.

Volatile Hydrocarbons and Hydrogen Sulfide

Concentrations of volatile hydrocarbons and H_2S were routinely determined in samples from Hole 1131A using standard Ocean Drilling Program (ODP) headspace or vacutainer sampling procedures. The striking results from Site 1131, as at Site 1127, are the high concentrations of methane (C_1) and H_2S in part of the section (Tables T5, T6). Four gas pockets occurred from 344.8 to 388.4 mbsf. These were sampled directly through the core liner using a gas-tight syringe (vacutainer). Methane concentrations in these gas pockets ranged from 61,093 to 81,267 ppm (Table T5). By comparison, gas pockets at Site 1127 were more abundant, and methane concentrations in the gas pockets at Site 1127 were about seven times greater, ranging from 329,000 to 585,000 (see "Organic Geochemistry," p. 17, in the "Site 1127" chapter).

T5. Vacutainer gas compositions, Hole 1131A, p. 66.

T6. Headspace gas compositions, Hole 1131A, p. 67.

Methane occurs at lower concentrations in the headspace samples from Hole 1131A; the lowest values are at the top and bottom of the sedimentary section, and the maximum values lie at ~200 mbsf (Table T6; Fig. F12). From 1.5 to 55.4 mbsf, methane values are <250 ppm. From 64.9 to 211.1 mbsf, methane increases to 11,458 ppm, the highest value, and then decreases steadily to 45 ppm at the bottom of the section. The C_1 headspace profile with depth tracks C_{org} values in the upper part of Hole 1131A. Low C_1 concentrations in the upper 100 mbsf and higher values from 100 to 200 mbsf correlate to a similar C_{org} pattern in the same depth intervals (see "Inorganic and Organic Carbon, Sulfur, and Nitrogen," p. 18). In contrast to the bimodal distribution

F12. Headspace gas compositions in samples from Hole 1131A, p. 40.

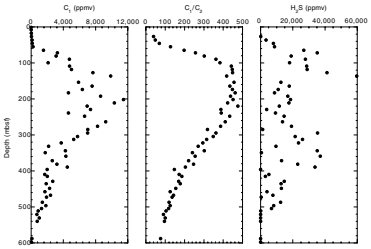

of C_1 at Site 1127 (see "Organic Geochemistry," p. 17, in the "Site 1127" chapter), methane has a unimodal distribution in Hole 1131A.

Ethane (C_2) was present from 26.9 mbsf to the base of Hole 1131A at concentrations as high as 25 ppm in headspace samples; most values are between 10 and 20 ppm (Table T6). The C_1/C_2 values in headspace samples from the same depth interval first increase from 40 to 476 and then decrease to a low of 76 at the base of the section (Table T6; Fig. F12). Although the initial increase and subsequent decrease in the C_1/C_2 ratio is atypical for sedimentary basins, and the values are in the range indicative of thermogenic hydrocarbon sources based on the ODP "Guidelines for Pollution Prevention and Safety" (JOIDES PPSP, 1992), the change in ratio with depth mirrors the increase and decrease in methane concentration. That is, C_2 concentrations do not vary significantly from 72.1 mbsf to the base of Hole 1131A; the change in C_1/C_2 results entirely from variations in C_1. Heavier hydrocarbon gases (C_{3+}) were detected in a few headspace samples from 359.1 to 530.6 mbsf, as well as in the four gas pockets.

The concentrations of H_2S in the four gas pockets in Hole 1131A range from 107,651 to 156,608 ppm, exceeding the highest value measured at Site 1127 and possibly any other ODP site (Table T5). The H_2S in headspace samples from Hole 1131A reaches concentrations as high as 59,681 ppm and shows a bimodal distribution with maxima at 136.4 and 359.1 mbsf. The headspace concentrations are lower than those found in gas pockets, although, as with the gas pockets, the H_2S values are higher in Hole 1131A than at Site 1127 (Table T6; see "Organic Geochemistry," p. 17, in the "Site 1127" chapter).

Inorganic and Organic Carbon, Sulfur, and Nitrogen

Throughout Hole 1131A, carbonate values are uniform and range primarily from 86 to 94 wt% (Table T7; Fig. F13).

Organic carbon (C_{org}) reaches values as high as 1.0 wt% (Table T7; Fig. F13). From the surface to a depth of ~125 mbsf, C_{org} values are primarily <0.4 wt%. In the interval from 125 mbsf to total depth, C_{org} values increase to between 0.4 and 1.0 wt%. Methane concentration in the interval from 125 to ~300 mbsf is also relatively high, apparently related to the higher C_{org} content.

Nitrogen concentrations are all <0.1 wt%, and many samples have no detectable nitrogen. Sulfur was detected in only three samples (Table T7).

T7. $CaCO_3$, C_{org}, N, and S data, Hole 1131A, p. 68.

F13. $CaCO_3$ and C_{org} contents in samples from Hole 1131A, p. 41.

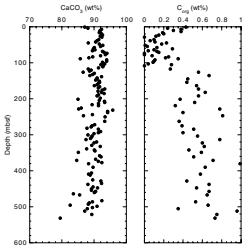

INORGANIC GEOCHEMISTRY

Interstitial Waters

Whole-round cores for interstitial water analysis were taken from Hole 1131A at a rate of one sample per section from the upper 15 cores and every other core thereafter, recovery permitting. Samples were analyzed according to the procedures outlined in "Inorganic Geochemistry," p. 18, in the "Explanatory Notes" chapter. These data are presented in Table T8 and Figures F14, F15, and F16.

T8. Interstitial water geochemistry, p. 70.

Salinity, Chlorinity, Potassium, and Sodium

Salinity shows a uniform increase to a value of 72 at 173.7 mbsf. Below this depth, the increase continues but is erratic, perhaps resulting from minor amounts of contamination by surface seawater (Fig. F14). A maximum value of 84 is reached at a depth of 448.4 mbsf. A similar pattern is observed in the concentration of Cl^-, which attains a maximum concentration of 1574 mM at 467.4 mbsf. The Na^+/Cl^- ratio increases from seawater values of 0.83 to a maximum of 1.1 ± 0.1 between 81.0 and 173.7 mbsf and then returns to seawater values near the base of the cored interval (Fig. F14). The concentration of K^+ mirrors the increase in Cl^-, and the K^+/Cl^- value does not deviate significantly from that of seawater.

Calcium, Magnesium, Lithium, Silica, and Strontium

The concentrations of Mg^{2+} and Ca^{2+} exhibit significant decreases in the upper 300 mbsf, with Mg^{2+} falling as low as 9.81 mM and Ca^{2+} to 2.22 mM at 108.9 mbsf (Fig. F15). Below this depth, concentrations steadily rise toward the base of the cored interval, although normalized ratios are still lower than in normal seawater (Fig. F15). The concentration of Sr^{2+} shows two principal increases, the first between the sediment/seawater interface and 45.8 mbsf, and the second between 192.6 and 294.8 mbsf (Fig. F15). Both these increases represent the recrystallization of aragonite and high-Mg calcite (HMC) to low-Mg calcite (LMC) and dolomite. The first is associated with the loss of HMC from the core and the appearance of dolomite, whereas the second is associated with increasing cementation (see "Lithostratigraphy," p. 3) and decreasing aragonite.

Sulfate, Alkalinity, Ammonium, Iron, and pH

The concentration of SO_4^{2-} shows a slight increase in the upper portion of Site 1131, before decreasing to a concentration of 14.7 mM at a depth of 275.8 mbsf (Fig. F16). When normalized to Cl^-, this decrease represents a depletion of SO_4^{2-} in the pore water by almost 90%. Over the same interval, the NH_4^+ concentration reaches 26.9 mM (Table T8). Iron was only present at or below detection limits throughout the majority of the cored interval, the exception being in the uppermost 45.8 m and in several samples at the base of the hole.

Alkalinity shows a maximum value of 135.02 mM at a depth of 173.7 mbsf. Toward the bottom of the hole, alkalinity decreases to a value of 2.93 mM. Values for pH and pH determined using the push-in electrode (ppH) are relatively consistent, decreasing to 5.9 at a depth of 486.9 mbsf (Fig. F16).

X-Ray Mineralogy

The sediments at Site 1131 are composed of LMC, HMC, quartz, aragonite, and dolomite (Table T9, also in ASCII format; Fig. F17). At the top of the core, HMC is the dominant mineral; however, the concentration of HMC decreases downward to zero at the boundary between lithostratigraphic Units I and II (see "Lithostratigraphy," p. 3). The decrease in HMC is concurrent with the increase in dolomite, which reaches sustained concentrations of ~20% with a maximum concentra-

F14. Interstitial water trends, p. 42.

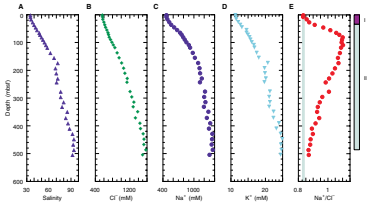

F15. Concentration depth profiles, p. 43.

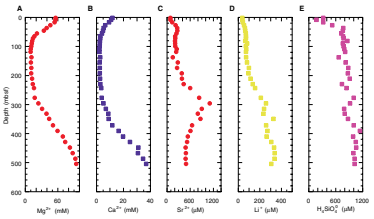

F16. Variations in pH and interstitial water compositions, p. 44.

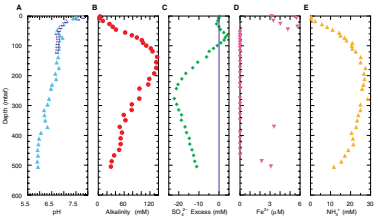

T9. XRD data, p. 71.

F17. Variations in mineral concentrations, p. 45.

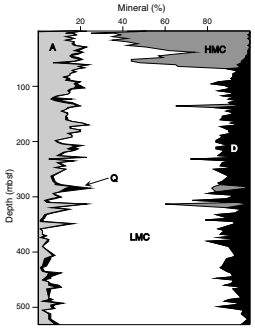

tion of 30%. At the base of Unit II, the concentration of aragonite decreases to ~5%.

Discussion

Carbonate Diagenesis

Site 1131 is characterized by a significant amount of carbonate recrystallization associated with the oxidation of organic material by sulfate-reducing bacteria and the consequent formation of H_2S. This recrystallization is evident from (1) the increase in the concentration of Sr^{2+} in the pore fluid (Fig. F15), (2) changes in mineralogy noted from the X-ray diffraction analyses (Fig. F17), and (3) observation of increased cementation (see "Lithostratigraphy," p. 3). Although the recrystallization occurs throughout the sediments, the nature of the Sr^{2+} profile indicates that the most significant region is between 200 and 300 mbsf where the concentration of Sr^{2+} exceeds 1000 µM. The second region of intensive recrystallization is in the upper 40 mbsf, coincident with the disappearance of HMC from the sediments and the appearance of dolomite. However, because the disappearance of HMC coincides with the boundary between lithostratigraphic Unit I and II, at least part of the decrease may be sedimentological in nature, rather than diagenetic.

An important observation is the presence of excess SO_4^{2-} in the upper portion of the core between 64.8 and 108.9 mbsf. The most probable source for this extra SO_4^{2-} is oxidation of H_2S, which diffuses from lower in the core where high concentrations of this gas are present (see "Organic Geochemistry," p. 17).

Origin of Saline Fluids

As was the case at Sites 1126, 1127, and 1130, Site 1131 is characterized by the presence of a saline brine within the drilled section. The maximum salinity determined is similar to that measured at Sites 1126 and 1127. An intriguing observation is the presence of a maximum in the Na^+/Cl^- ratio, which occurs at a depth between 90 and 110 mbsf. Although it is possible that this high ratio could be an analytical artifact, its presence has been replicated using the concentrations of (1) Na^+ calculated by charge difference, (2) Na^+ measured using the ion chromatograph, and (3) Cl^- determined by titration and ion chromatography. Based on the concurrence of the results from these different techniques, we feel confident that these sediments contain a brine that had a Na^+/Cl^- ratio close to unity and, therefore, had been involved in the dissolution and precipitation of halite and other evaporite minerals. If these observations are correct, then the question arises as to why the region with the highest Na^+/Cl^- ratio is not located in the region of the highest salinity. One explanation may be that since the brines were emplaced in the sediments, the Na^+ and Cl^- ions have diffused into sediments of lower Na^+ and Cl^- content. Because the diffusion rate of these two ions is approximately similar (Li and Gregory, 1974), the original Na^+/Cl^- ratio of the brine has been maintained at the depth in the sediments at which the brine was first introduced, even though concentrations subsequently declined as a result of diffusion. The Na^+/Cl^- ratio decreases with depth because the brine was originally emplaced over a pre-existing brine, which had a Na^+/Cl^- ratio similar to that of seawater. The un-

derlying brine could have entered the sediments during a previous sea-level lowstand. It is possible that the sequence of brine emplacement followed by sea-level rise, sediment deposition, and diffusion could have occurred a number of times coincident with the major sea-level changes during the Pleistocene.

Charge Anomaly

A comparison of the analyses of anions and cations from Site 1131 samples revealed the presence of excess negative charge. This phenomenon was also noticed on Leg 166 for samples from Site 1007 (Shipboard Scientific Party, 1997). As a result of the positive association between the charge-balance anomaly and the normalized concentration of Mg^{2+} at Site 1007, the anomaly was postulated to result from complexing between SO_4^{2-} and Mg^{2+}. The same association was recognized at Site 1131 (Fig. **F18**). Although we have no definitive explanation for this association, we note that the anomaly was not seen at other sites drilled during Leg 182. These other sites also did not exhibit a combination of large sulfate and Mg^{2+} depletions. Hence, we concur with the idea that the imbalance must be linked to the systematic presence of an ion pair in the pore waters.

PHYSICAL PROPERTIES

Introduction

Measurements of physical properties at Site 1131 followed the procedures outlined in **"Physical Properties,"** p. 19, in the "Explanatory Notes" chapter. These included nondestructive measurements of *P*-wave velocity (every 4 cm; Table **T10,** also in **ASCII format**), GRA bulk density (every 4 cm; Table **T11,** also in **ASCII format**), magnetic susceptibility (every 8 cm; Table **T12,** also in **ASCII format**), and NGR (every 16 cm; Table **T13,** also in **ASCII format**) using the MST. The *P*-wave logger (PWL) was activated only on APC cores. Thermal conductivity was measured in unconsolidated sediment at a frequency of one per core (Table **T14,** also in **ASCII format**), with one additional sample per core analyzed after deployments of the Adara tool and the DVTP (Table **T15,** also in **ASCII format**). A minimum of two discrete *P*-wave velocity measurements per section were made on the working half of the split cores (Table **T16,** also in **ASCII format**). Measurement frequency was increased to five per section after the PWL was turned off. Standard index properties (Table **T17,** also in **ASCII format**) and undrained shear strength (only in unconsolidated sediments) (Table **T18,** also in **ASCII format**) were measured at a frequency of one per section. Difficulties occurred with the pycnometer used for determination of dry volume for index properties measurements (see **"Index Properties,"** p. 21, in the "Explanatory Notes" chapter).

The following sections describe downhole variations in sediment physical properties and their relationships to lithology and downhole logging measurements. Variations in magnetic susceptibility are described in **"Paleomagnetism,"** p. 14.

F18. Charge imbalance vs. concentration of Mg^{2+}, **p. 46.**

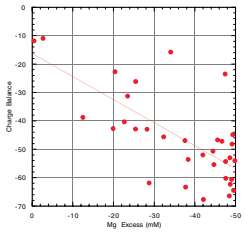

T10. *P*-wave velocity measurements, **p. 73.**

T11. GRA-densiometry measurements, Site 113, **p. 74.**

T12. Magnetic susceptibility measurements, **p. 75.**

T13. Natural gamma-ray measurements, **p. 76.**

T14. Thermal conductivity measurements, **p. 77.**

T15. In situ formation temperature estimates, **p. 78.**

T16. Discrete *P*-wave velocity measurements, **p. 79.**

T17. Index properties measurements, **p. 80.**

T18. Undrained shear strength measurements, **p. 81.**

Index Properties, *P*-Wave Velocity, Natural Gamma Radiation, and GRA Densiometry

Sediment physical properties data reflect the homogeneous sediments recovered at Site 1131. An offset was seen between the discrete bulk density measurements and the GRA densiometry measurements of the MST. This offset was corrected using the equation of Boyce (1976), as described in "Index Properties," p. 21, in the "Explanatory Notes" chapter. Although high concentrations of gas were present, sediment physical properties were not disturbed to the extent of those at Site 1127. Despite this, small voids caused by gas expansion consistently interfered with the sonic travel through the sediment and, as a result, most of the PWL data are invalid.

A close association was seen between downhole logging data (see "Downhole Measurements," p. 23) and sediment physical properties measurements. Natural gamma radiation values from both whole core and the gamma-ray downhole log show an excellent correlation that supports the integrity of both data sets. Gamma-ray attenuation and moisture and density data have similar patterns but lower values than the downhole logging data. This difference probably results from the fact that in situ density includes the influence of sediment overburden and hydrostatic pressure, whereas the laboratory measurements do not. A similar effect is seen in the *P*-wave velocities, particularly below 140 mbsf, where in situ velocities are higher than those measured in discrete samples.

Physical properties data can be divided into two units on the basis of trends in the measured parameters. Physical properties Unit (PP Unit) 1 (0–30 mbsf) is characterized by a rapid increase in NGR (<5–45 cps) to the base of the unit (Fig. F19). This increase appears to result from increasing uranium concentration, as indicated by the spectral gamma-ray log (see "Downhole Measurements," p. 23), and to correlate with the disappearance of HMC in the sedimentary section (see "Inorganic Geochemistry," p. 18). Bulk density (1.4–1.62 g/cm³) shows a small increase with depth, whereas *P*-wave velocity remains constant near 1.55 km/s (Fig. F19). Physical properties Unit 1 corresponds to lithostratigraphic Unit I (see "Lithostratigraphy," p. 3). High but decreasing porosity values (62%–55%) in this unit correspond to the recovered packstone facies. Overall increases seen in bulk density and *P*-wave velocity and decreases in porosity within PP Unit 1 are likely to reflect sediment compaction.

Physical Properties Unit 2 (30–530 mbsf) is characterized by distinct cyclicity in NGR data (Fig. F19) with values between 5 and 62 cps. This cyclicity is likely to be related to Milankovitch-induced sea-level variability and the resultant changes in sedimentology at Site 1131. From 30 to 130 m within PP Unit 2, *P*-wave velocity shows a slight increase (1.6–1.65 km/s) accompanied by a small increase in bulk density (from 1.7 to 2 g/cm³). At 130 mbsf, a sudden increase in *P*-wave velocity is observed (Fig. F19), which corresponds to a change to the PWS3 measurement probe (see "Sonic Velocity," p. 23, in the "Explanatory Notes" chapter). Below this offset, *P*-wave velocity generally increases from average values of 1.8 to 2.0 k/ms (Fig. F19). Within the sedimentary sequence, *P*-wave velocity often correlates to high NGR values. These instances correspond to firmgrounds within the sediment section. Within PP Unit 2, bulk density shows a general increase from 1.55 to 1.7 with higher frequency variability superimposed on this trend. Accompanying this increase in density is a decrease in porosity from 50%

F19. Discrete *P*-wave velocity, bulk density, porosity, magnetic susceptibility, and NGR measurements, p. 47.

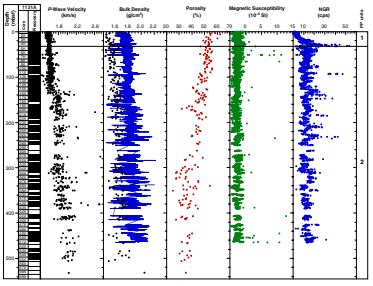

to 30% (Fig. F19). Both of these changes result from lithostatic compaction.

Shear Strength

Undrained peak and residual shear strength were measured on unconsolidated sediments from 0 to 155 mbsf (Fig. F20). Shear strength from Site 1131 shows an overall downhole increase (2–30 kPa) resulting from compaction. Increased variability occurs below 30 mbsf, which corresponds to the PP Unit 1/Unit 2 boundary. This variability is caused in part by alternations in sediment lithification, but may also result from drilling disturbance or cracking of the sediment before failure, producing lower values for peak strength.

Thermal Conductivity

Thermal conductivity values at Site 1131 range from 0.76 to 1.16 W/(m·K) (Fig. F21). Thermal conductivity is correlated to increases in sediment bulk density at Site 1131 (Fig. F21) and thus is likely to be controlled by compaction and diagenetically controlled changes in sediment induration.

In Situ Temperature Measurements

Only three in situ temperature measurements were made at Site 1131, two using the Adara tool and one using the DVTP (Fig. F22). There was considerable variation in estimates of mudline temperature from 11.98° to 13.55°C. An additional estimate of seafloor temperature was obtained using an expendable bathythermograph. This yielded a value lower than those obtained from the in situ temperature tools, possibly because of differences in temperature calibration. None of the in situ temperature measurements were affected by postemplacement movement of the probe, and differences between data fits gave only minor differences in temperature (Table T15).

In situ temperature data define a linear temperature-depth trend that defines a geothermal gradient of 42.6° ± 0.5°C/km (r^2 = 0.99; N = 6) (all uncertainties are 1 standard deviation). The geometric mean of thermal conductivity between 0 and 115 mbsf was used for determination of heat flow (0.95 ± 0.089 W/[m·K]) (Fig. F22). Using this value and the geothermal gradient determined above, heat flow at the site is estimated to be 40.5 mW/m². This value is higher than that determined at Site 1130, which has similar low thermal conductivity sediments and is in a similar position and depth on the shelf margin, although it is lower than the value determined in much deeper water off the platform margin at Site 1128.

DOWNHOLE MEASUREMENTS

Logging Operations

After completion of drilling operations at Hole 1131A, the borehole was prepared for logging (see "Operations," p. 2). The end of the BHA was placed at 99 mbsf. The WHC was used during all logging runs and coped well with the moderate heave conditions. Three different logging strings were deployed in the following order: (1) triple combo including

F20. Maximum shear strength with physical properties units for Hole 1131A, p. 48.

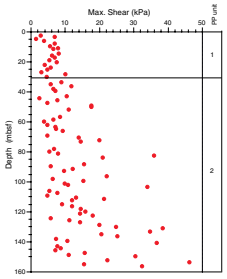

F21. Thermal conductivity measurements, p. 49.

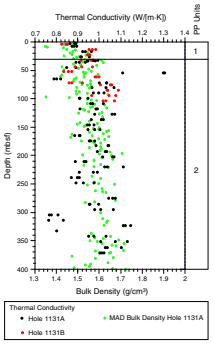

F22. Variation of formation temperature with depth, p. 50.

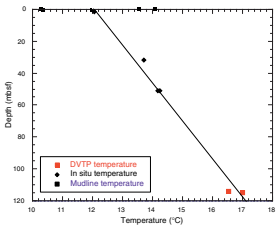

the Lamont-Doherty Earth Observatory high-resolution temperature/acceleration/pressure tool (LDEO-TAP), (2) FMS/sonic, and (3) WST (see "Downhole Measurements," p. 25, in the "Explanatory Notes" chapter). The base of the hole became progressively shallower during logging operations because of fill accumulation (Table T19).

Before the main run with the triple combo, a short quality-control run was made from base of hole at 585 mbsf (31 m short of drilled depth) to 494 mbsf. The main run covered the interval from 578 mbsf to the mudline. A single pass with the FMS/sonic was made from 572.5 mbsf to 144 mbsf. The WST was used to record eight check-shot stations (stacks of seven shots) at 30- to 100-m intervals between 560 and 140 mbsf. Check-shot locations were located at log breaks and at the estimated depths of significant seismic reflectors (see "Seismic Stratigraphy," p. 26, in the "Site 1127" chapter).

T19. Tool strings, intervals logged, and logging speeds; Hole 1131A, p. 82.

Data Quality

Caving was significant in the upper 240 m of the open-hole logged interval, where hole diameter reached 45 cm, occasionally saturating the hostile environment lithodensity sonde and FMS calipers. Despite caving, FMS images were generally of high quality. With the exception of the accelerator porosity sonde, which in some intervals was affected by large borehole diameter (see "Logging Unit 2: 27–529 mbsf," p. 25), the triple combo string performed well. Hole-centered tools (sonic digital tool and dual induction tool) were less sensitive to borehole conditions and produced high-quality sonic and resistivity logs. The check-shot data contained consistent background noise (~35 Hz) of undetermined origin, and clipping of the recorded signal was observed at some stations. However, the recorded wavelets show a distinct first break suitable for check-shot purposes.

Despite low core recovery in some intervals, there is good agreement between the gamma-ray log (HSGR) and NGR from core (see "Physical Properties," p. 21). Core velocity is consistently lower than sonic velocity measured downhole. This difference increases with depth, as discrete velocity measurements on cores were not measured at in situ pressures.

F23. Summary of spectral gamma-ray logs from the HNGS for the open-hole logged interval, p. 51.

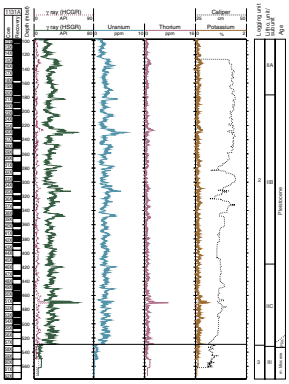

Preliminary Interpretation

Sediments at Site 1131 are generally high in calcium carbonate (see "Organic Geochemistry," p. 17). The most striking feature of the logs at Site 1131 is the distinct "Milankovich-like" cyclicity of the gamma radiation log (Fig. F23). This cyclicity dominantly results from variations in uranium concentrations (Fig. F23). These changes in uranium may be associated with organic matter and/or diagenetic horizons, although blackened grains observed in the recovered core may be another potential source. Cyclicity in gamma radiation at Site 1131 correlates well with cyclicity at Site 1127. Three major logging units have been defined at Site 1131, mainly on the basis of variations in gamma-ray and sonic logs.

F24. Summary of spectral gamma-ray logs from the HNGS for the interval logged through pipe, p. 52.

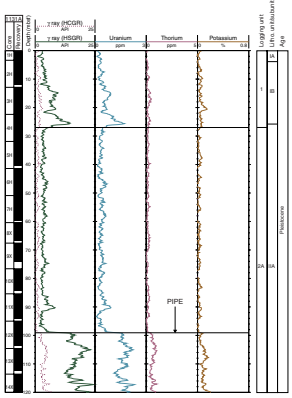

Logging Unit 1: 0–27 mbsf

Unit 1 is defined by an increasing trend of cyclic variations in gamma radiation (Fig. F24). The base of Unit 1 is defined at a marked drop in gamma-ray values caused by a drop in the uranium content of

the formation (Fig. F24). Logging Unit 1 coincides with lithostratigraphic Unit 1, which is interpreted as a succession of bryozoan mounds (see "Lithostratigraphy," p. 3).

Logging Unit 2: 27–529 mbsf

Unit 2 was logged through pipe to 99 mbsf, with low variability in gamma-ray values (Fig. F24). The open-hole logged interval displays more variation, with gamma-ray values fluctuating between 20 and 60 American Petroleum Institute (API) units (Fig. F23). Throughout logging Unit 2, density values show a steady increase, with periodic excursions to higher values associated with peaks in sonic velocity and resistivity (Fig. F25). These intervals probably represent firmgrounds in the sedimentary sequence and are often accompanied by increased gamma radiation. These lithified horizons are also observed in FMS images as thin (~1–2 m), highly resistive intervals (Fig. F26). A few lithified horizons (e.g., at 260 and 323 mbsf) in Unit 2 are associated with cross-overs (negative separation) of porosity and density and low gamma-ray values and may be interpreted as chert horizons. As with bulk density, sonic velocity also shows a steadily increasing downhole trend typical of a compaction profile (Fig. F25). Resistivity values are nearly constant throughout Unit 2, with the exception of excursions found within firmgrounds (Fig. F25). Porosity values are highly variable above 340 mbsf in Unit 2, result partly from variations in borehole diameter. Below 340 mbsf, porosity values remain moderately constant (45%) (Fig. F25). Photoelectric effect (PEF) values within logging Unit 2 show a slight downhole increase with low to moderate variability. The base of logging Unit 2 coincides with a major hiatus between the Pliocene and the middle Miocene, the boundary between lithostratigraphic Units II and III, and the base of seismic Sequence 2 (see "Biostratigraphy," p. 9, "Lithostratigraphy," p. 3; also see "Seismic Stratigraphy," p. 26, in the "Site 1127" chapter).

Logging Unit 3: 529–575 mbsf

Logging Unit 3 correlates with lithostratigraphic Unit III (see "Lithostratigraphy," p. 3). This portion of the sedimentary section had only minimal recovery; thus, the downhole logs of logging Unit 3 provide important information on the sediments in this interval. Unit 3 is characterized by a shift to uniformly low gamma-ray values (<10 API units) and a higher variability of all other logs except density (Fig. F25). Photoelectric effect values fluctuate between 3.5 and 4.5 barn/e⁻, and the porosity curve shows frequent cross-overs with density. Within logging Unit 3, there are numerous excursions in shallow resistivity, indicating fluid invasion into the sequence (Fig. F25). Peak sonic velocities reach 2.9 km/s (Fig. F25). Downhole measurements indicate a change to a succession of thinly bedded cherts (porosity-density cross-over and low PEF values; high resistivity and sonic values), alternating with layers rich in calcium carbonate (no cross-over and high PEF values). The sediments of Unit 3 are well imaged by the FMS, which clearly identifies individual chert layers as thin (~ 20 cm), highly resistive intervals interbedded with thicker (1–2 m), less resistive grainstones (Fig. F27). This conclusion is supported by the limited core recovery in this interval.

F25. Summary of triple combo and sonic logs vs. depth for the open-hole logged interval, p. 53.

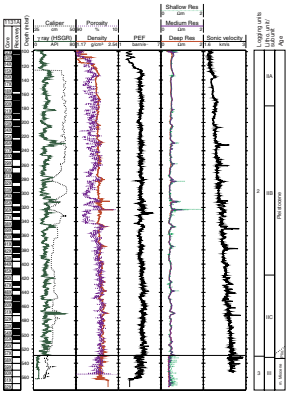

F26. FMS image showing a firmground between Subunits 2A and 2B, p. 54.

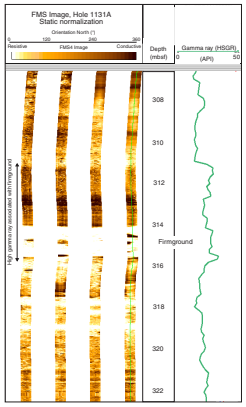

F27. FMS image showing logging Unit 2/Unit 3 boundary and lithostratigraphic Unit II/Unit III boundary, p. 55.

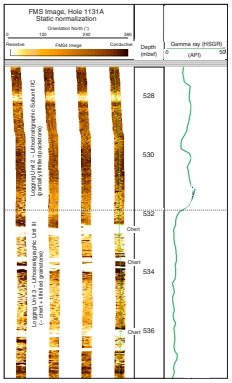

Temperature Measurements

The measurements of the LDEO-TAP tool define a very smooth temperature gradient (~17°C/km) below the pipe (Fig. F28), indicating that flow into the borehole is insignificant. This is dissimilar to the situation at Hole 1127B, immediately downslope from Hole 1131A.

F28. Downhole variations in borehole temperature, p. 56.

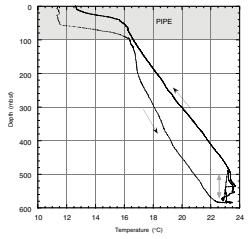

SEISMIC STRATIGRAPHY

The seismic stratigraphic results from Sites 1127, 1129, and 1131 are considered together, as these sites represent a transect of three closely spaced sample points through the same sequences that form spectacular clinoforms beneath the modern shelf edge. For a discussion of these results, see "Seismic Stratigraphy," p. 26, in the "Site 1127" chapter.

REFERENCES

Berggren, W.A., Kent, D.V., Swisher, C.C., III, and Aubry, M.-P., 1995. A revised Cenozoic geochronology and chronostratigraphy. *In* Berggren, W.A., Kent, D.V., Aubry, M.-P., and Hardenbol, J. (Eds.), *Geochronology, Time Scales and Global Stratigraphic Correlation*. Spec. Publ.—Soc. Econ. Paleontol. Mineral. (Soc. Sediment. Geol.), 54:129–212.

Bone, Y., and James, N.P., 1993. Bryozoans as carbonate sediment producers on the cool-water Lacepede Shelf, Southern Australia. *Sediment. Geol.,* 86:247–271.

Boyce, R.E., 1976. Definitions and laboratory techniques of compressional sound velocity parameters and wet-water content, wet-bulk density, and porosity parameters by gravimetric and gamma-ray attenuation techniques. *In* Schlanger, S.O., Jackson, E.D., et al., *Init. Repts. DSDP,* 33: Washington (U.S. Govt. Printing Office), 931–958.

Chaproniere, G.C.H., Shafik, S., Truswell, E.M., MacPhail, M.K., and Partridge, A.D., 1995. Cainozoic. In *Australian Phanerozoic Time Scale.* Aust. Geol. Surv. Org., 10.

Cisowski, S., 1981. Interacting vs. non-interacting single domain behavior in natural and synthetic samples. *Phys. Earth Planet. Inter.,* 26:56–62.

Feary, D.A., and James, N.P., 1995. Cenozoic biogenic mounds and buried Miocene (?) barrier reef on a predominantly cool-water carbonate continental margin, Eucla Basin, western Great Australian Bight. *Geology,* 23:427–430.

————, 1998. Seismic stratigraphy and geological evolution of the Cenozoic, cool-water, Eucla Platform, Great Australian Bight. *AAPG Bull.,* 82:792–816.

James, N.P., 1997. The cool water carbonate depositional realm. *Spec. Publ.—Soc. Econ. Paleontol. Mineral.,* 56:1–20.

James, N.P., and Bourque, P.-A., 1990. Reefs and mounds. *In* Walker, R.G., and James, N.P. (Eds.), *Facies Models*. Geol. Assoc. Can., 323–348.

James, N.P., and von der Borch, C.C., 1991. Carbonate shelf edge off southern Australia: a prograding open-platform margin. *Geology,* 19:1005–1008.

Jenkins, D.G., 1985. Southern mid-latitude Paleocene to Holocene planktic foraminifera. *In* Bolli, H.M., Saunders, J.B., and Perch-Nielsen, K. (Eds.), *Plankton Stratigraphy:* Cambridge (Cambridge Univ. Press), 263–282.

————, 1993. Cenozoic southern mid- and high-latitude biostratigraphy and chronostratigraphy based on planktonic foraminifera. *In* Kennett, J.P., and Warnke, D.A. (Eds.), *The Antarctic Paleoenvironment: A Perspective on Global Change.* Antarct. Res. Ser., 60:125–144.

JOIDES PPSP, 1992. Ocean Drilling Program guidelines for pollution prevention and safety. *JOIDES J.,* 18.

Li, Q., and McGowran, B., in press. Miocene foraminifera from Lakes Entrance oil shaft, southeastern Australia. *Assoc. Australas. Paleontol. Mem. Ser.*

Li, Y., and Gregory, S., 1974. Diffusion of ions in sea water and in deep-sea sediments. *Geochim. Cosmochim. Acta.,* 38:703–714.

Shipboard Scientific Party, 1997. Site 1007. *In* Eberli, G.P., Swart, P.K., Malone, M.J., et al., *Proc. ODP, Init. Repts.,* 166: College Station, TX (Ocean Drilling Program), 289–345.

Valet, J.-P., and Meynadier, L., 1993. Geomagnetic field intensity and reversals during the past four million years. *Nature,* 336:234–238.

Figure F1. Map showing the location of Site 1131 (on the eastern Eyre Terrace uppermost slope) in relation to other Leg 182 sites and the Australian Geological Survey Organisation Survey 169 (AGSO169) seismic lines.

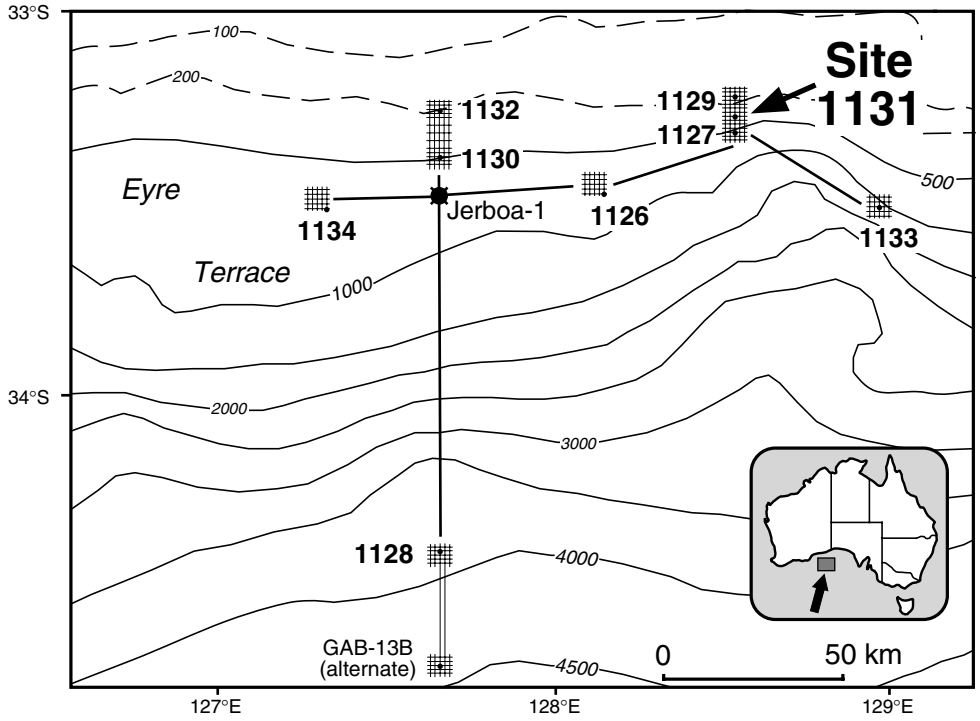

Figure F2. Portion of seismic Line AGSO169/05a showing interpreted seismic stratigraphic sequences planned (shown in white) and actually intersected (shown in black) at Site 1131. Note the extremely thick section of Sequence 2 sigmoidal clinoforms.

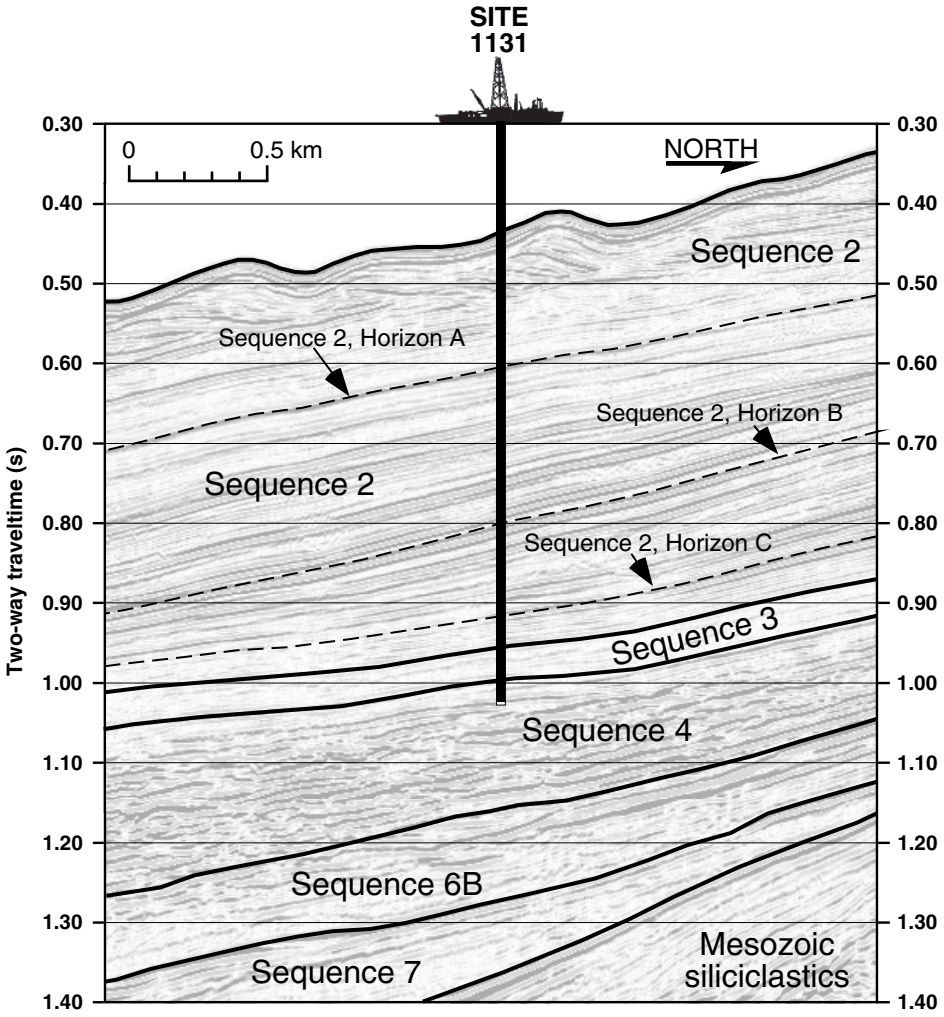

Figure F3. Summary of lithostratigraphy at Site 1131, showing subdivision into lithostratigraphic units and subunits. Age and paleomagnetic data are from **"Biostratigraphy,"** p. 9, and **"Paleomagnetism,"** p. 14.

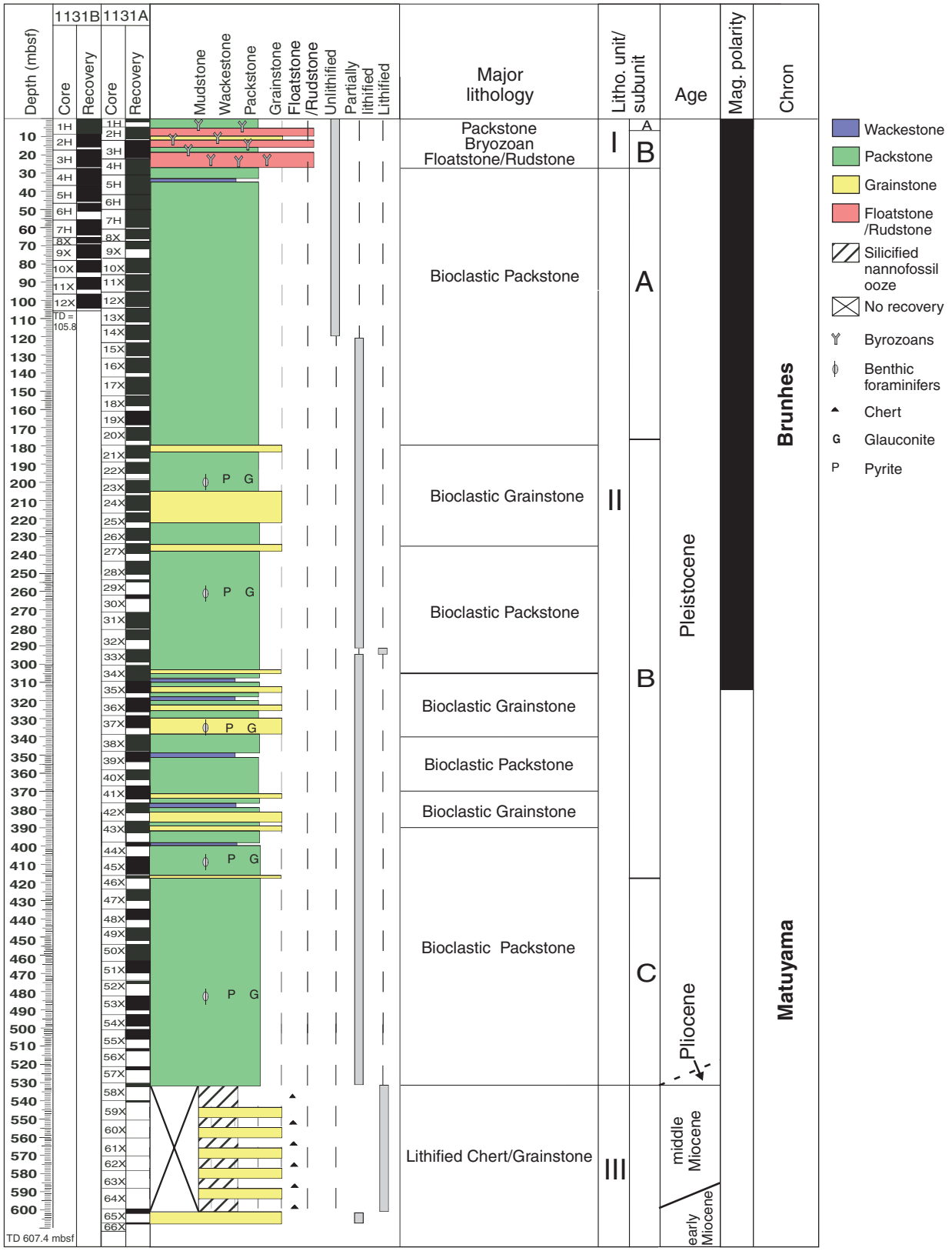

Figure F4. Stratigraphic position of calcareous nannofossil and planktonic foraminifer zones and benthic foraminifer assemblages at Site 1131. Dashed boundaries imply uncertainty. No recovery means that no material was recovered in a core. The lithostratigraphic units are taken from "Lithostratigraphy," p. 3. (Continued on next page.)

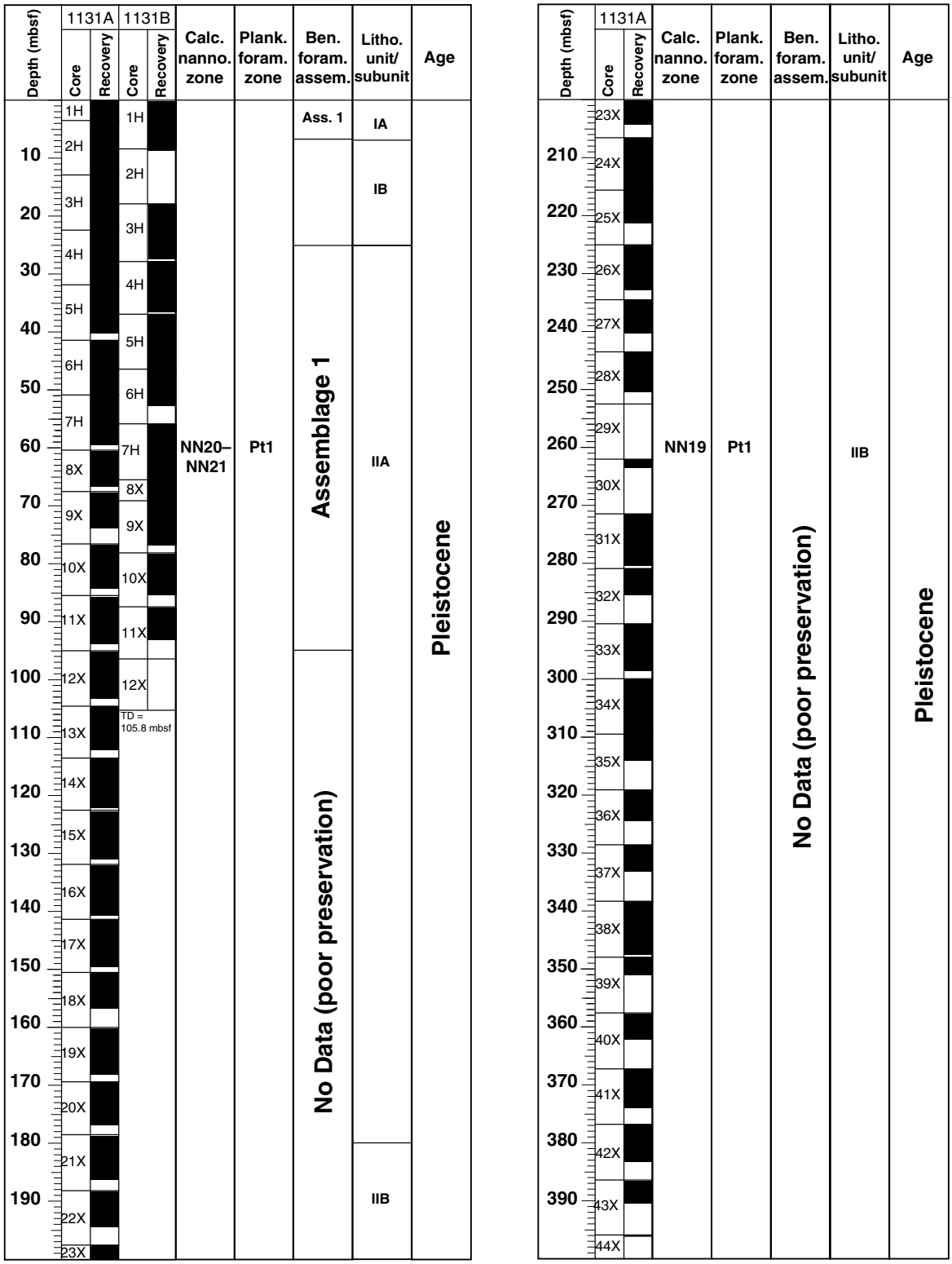

Figure F4 (continued).

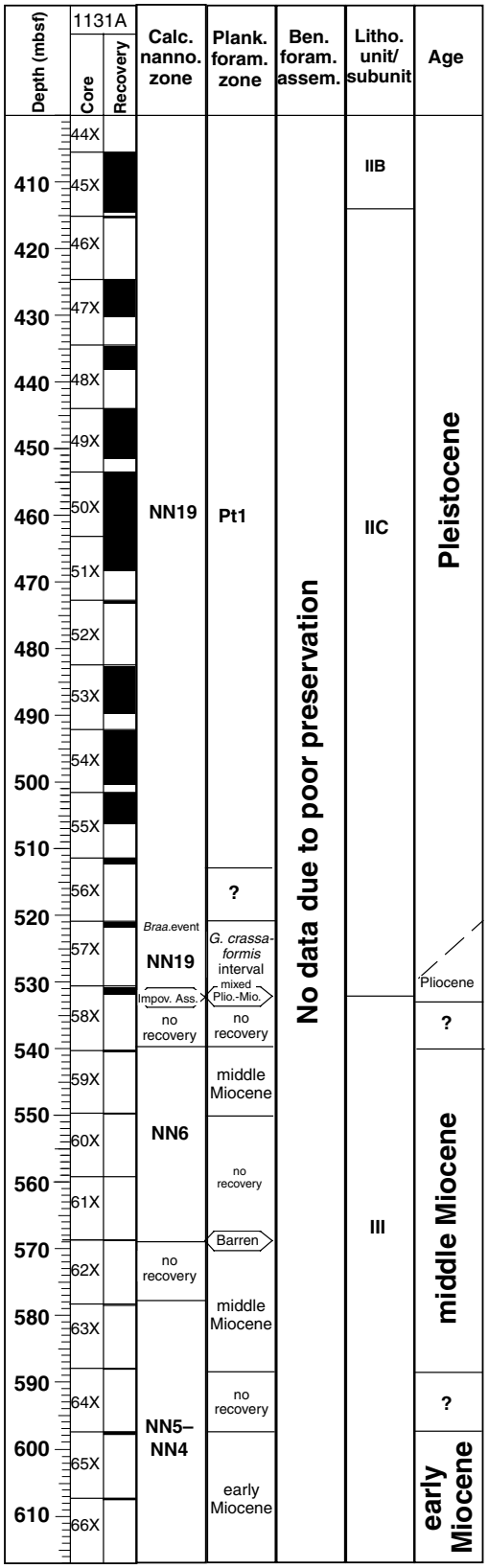

Figure F5. Sedimentation rate curve constructed from the datum levels listed in Table T2, p. 59. Stratigraphic error is indicated by the length of the error bars.

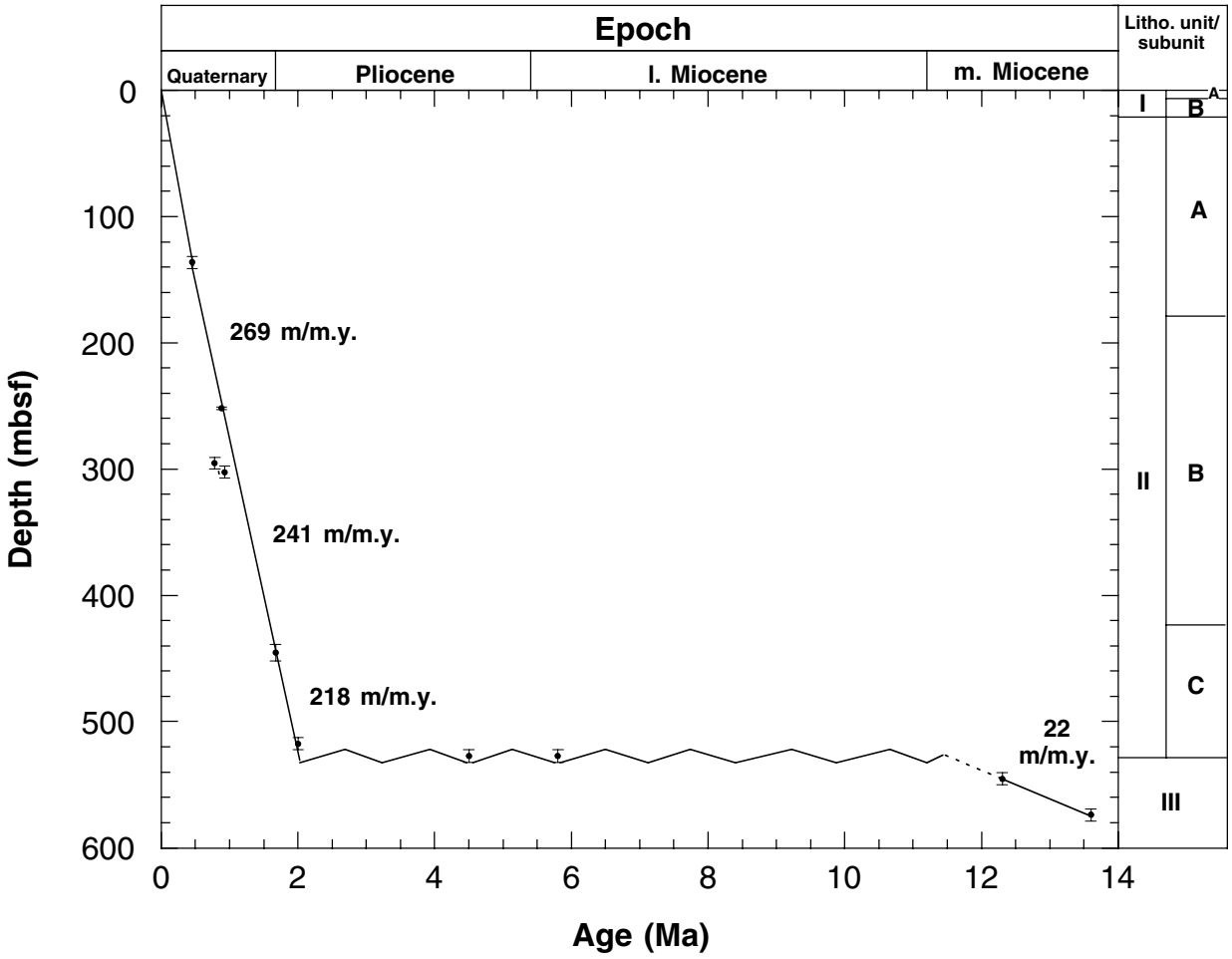

Figure F6. Downhole inclination determined **(A)** from natural remanent magnetization (NRM) long-core measurements and **(B)** after partial demagnetization at 20 mT, together with interpreted magnetostratigraphy from Hole 1131A. Long-core measurements (crosses) are compared with results from discrete samples (open squares). Magnetic polarity is shown in the far right column.

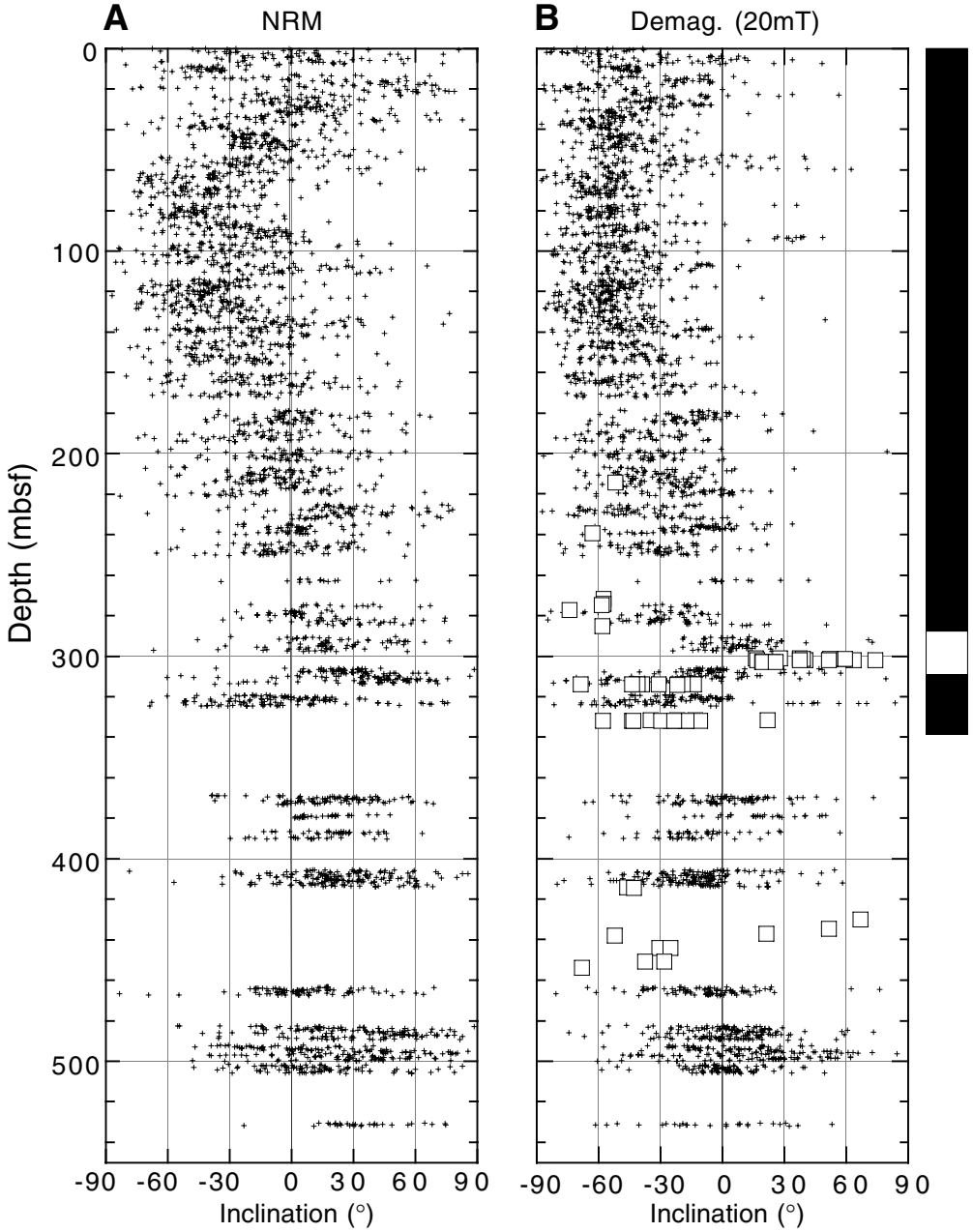

Figure F7. Normalized intensity decay (left), demagnetization diagrams (center), and stereoplot of representative samples (right). **A.** Alternating field (AF) demagnetization showing two-component magnetization with a characteristic magnetization of normal polarity (Sample 182-1131A-31X-1, 27–34 cm.) **B.** AF demagnetization showing a prominent overprint and a reverse polarity characteristic magnetization (Sample 182-1131A-48X-1, 45–47 cm.). Demagnetization diagrams show projections of the natural remanent magnetization vector in the vertical (open symbols) and horizontal (solid symbols) planes during progressive demagnetization.

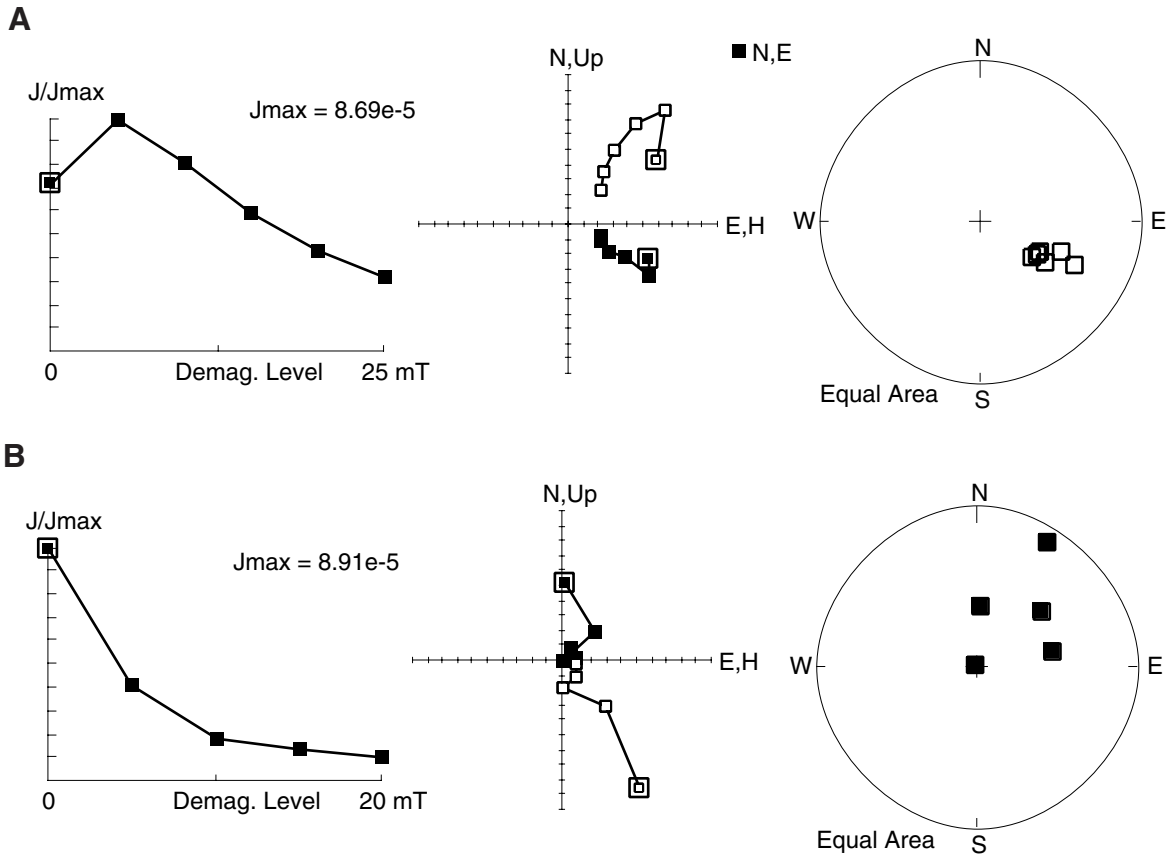

Figure F8. Long-core measurements of **(A, B)** declination, **(C)** inclination, and **(D)** intensity of remanent magnetization after partial demagnetization (20 mT) for the upper 180 mbsf. Declinations for Hole 1131A (B) and Hole 1131B (A) are shown before (small symbols) and after (large symbols) orientation using the magnetic Tensor tool. In C and D, open symbols are used for data from Hole 1131B.

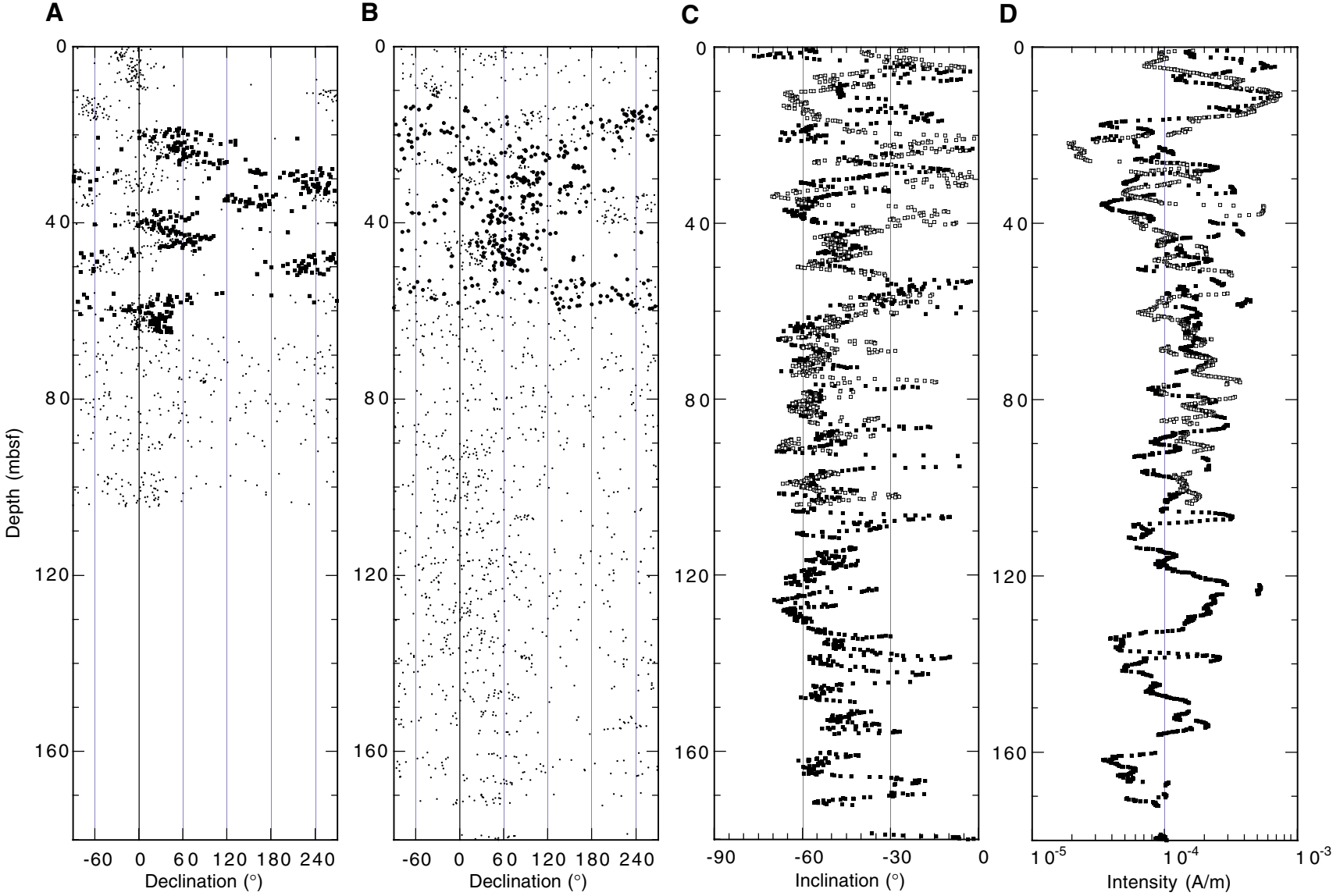

Figure F9. Acquisition of isothermal remanent magnetization (IRM) and its alternating field demagnetization for representative samples from APC and XCB cores.

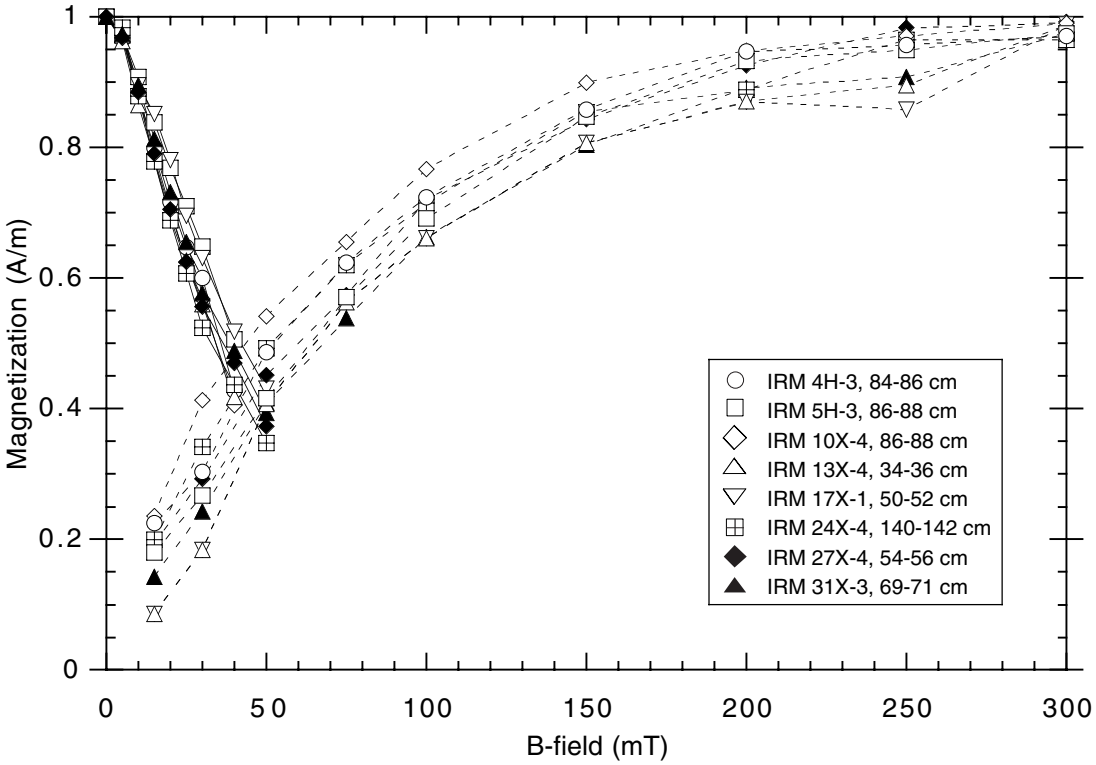

Figure F10. Composite depth section produced using the Splicer software. The black line represents data from Hole 1131A, and the red line represents data from Hole 1131B. Data from Hole 1131B are offset for ease of comparison. NGR = natural gamma radiation. All depths use the meters composite depth (mcd) scale. For conversions from mcd to meters below seafloor (mbsf), see Table T3, p. 60.

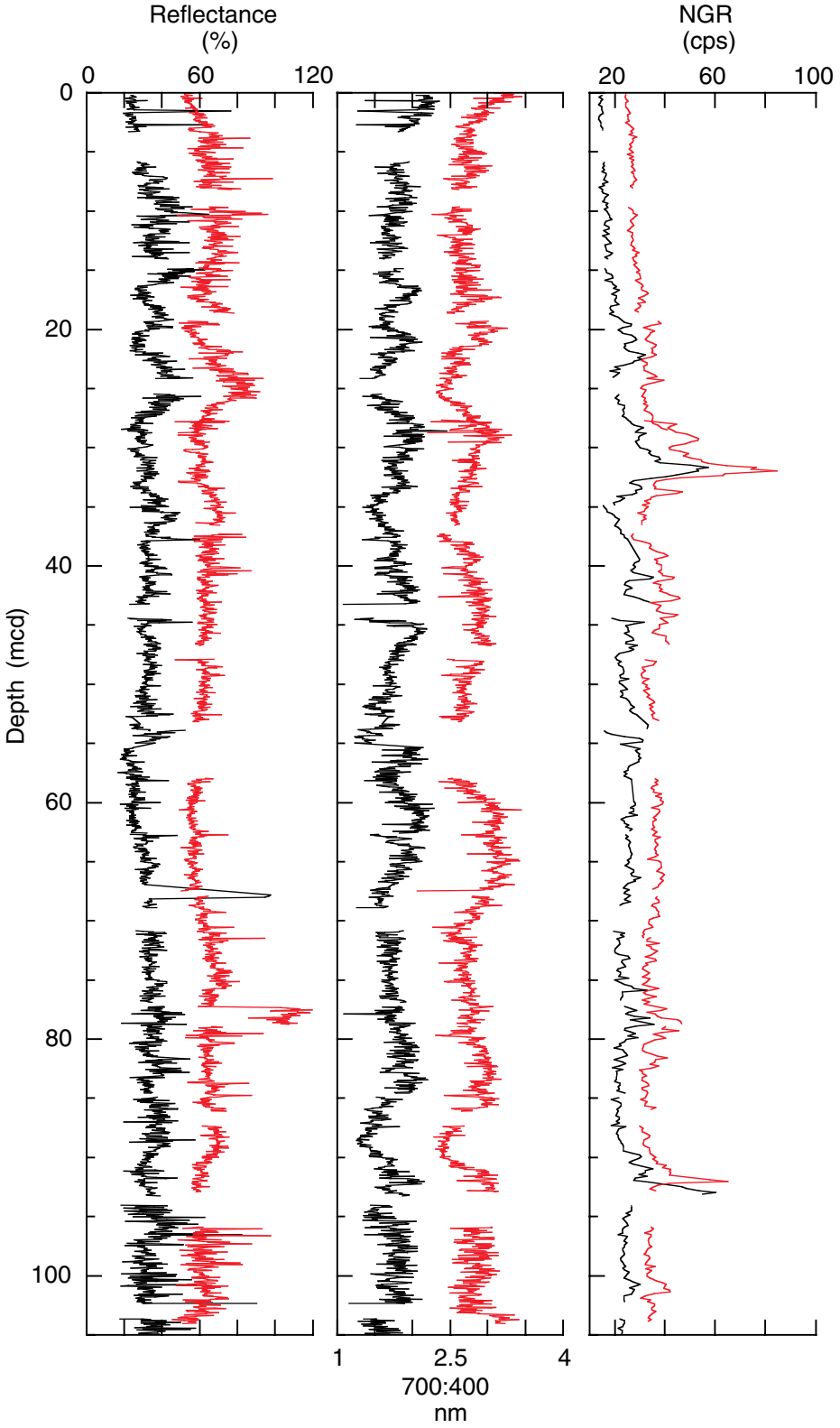

Figure F11. Spliced section of smoothed color reflectance ratio data (700:400 nm), smoothed 400-nm color reflectance data, and smoothed natural gamma radiation (NGR) data produced using the Splicer software. These data are a spliced composite of correlated data from Holes 1131A and 1131B.

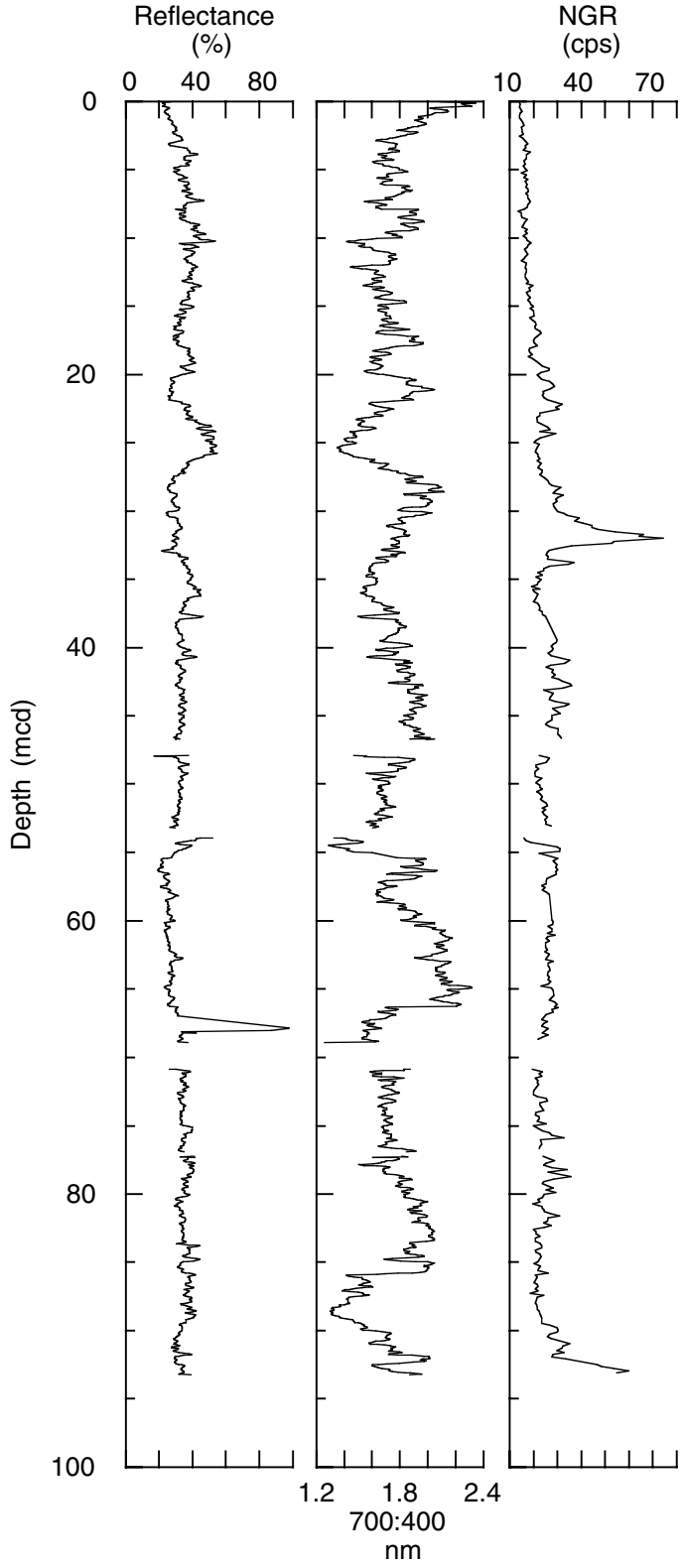

Figure F12. Methane (C_1) concentration, methane/ethane (C_1/C_2) values, and hydrogen sulfide (H_2S) concentration of headspace gases from Hole 1131A; ppmv = parts per million by volume.

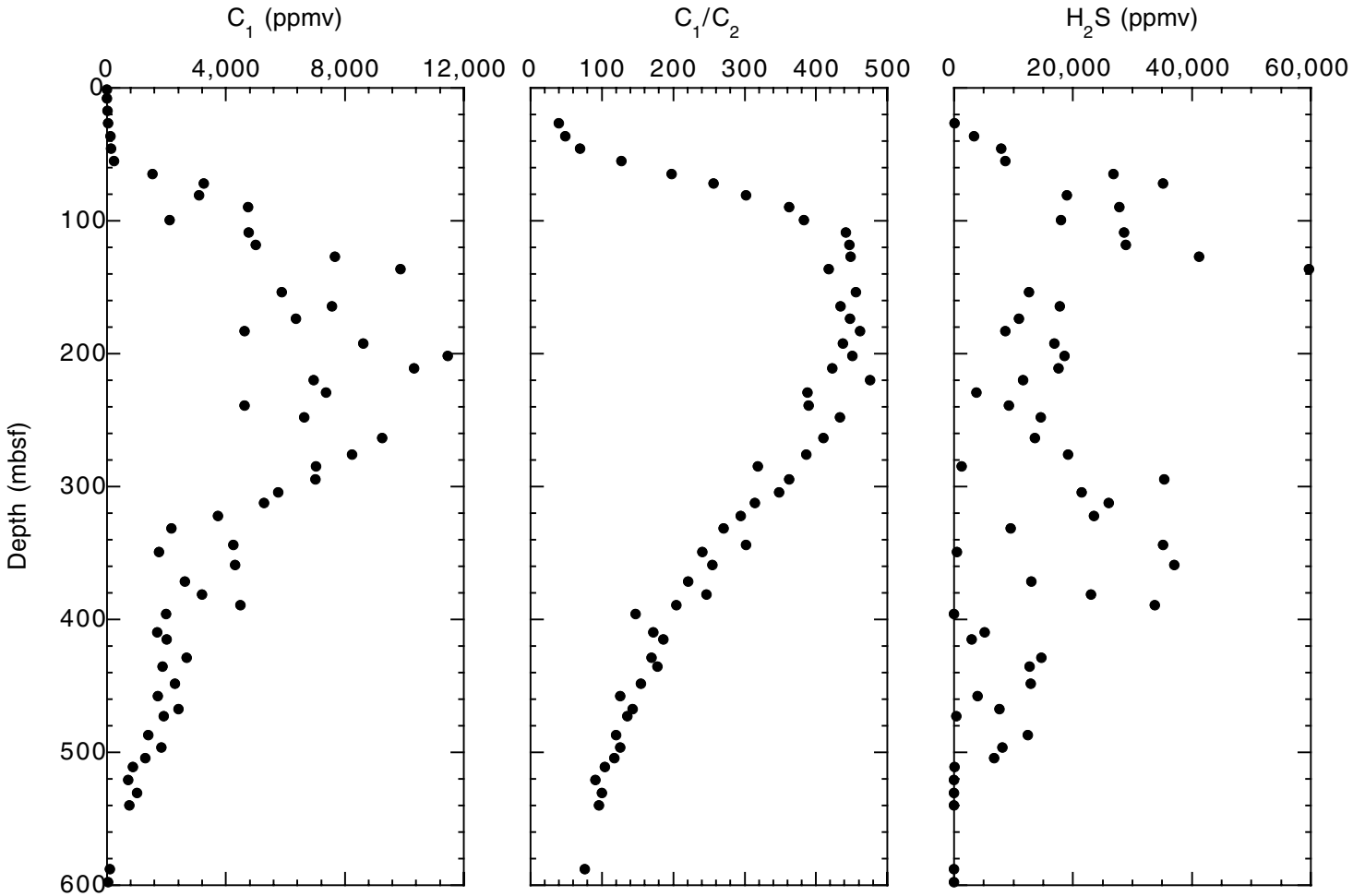

Figure F13. Calcium carbonate and organic carbon contents in samples from Hole 1131A.

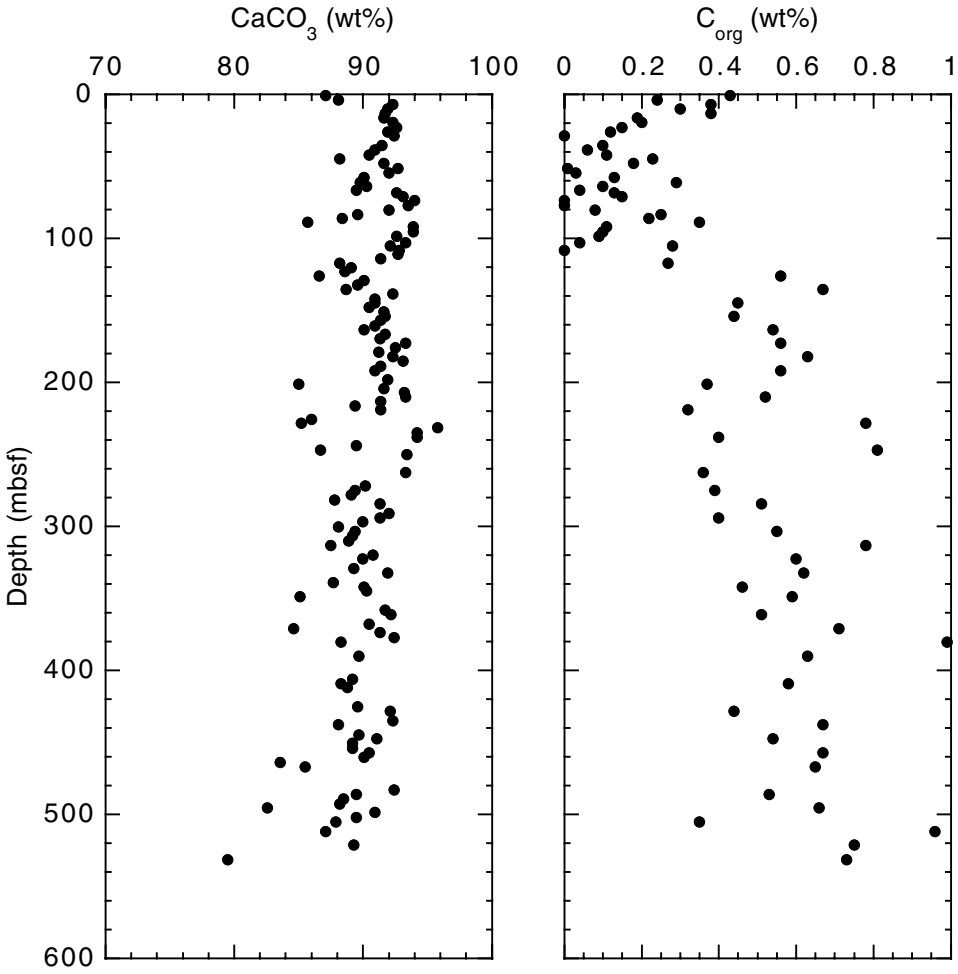

Figure F14. Summary trends in (**A**) salinity, (**B**) Cl^-, (**C**) Na^+, (**D**) K^+, and (**E**) Na^+/Cl^-. Although the trends of the concentrations in these ions show a diffusive profile, the Na^+/Cl^- ratio shows a maximum between 90 and 120 mbsf. Lithostratigraphic units are shown on the right side of the figure.

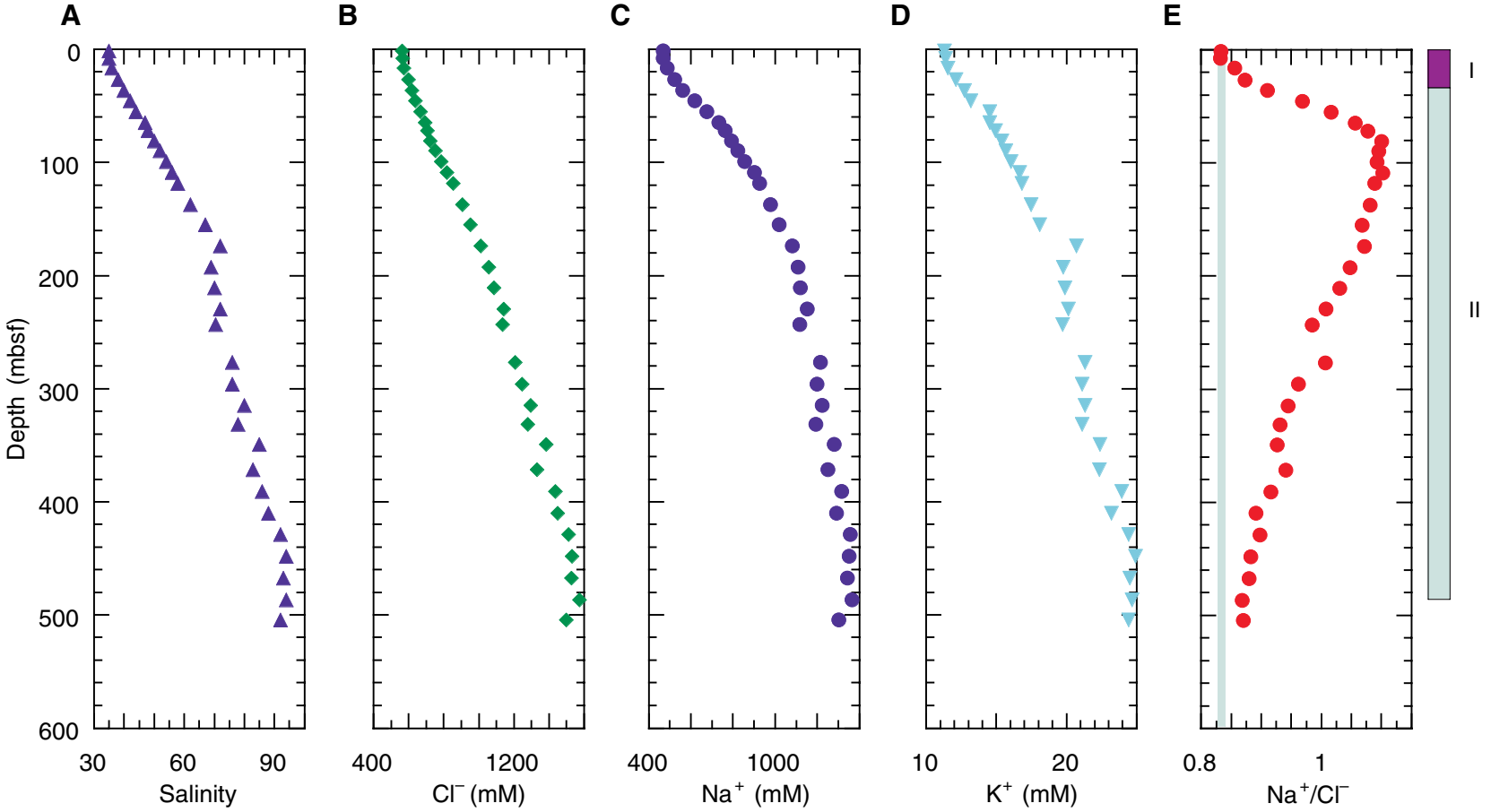

Figure F15. Concentrations of **(A)** Mg^{2+}, **(B)** Ca^{2+}, **(C)** Sr^{2+}, **(D)** Li^{+}, and **(E)** $H_4SiO_4^0$. Note the large decrease in the concentration of Ca^{2+} and Mg^{2+} in the upper 300 mbsf and the rapid increase in Sr^{2+} between 200 and 300 mbsf.

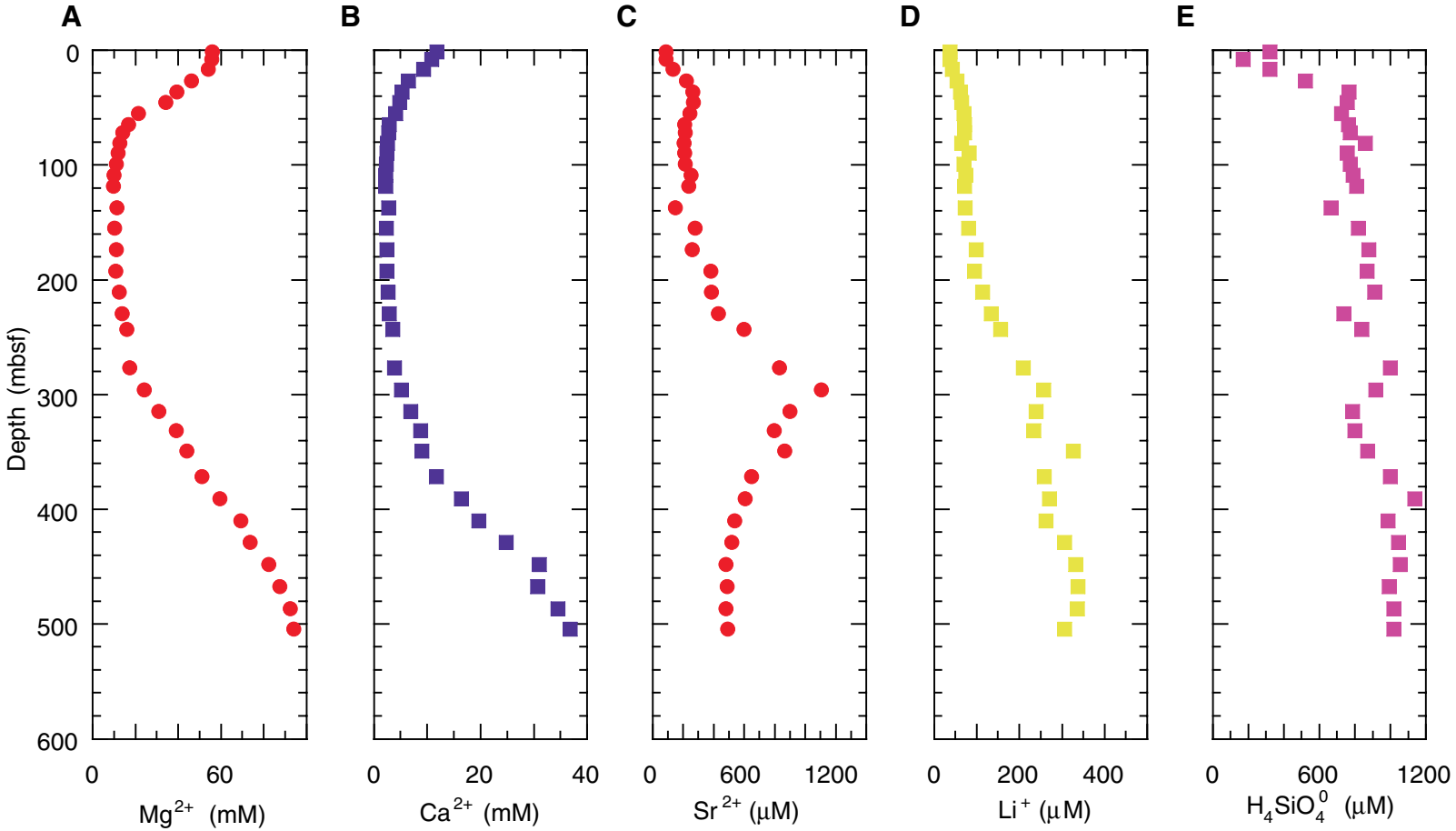

Figure F16. Variations in **(A)** pH (the punch-in pH values are shown by the open triangles), **(B)** alkalinity, **(C)** SO_4^{2-}, **(D)** Fe^{2+}, and **(E)** NH_4^+ from Site 1131.

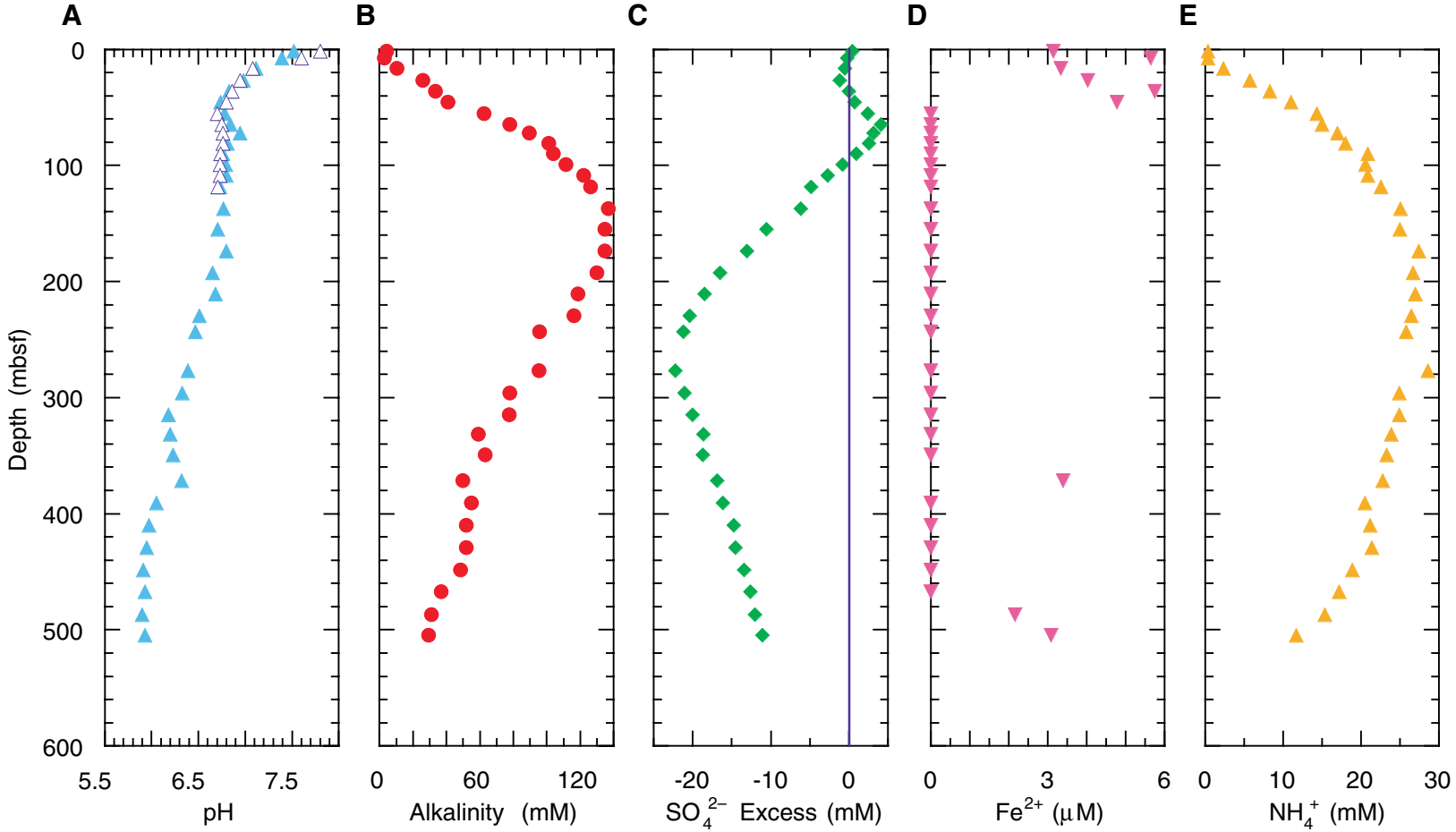

Figure F17. Variations in the concentration of aragonite (A), high-Mg calcite (HMC), quartz (Q), low-Mg calcite (LMC), and dolomite (D) at Site 1131.

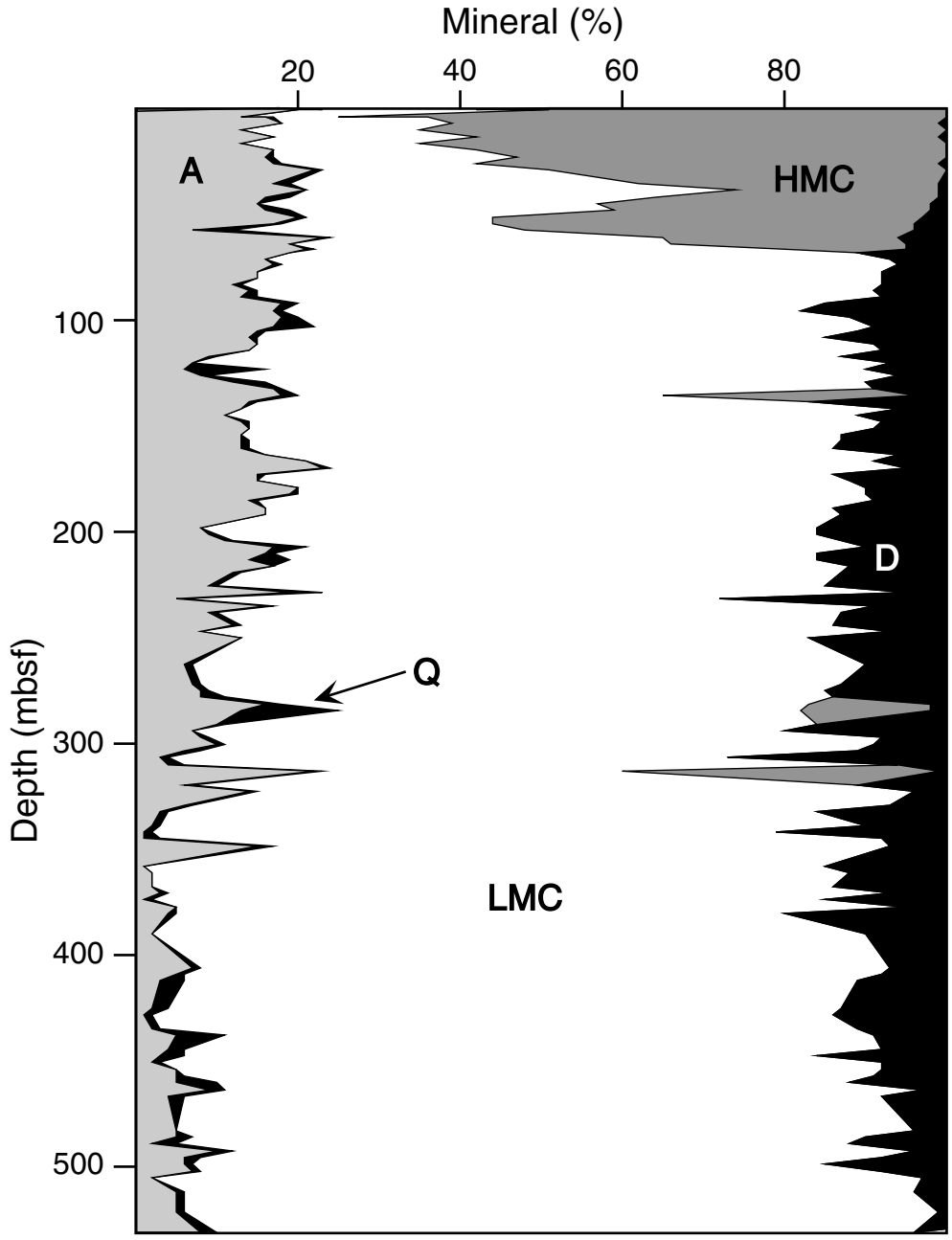

Figure F18. Correspondence between the charge imbalance and the concentration of Mg^{2+} for Site 1131, which suggests that the imbalance is associated with the loss of Mg^{2+}.

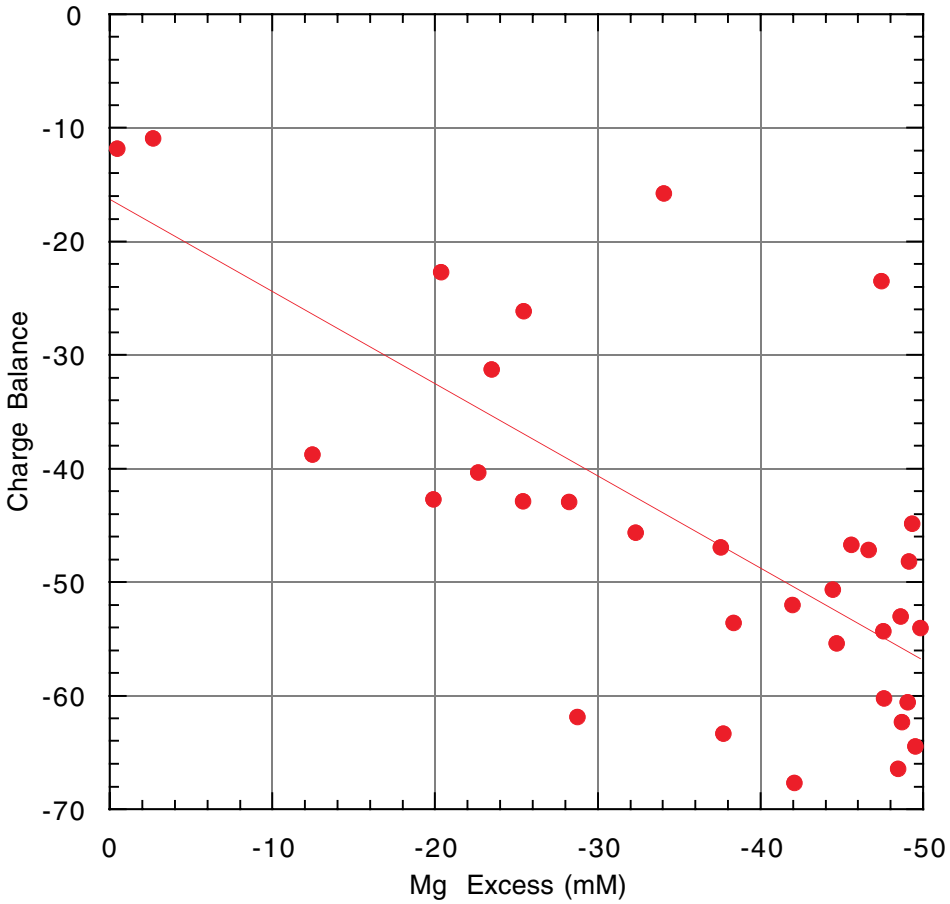

Figure F19. Combined plot of discrete *P*-wave velocity (black dots), gamma-ray attenuation (GRA; lines) and moisture-and-density (MAD; dots) bulk densities, porosity, magnetic susceptibility, and natural gamma radiation (NGR) measurements. Core recovery is shown on the left, and physical properties units (PP units) are shown on the right.

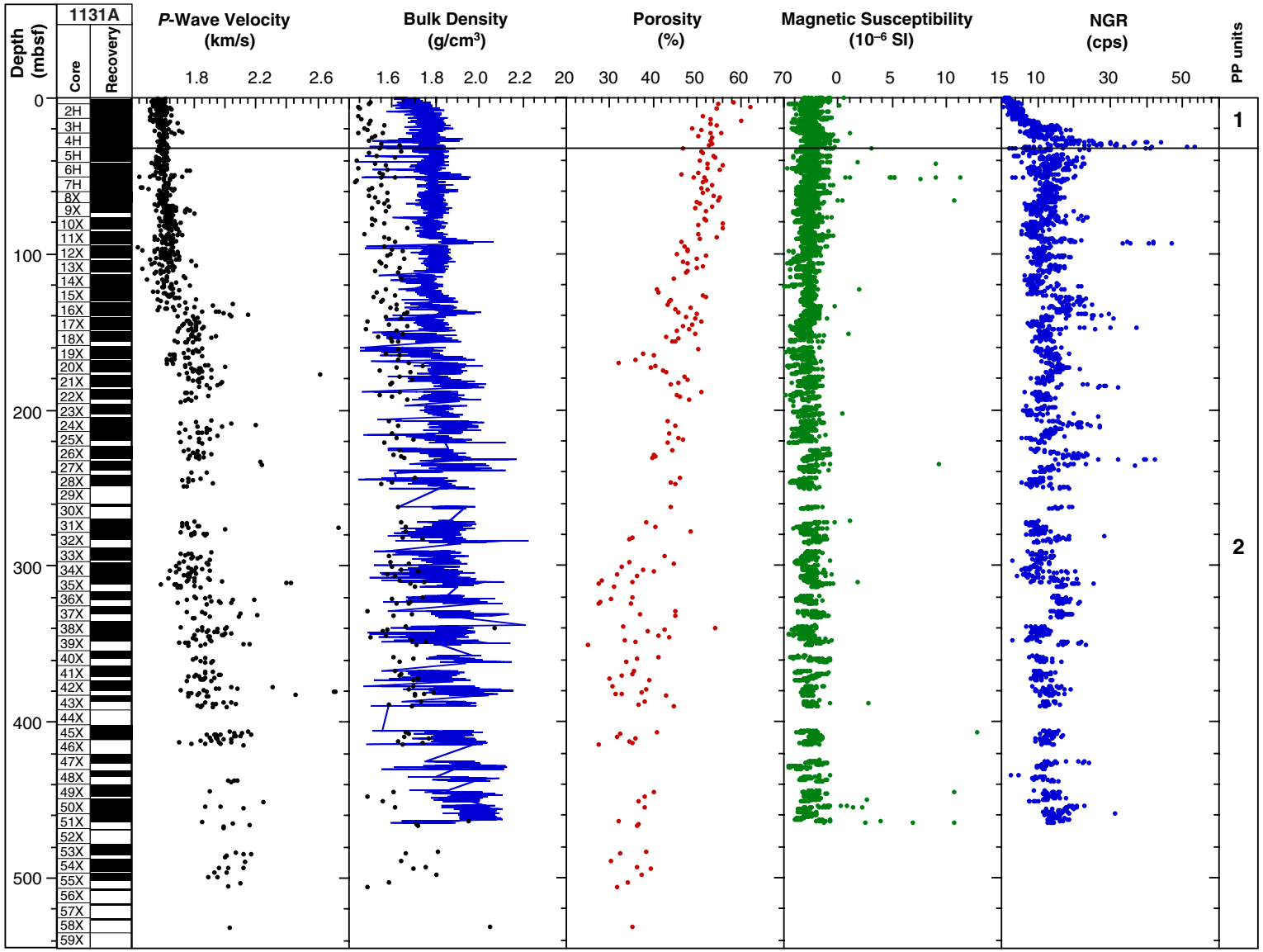

Figure F20. Maximum shear strength data with physical properties units (PP units) for Hole 1131A.

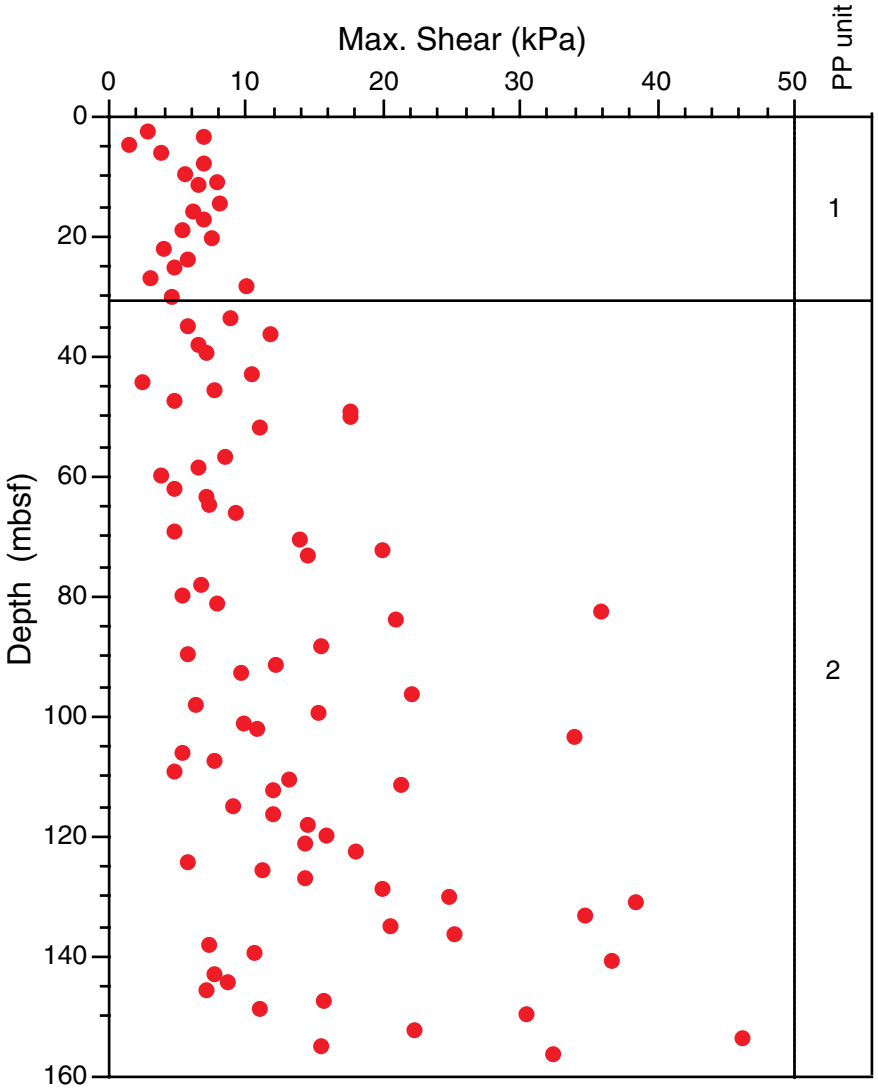

Figure F21. Thermal conductivity measurements with physical properties units (PP units) for Site 1131. MAD = moisture and density.

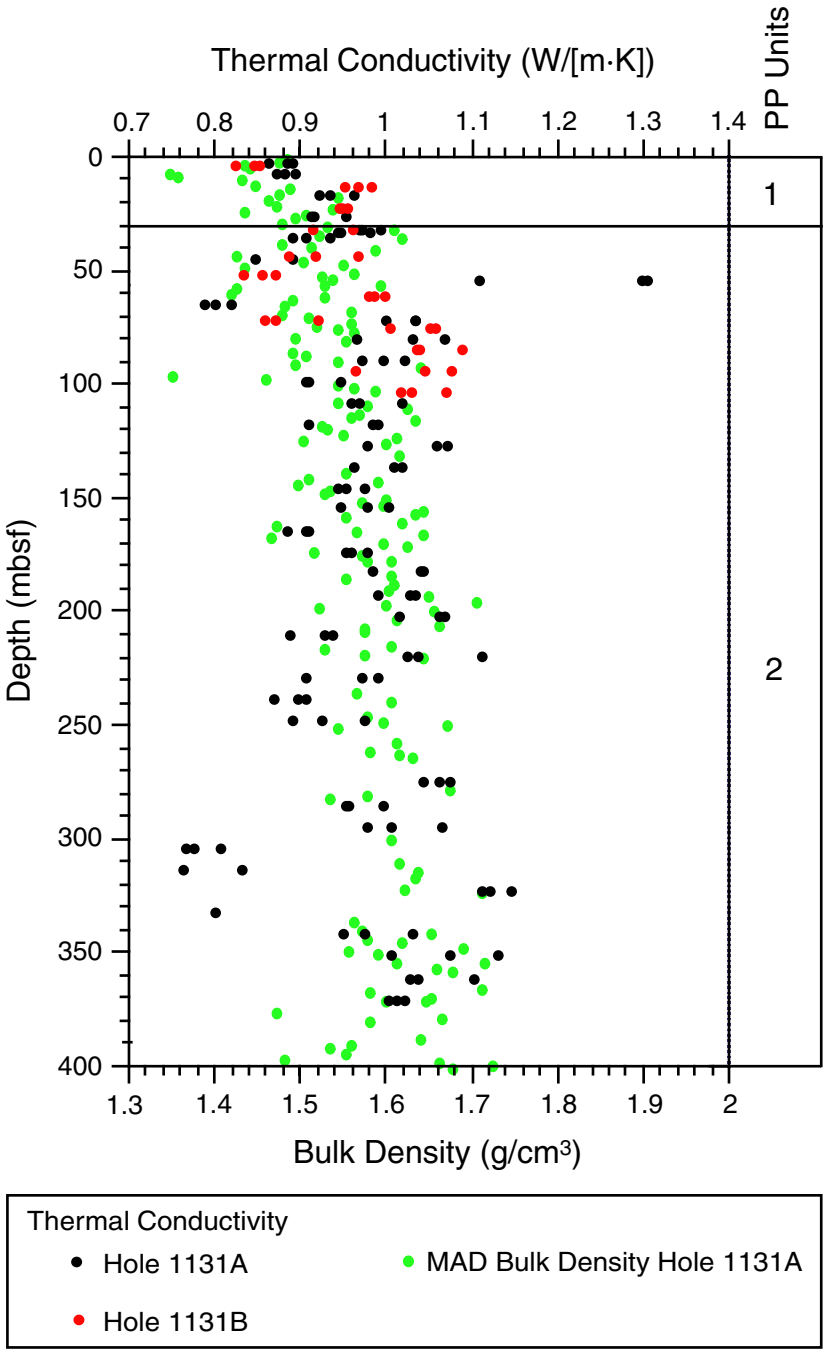

Figure F22. Variation of formation temperature with depth at Site 1131: Davis-Villinger temperature probe temperature (DVTP; red square), in situ Adara temperature (black diamond), and expendable bathythermograph mudline temperature (black square).

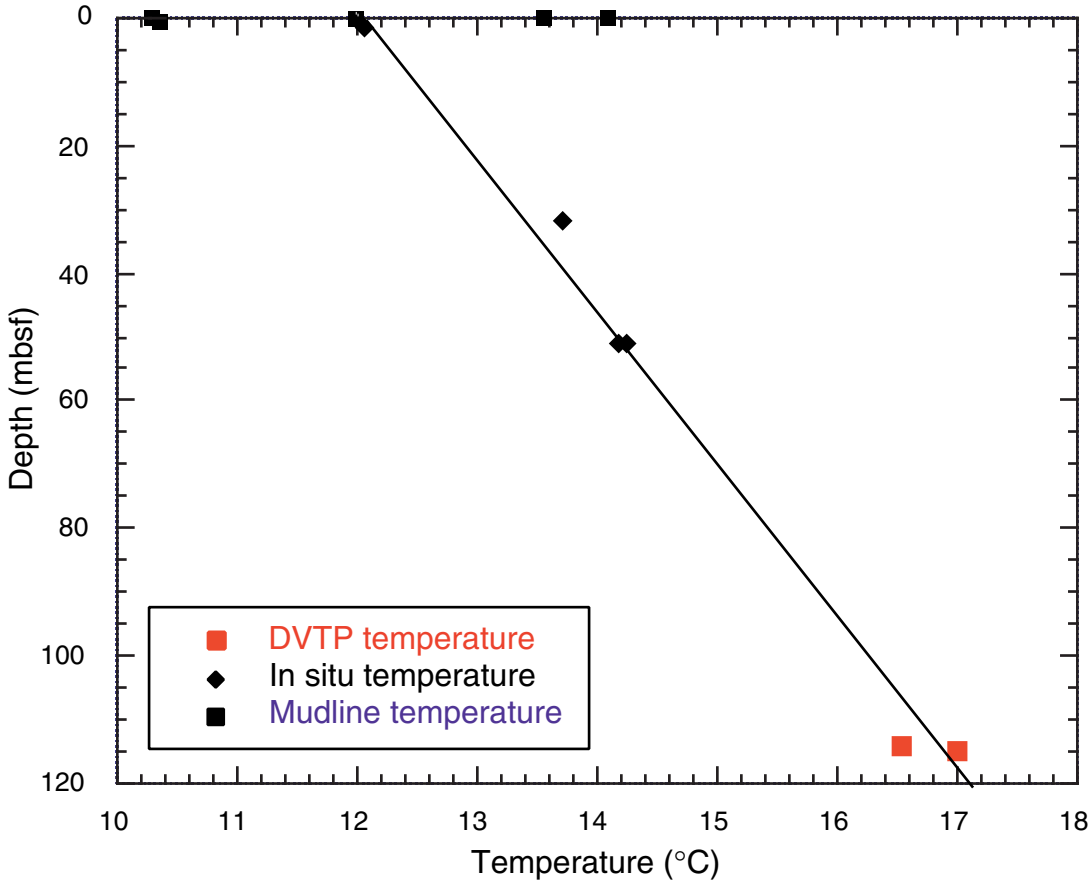

Figure F23. Summary of spectral gamma-ray logs from the hostile environment natural gamma-ray sonde plotted vs. depth (mbsf) for the open-hole logged interval. From left to right, columns are core recovery, total gamma radiation (HSGR) and computed (uranium free) gamma radiation (HCGR), uranium, thorium, potassium and caliper, logging units, lithostratigraphic units, and biostratigraphic ages.

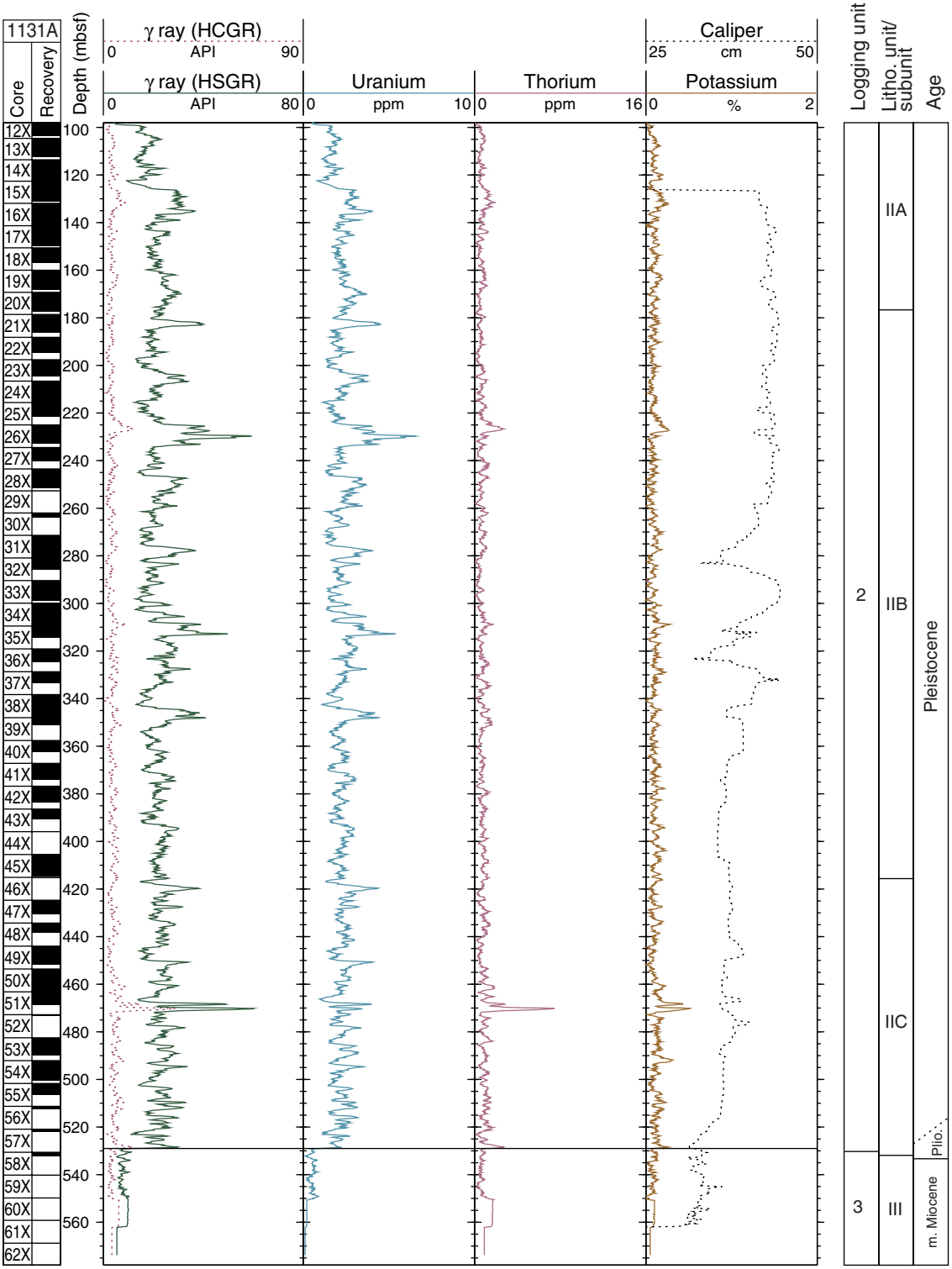

Figure F24. Summary of spectral gamma-ray logs from the hostile environment natural gamma-ray sonde plotted on an expanded depth scale (mbsf) to highlight variations in the interval logged through pipe. From left to right, columns are core recovery, total gamma radiation (HSGR) and computed (uranium free) gamma radiation (HCGR), uranium, thorium, potassium, logging units, lithostratigraphic units, and biostratigraphic ages.

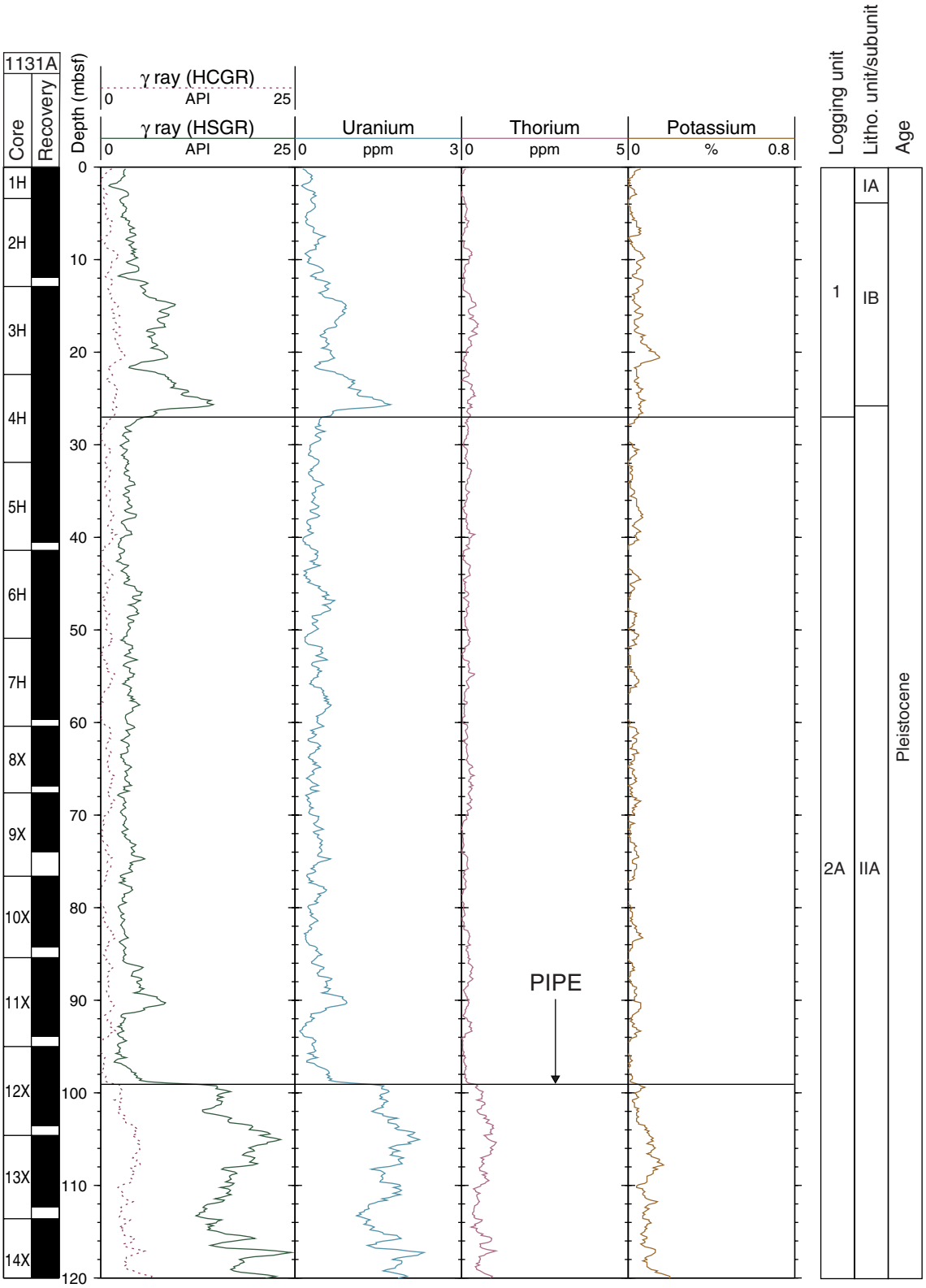

Figure F25. Summary of triple combination logging tool and sonic logs vs. depth (mbsf) for the open-hole logged interval. From left to right, columns are core recovery; total gamma radiation (HSGR) and caliper; porosity and density; photoelectric effect (PEF); shallow, medium and deep resistivity; sonic velocity; logging units; lithostratigraphic units, and biostratigraphic ages.

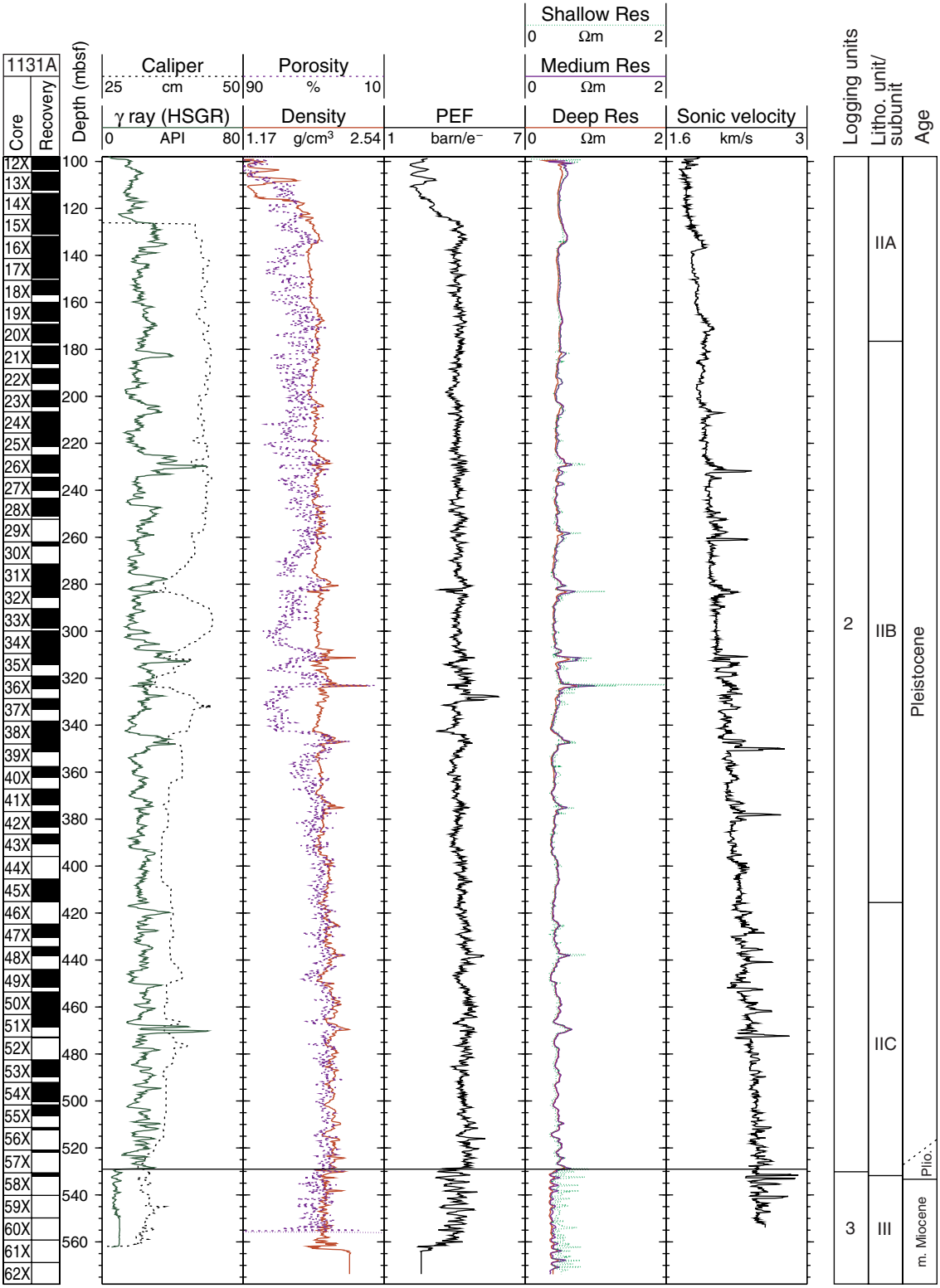

Figure F26. Formation MicroScanner (FMS) image showing a firmground (bright colored) within logging Unit 2. Elevated levels of gamma radiation (uranium) are associated with the firmground and the overlying 3-m interval.

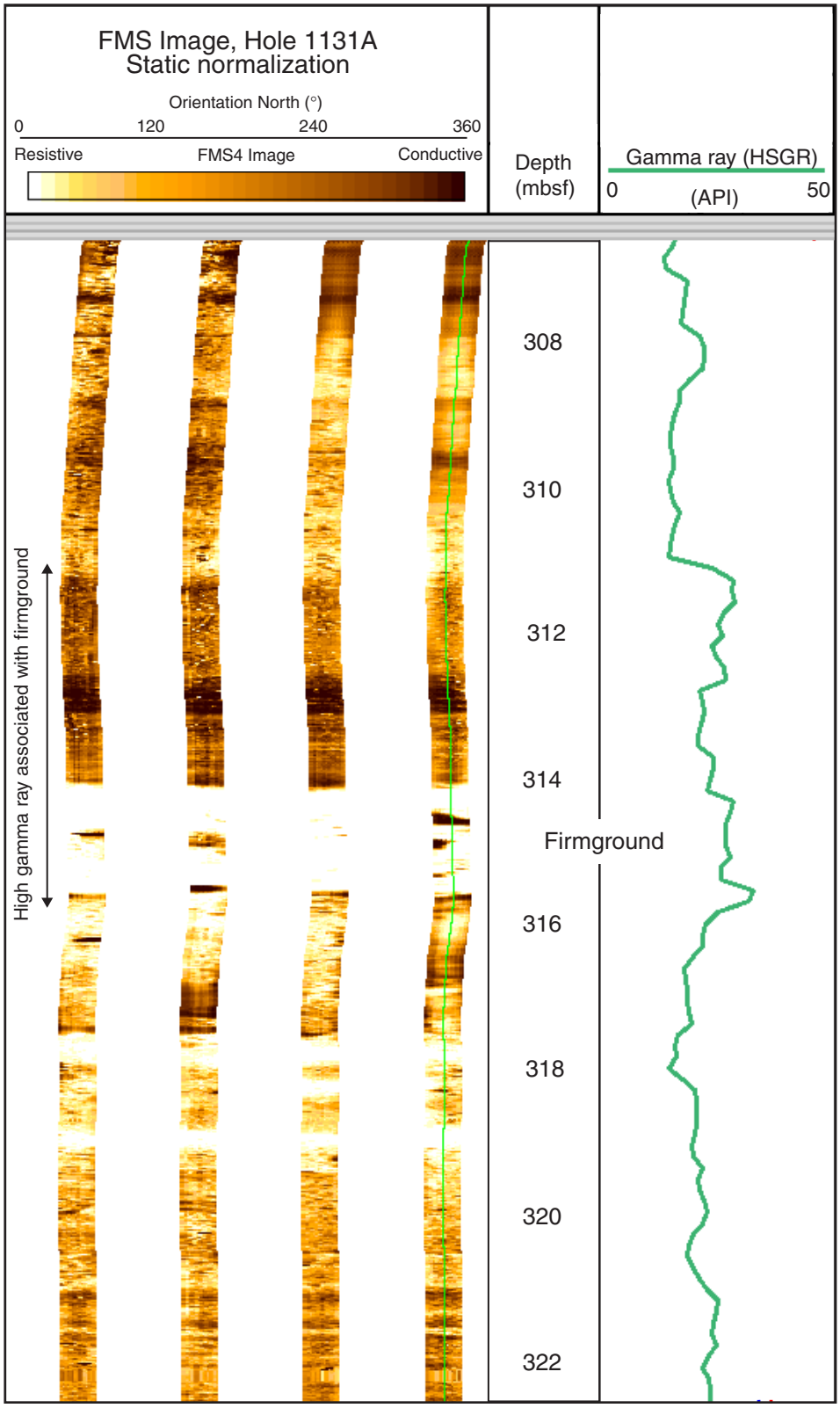

Figure F27. Formation MicroScanner (FMS) image showing the boundary (dotted line) between logging Units 2 and 3, coinciding with the boundary between lithostratigraphic Units II and III. Chert horizons in Unit 3 are imaged as resistive (bright) intervals, whereas the grainstone (Unit 3) and packstone (Unit 2) intervals are shown as more conductive (dark) intervals. The boundary between Units 2 and 3 is defined by the inflection in the gamma-ray curve immediately above 532 mbsf.

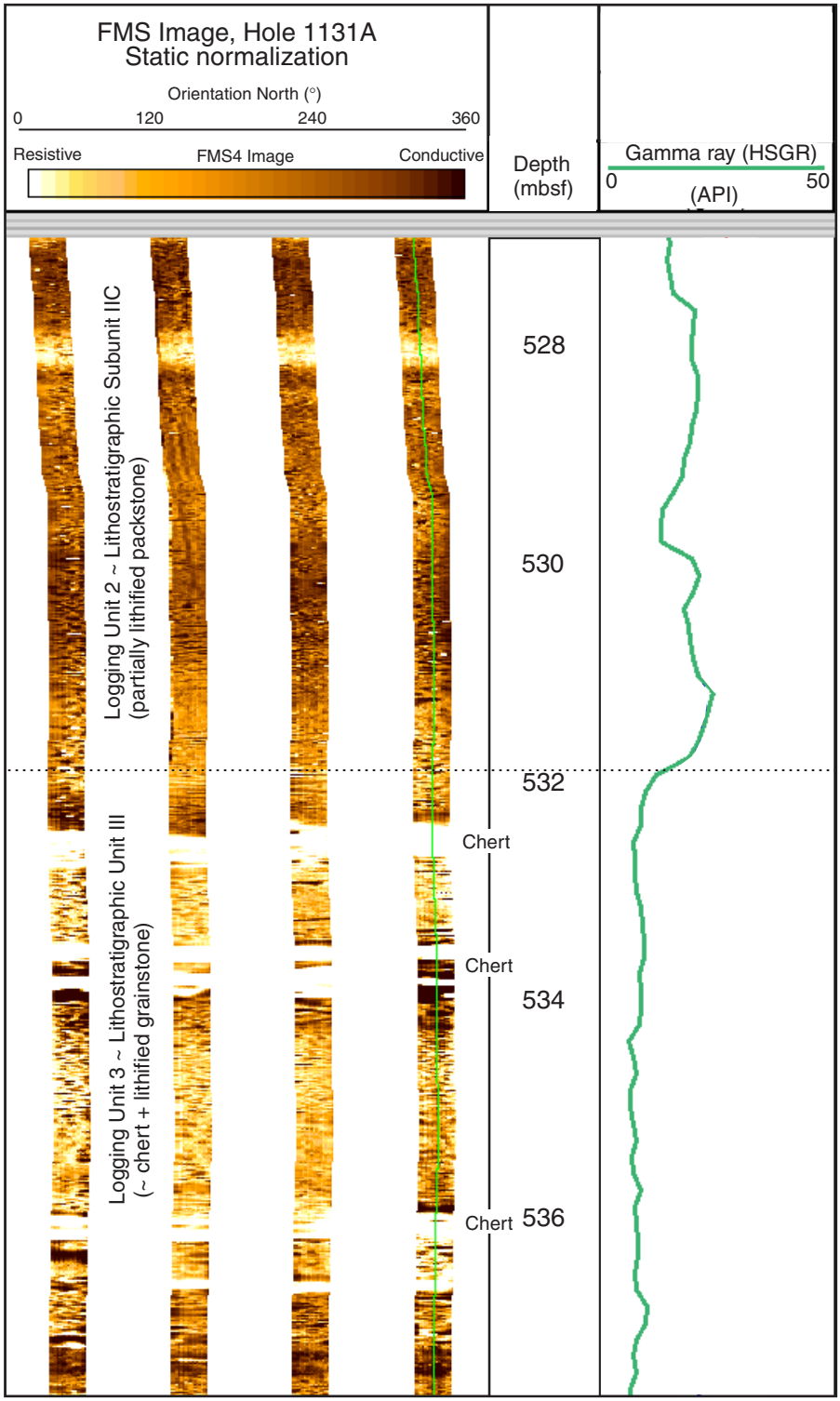

Figure F28. Downhole variations in borehole temperature measured by the Lamont-Doherty Earth Observatory high-resolution temperature/acceleration/pressure tool on the triple combination logging tool. Logging directions are indicated by arrows.

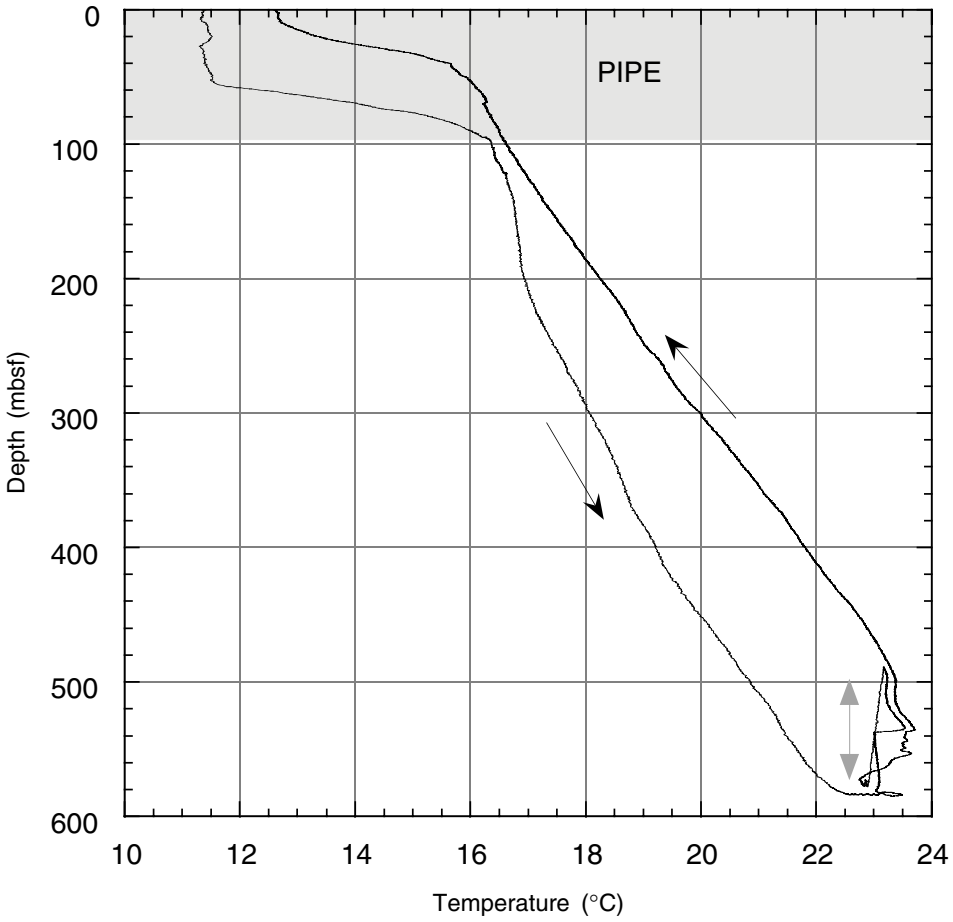

Table T1. Site 1131 coring summary. (See table note. Continued on next page.)

Hole 1131A

Latitude: –33.326090° (33°19.5654′S)
Longitude: 128.481200° (128°28.8720′E)
Seafloor (drill-pipe measurement from rig floor, mbrf): 345.1
Distance between rig floor and sea level (m): 11.7
Water depth (drill-pipe measurement from sea level, m): 333.4
Total depth (from rig floor, mbrf): 962.0
Penetration (mbsf): 616.9
Total number of cores: 66
Total length of cored section (m): 616.9
Total core recovered (m): 371.69
Core recovery (%): 60.3

Hole 1131B

Latitude: –33.325900° (33°19.5540′S)
Longitude: 128.480880° (128°28.8528′E)
Seafloor (drill-pipe measurement from rig floor, mbrf): 343.10
Distance between rig floor and sea level (m): 11.70
Water depth (drill-pipe measurement from sea level, m): 331.4
Total depth (from rig floor, mbrf): 448.9
Penetration (mbsf): 105.8
Total number of cores: 12
Total length of cored section (m): 105.8
Total core recovered (m): 95.34
Core recovery (%): 90.11

Core	Date (Nov 1998)	Time (UTC + 8 hr)	Depth (mbsf)	Length cored (m)	Length recovered (m)	Recovery (%)	Comment
180-1131A-							
1H	16	1615	0.00–3.40	3.4	3.39	99.7	
2H	16	1650	3.40–12.90	9.5	8.54	89.9	
3H	16	1730	12.90–22.40	9.5	9.56	100.6	Oriented
4H	16	1845	22.40–31.90	9.5	9.68	101.9	Oriented; H_2S
5H	16	1920	31.90–41.40	9.5	8.62	90.7	Oriented; H_2S
6H	16	2000	41.40–50.90	9.5	9.82	103.4	Oriented; H_2S
7H	16	2100	50.90–60.40	9.5	8.82	92.8	Oriented; H_2S
8X	16	2200	60.40–67.60	7.2	6.50	90.3	H_2S
9X	16	2235	67.60–76.60	9.0	6.46	71.8	H_2S
10X	16	2315	76.60–85.40	8.8	7.68	87.3	H_2S
11X	17	0015	85.40–95.00	9.6	8.60	89.6	H_2S
12X	17	0100	95.00–104.60	9.6	8.61	89.7	H_2S
13X	17	0145	104.60–113.60	9.0	7.72	85.8	H_2S
14X	17	0220	113.60–122.60	9.0	8.84	98.2	H_2S
15X	17	0315	122.60–131.90	9.3	8.60	92.5	H_2S
16X	17	0355	131.90–141.30	9.4	9.09	96.7	H_2S
17X	17	0435	141.30–150.60	9.3	8.46	91.0	H_2S
18X	17	0515	150.60–160.00	9.4	6.32	67.2	H_2S
19X	17	0600	160.00–169.30	9.3	8.32	89.5	H_2S
20X	17	0640	169.30–178.60	9.3	7.90	85.0	H_2S
21X	17	0725	178.60–188.20	9.6	7.73	80.5	H_2S
22X	17	0805	188.20–197.60	9.4	6.43	68.4	H_2S
23X	17	0845	197.60–206.60	9.0	6.76	75.1	H_2S
24X	17	0925	206.60–215.60	9.0	9.01	100.1	H_2S
25X	17	1005	215.60–225.00	9.4	5.88	62.6	H_2S
26X	17	1050	225.00–234.50	9.5	8.01	84.3	H_2S
27X	17	1130	234.50–243.50	9.0	5.90	65.6	H_2S
28X	17	1215	243.50–252.50	9.0	7.19	79.9	H_2S
29X	17	1255	252.50–262.00	9.5	0.02	0.2	H_2S
30X	17	1335	262.00–271.40	9.4	1.88	20.0	H_2S
31X	17	1420	271.40–280.90	9.5	9.19	96.7	H_2S
32X	17	1520	280.90–290.40	9.5	4.83	50.8	H_2S
33X	17	1600	290.40–299.90	9.5	8.40	88.4	H_2S
34X	17	1635	299.90–309.50	9.6	9.98	104.0	H_2S
35X	17	1720	309.50–319.10	9.6	4.68	48.8	H_2S
36X	17	1820	319.10–328.70	9.6	5.59	58.2	H_2S
37X	17	1900	328.70–338.30	9.6	4.67	48.7	H_2S
38X	17	1940	338.30–348.00	9.7	9.59	98.9	H_2S

Table T1 (continued).

Core	Date (Nov 1998)	Time (UTC + 8 hr)	Depth (mbsf)	Length cored (m)	Length recovered (m)	Recovery (%)	Comment
39X	17	2020	348.00–357.60	9.6	3.20	33.3	H_2S
40X	17	2140	357.60–367.20	9.6	4.63	48.2	H_2S
41X	17	2245	367.20–376.80	9.6	6.97	72.6	H_2S
42X	17	2340	376.80–386.40	9.6	6.86	71.5	H_2S
43X	18	0030	386.40–395.90	9.5	4.30	45.3	H_2S
44X	18	0210	395.90–405.50	9.6	0.21	2.2	H_2S
45X	18	0300	405.50–415.10	9.6	9.26	96.5	H_2S
46X	18	0350	415.10–424.70	9.6	0.23	2.4	H_2S
47X	18	0435	424.70–434.30	9.6	5.95	62.0	H_2S
48X	18	0525	434.30–444.00	9.7	4.25	43.8	H_2S
49X	18	0610	444.00–453.60	9.6	7.65	79.7	H_2S
50X	18	0700	453.60–463.20	9.6	9.95	103.7	H_2S
51X	18	0750	463.20–472.80	9.6	5.37	55.9	H_2S
52X	18	0840	472.80–482.50	9.7	0.59	6.1	H_2S
53X	18	0925	482.50–492.10	9.6	7.34	76.5	H_2S
54X	18	1015	492.10–501.70	9.6	8.40	87.5	H_2S
55X	18	1100	501.70–511.30	9.6	4.74	49.4	H_2S
56X	18	1155	511.30–520.90	9.6	1.23	12.8	H_2S
57X	18	1240	520.90–530.60	9.7	1.14	11.8	H_2S
58X	18	1320	530.60–540.20	9.6	1.47	15.3	H_2S
59X	18	1410	540.20–549.80	9.6	0.22	2.3	
60X	18	1510	549.80–559.20	9.4	0.02	0.2	
61X	18	1600	559.20–568.80	9.6	0.00	0.0	No recovery
62X	18	1730	568.80–578.40	9.6	0.02	0.2	
63X	18	1820	578.40–588.00	9.6	0.03	0.3	
64X	18	1935	588.00–597.60	9.6	0.04	0.4	
65X	18	2030	597.60–607.30	9.7	0.26	2.7	
66X	18	2225	607.30–616.90	9.6	0.09	0.9	
Totals:				616.9	371.69	60.3	
182-1131B-							
1H	20	0600	0.00–8.40	8.4	8.40	100.0	
2H	20	0635	8.40–17.90	9.5	9.27	97.6	
3H	20	0725	17.90–27.40	9.5	9.59	101.0	
4H	20	0755	27.40–36.90	9.5	9.41	99.1	
5H	20	0830	36.90–46.40	9.5	9.68	101.9	H_2S
6H	20	0945	46.40–55.90	9.5	5.47	57.6	H_2S
7H	20	1040	55.90–65.40	9.5	9.67	101.8	H_2S
8X	20	1200	65.40–69.10	3.7	3.97	107.3	H_2S
9X	20	1240	69.10–78.10	9.0	7.95	88.3	H_2S
10X	20	1320	78.10–87.40	9.3	7.55	81.2	H_2S
11X	20	1400	87.40–96.40	9.0	5.91	65.7	H_2S
12X	20	1445	96.40–105.80	9.4	8.47	90.1	H_2S
Totals:				105.8	95.34	90.1	

Note: UTC = Universal Time Coordinated.

Table T2. Datum levels used for the calculation of the Site 1131 sedimentation rate.

Datum type	Datum level	Age (Ma)	Midpoint (mbsf)	Stratigraphic error (m)	Fossil group	Upper sample		Lower sample	
						Core, section, interval (cm)	Depth (mbsf)	Core, section, interval (cm)	Depth (mbsf)
						182-1131A-		182-1131A-	
T	*Pseudoemiliania lacunosa*	0.45	136.10	4.90	1	15X-CC, 19-22	131.17	16X-CC, 16-19	140.96
T	*Reticulofenestra asanoi*	0.88	251.60	0.92	1	28X-CC, 12-15	250.66	29X-CC, 0-2	252.50
	Brunhes/Matuyama	0.78	295.15	4.75					
	Top of Jaramillo	0.99	333.50	4.80					
T	*Calcidiscus macintyrei*	1.67	445.10	6.55	1	48X-CC, 29-32	438.47	49X-CC, 33-36	451.62
B	*Globorotalia truncatulinoides*	2	517.26	4.76	4	56X-CC, 28-31	512.50	57X-CC, 47-50	522.01
B	*Globorotalia crassaformis*	4.5	527.03	5.02	4	57X-CC, 47-50	522.01	58X-CC, 0-3	532.04
T	*Globoquadrina dehiscens*	5.8	527.05	5.02	4	57X-CC, 47-50	522.01	58X-CC, 0-3	532.04
B	*C. macintyrei*	12.3	545.09	4.71	1	59X-CC, 19-22	540.39	60X-CC, 0-2	549.80
T	*Sphenolithus heteromorphus*	13.6	573.62	4.81	1	62X-CC, 0-2	568.80	63X-CC, 0-3	578.40

Notes: T = top of taxon stratigraphic range, B = bottom of taxon stratigraphic range. Midpoint = the middle depth between the sample where the taxon occurs and the adjacent sample where it does not occur. Stratigraphic error = one-half the distance between these two samples. Datum level code = the number assigned to the datum level on Figure **F5,** p. 33. Fossil groups: 1 = calcareous nannofossils, 4 = planktonic foraminifers.

Table T3. Core and section depths in mcd and mbsf, Site 1131. (See table notes. Continued on next four pages.)

Leg	Site	Hole	Core	Type	Section	Depth (mbsf)	Offset (m)	Depth (mcd)
182	1131	A	1	H	1	0.00	0.16	0.16
182	1131	A	1	H	2	1.50	0.16	1.66
182	1131	A	1	H	3	2.60	0.16	2.76
182	1131	A	2	H	1	3.40	2.40	5.80
182	1131	A	2	H	2	4.90	2.40	7.30
182	1131	A	2	H	3	6.40	2.40	8.80
182	1131	A	2	H	4	7.90	2.40	10.30
182	1131	A	2	H	5	9.45	2.40	11.85
182	1131	A	2	H	6	10.92	2.40	13.32
182	1131	A	3	H	1	12.90	1.91	14.81
182	1131	A	3	H	2	14.40	1.91	16.31
182	1131	A	3	H	3	15.90	1.91	17.81
182	1131	A	3	H	4	17.40	1.91	19.31
182	1131	A	3	H	5	18.90	1.91	20.81
182	1131	A	3	H	6	20.40	1.91	22.31
182	1131	A	3	H	7	21.90	1.91	23.81
182	1131	A	4	H	1	22.40	3.03	25.43
182	1131	A	4	H	2	23.90	3.03	26.93
182	1131	A	4	H	3	25.40	3.03	28.43
182	1131	A	4	H	4	26.90	3.03	29.93
182	1131	A	4	H	5	28.40	3.03	31.43
182	1131	A	4	H	6	29.90	3.03	32.93
182	1131	A	4	H	7	31.40	3.03	34.43
182	1131	A	5	H	1	31.90	2.96	34.86
182	1131	A	5	H	2	33.40	2.96	36.36
182	1131	A	5	H	3	34.90	2.96	37.86
182	1131	A	5	H	4	36.40	2.96	39.36
182	1131	A	5	H	5	37.90	2.96	40.86
182	1131	A	5	H	6	39.40	2.96	42.36
182	1131	A	6	H	1	41.40	2.96	44.36
182	1131	A	6	H	2	42.90	2.96	45.86
182	1131	A	6	H	3	44.40	2.96	47.36
182	1131	A	6	H	4	45.90	2.96	48.86
182	1131	A	6	H	5	47.40	2.96	50.36
182	1131	A	6	H	6	48.90	2.96	51.86
182	1131	A	6	H	7	50.40	2.96	53.36
182	1131	A	7	H	1	50.90	2.96	53.86
182	1131	A	7	H	2	52.40	2.96	55.36
182	1131	A	7	H	3	53.90	2.96	56.86
182	1131	A	7	H	4	55.40	2.96	58.36
182	1131	A	7	H	5	56.90	2.96	59.86
182	1131	A	7	H	6	58.40	2.96	61.36
182	1131	A	8	X	1	60.40	2.24	62.64
182	1131	A	8	X	2	61.90	2.24	64.14
182	1131	A	8	X	3	63.40	2.24	65.64
182	1131	A	8	X	4	64.90	2.24	67.14
182	1131	A	8	X	5	65.90	2.24	68.14
182	1131	A	9	X	1	67.60	3.20	70.80
182	1131	A	9	X	2	69.10	3.20	72.30
182	1131	A	9	X	3	70.60	3.20	73.80
182	1131	A	9	X	4	72.10	3.20	75.30
182	1131	A	9	X	5	73.10	3.20	76.30
182	1131	A	10	X	1	76.60	0.58	77.18
182	1131	A	10	X	2	78.10	0.58	78.68
182	1131	A	10	X	3	79.60	0.58	80.18
182	1131	A	10	X	4	81.10	0.58	81.68
182	1131	A	10	X	5	82.60	0.58	83.18
182	1131	A	11	X	1	85.40	–0.51	84.89
182	1131	A	11	X	2	86.90	–0.51	86.39
182	1131	A	11	X	3	88.40	–0.51	87.89
182	1131	A	11	X	4	89.90	–0.51	89.39
182	1131	A	11	X	5	91.40	–0.51	90.89
182	1131	A	11	X	6	92.90	–0.51	92.39
182	1131	A	12	X	1	95.00	–1.01	93.99
182	1131	A	12	X	2	96.50	–1.01	95.49
182	1131	A	12	X	3	98.00	–1.01	96.99
182	1131	A	12	X	4	99.50	–1.01	98.49
182	1131	A	12	X	5	101.00	–1.01	99.99

Table T3 (continued).

Leg	Site	Hole	Core	Type	Section	Depth (mbsf)	Offset (m)	Depth (mcd)
182	1131	A	12	X	6	102.50	–1.01	101.49
182	1131	A	13	X	1	104.60	–1.01	103.59
182	1131	A	13	X	2	106.10	–1.01	105.09
182	1131	A	13	X	3	107.60	–1.01	106.59
182	1131	A	13	X	4	109.10	–1.01	108.09
182	1131	A	13	X	5	110.60	–1.01	109.59
182	1131	A	13	X	6	111.60	–1.01	110.59
182	1131	A	14	X	1	113.60	–1.01	112.59
182	1131	A	14	X	2	115.10	–1.01	114.09
182	1131	A	14	X	3	116.60	–1.01	115.59
182	1131	A	14	X	4	118.10	–1.01	117.09
182	1131	A	14	X	5	119.60	–1.01	118.59
182	1131	A	14	X	6	121.10	–1.01	120.09
182	1131	A	15	X	1	122.60	–1.01	121.59
182	1131	A	15	X	2	124.10	–1.01	123.09
182	1131	A	15	X	3	125.60	–1.01	124.59
182	1131	A	15	X	4	127.10	–1.01	126.09
182	1131	A	15	X	5	128.60	–1.01	127.59
182	1131	A	15	X	6	130.10	–1.01	129.09
182	1131	A	16	X	1	131.90	–1.01	130.89
182	1131	A	16	X	2	133.40	–1.01	132.39
182	1131	A	16	X	3	134.90	–1.01	133.89
182	1131	A	16	X	4	136.40	–1.01	135.39
182	1131	A	16	X	5	137.90	–1.01	136.89
182	1131	A	16	X	6	139.40	–1.01	138.39
182	1131	A	17	X	1	141.30	–1.01	140.29
182	1131	A	17	X	2	142.80	–1.01	141.79
182	1131	A	17	X	3	144.30	–1.01	143.29
182	1131	A	17	X	4	145.80	–1.01	144.79
182	1131	A	17	X	5	147.30	–1.01	146.29
182	1131	A	17	X	6	148.80	–1.01	147.79
182	1131	A	18	X	1	150.60	–1.01	149.59
182	1131	A	18	X	2	152.10	–1.01	151.09
182	1131	A	18	X	3	153.60	–1.01	152.59
182	1131	A	18	X	4	155.10	–1.01	154.09
182	1131	A	18	X	5	156.10	–1.01	155.09
182	1131	A	19	X	1	160.00	–1.01	158.99
182	1131	A	19	X	2	161.50	–1.01	160.49
182	1131	A	19	X	3	163.00	–1.01	161.99
182	1131	A	19	X	4	164.50	–1.01	163.49
182	1131	A	19	X	5	166.00	–1.01	164.99
182	1131	A	19	X	6	167.50	–1.01	166.49
182	1131	A	20	X	1	169.30	–1.01	168.29
182	1131	A	20	X	2	170.80	–1.01	169.79
182	1131	A	20	X	3	172.30	–1.01	171.29
182	1131	A	20	X	4	173.80	–1.01	172.79
182	1131	A	20	X	5	175.30	–1.01	174.29
182	1131	A	21	X	1	178.60	–1.01	177.59
182	1131	A	21	X	2	180.10	–1.01	179.09
182	1131	A	21	X	3	181.60	–1.01	180.59
182	1131	A	21	X	4	183.10	–1.01	182.09
182	1131	A	21	X	5	184.60	–1.01	183.59
182	1131	A	22	X	1	188.20	–1.01	187.19
182	1131	A	22	X	2	189.70	–1.01	188.69
182	1131	A	22	X	3	191.20	–1.01	190.19
182	1131	A	22	X	4	192.70	–1.01	191.69
182	1131	A	23	X	1	197.60	–1.01	196.59
182	1131	A	23	X	2	199.10	–1.01	198.09
182	1131	A	23	X	3	200.60	–1.01	199.59
182	1131	A	23	X	4	202.10	–1.01	201.09
182	1131	A	23	X	5	203.60	–1.01	202.59
182	1131	A	24	X	1	206.60	–1.01	205.59
182	1131	A	24	X	2	208.10	–1.01	207.09
182	1131	A	24	X	3	209.60	–1.01	208.59
182	1131	A	24	X	4	211.10	–1.01	210.09
182	1131	A	24	X	5	212.60	–1.01	211.59
182	1131	A	24	X	6	214.10	–1.01	213.09
182	1131	A	25	X	1	215.60	–1.01	214.59
182	1131	A	25	X	2	217.10	–1.01	216.09

Table T3 (continued).

Leg	Site	Hole	Core	Type	Section	Depth (mbsf)	Offset (m)	Depth (mcd)
182	1131	A	25	X	3	218.60	–1.01	217.59
182	1131	A	25	X	4	220.10	–1.01	219.09
182	1131	A	26	X	1	225.00	–1.01	223.99
182	1131	A	26	X	2	226.50	–1.01	225.49
182	1131	A	26	X	3	228.00	–1.01	226.99
182	1131	A	26	X	4	229.50	–1.01	228.49
182	1131	A	26	X	5	231.00	–1.01	229.99
182	1131	A	27	X	1	234.50	–1.01	233.49
182	1131	A	27	X	2	236.00	–1.01	234.99
182	1131	A	27	X	3	237.50	–1.01	236.49
182	1131	A	27	X	4	239.00	–1.01	237.99
182	1131	A	28	X	1	243.50	–1.01	242.49
182	1131	A	28	X	2	245.00	–1.01	243.99
182	1131	A	28	X	3	246.50	–1.01	245.49
182	1131	A	28	X	4	248.00	–1.01	246.99
182	1131	A	28	X	5	249.50	–1.01	248.49
182	1131	A	30	X	1	262.00	–1.01	260.99
182	1131	A	31	X	1	271.40	–1.01	270.39
182	1131	A	31	X	2	272.90	–1.01	271.89
182	1131	A	31	X	3	274.40	–1.01	273.39
182	1131	A	31	X	4	275.90	–1.01	274.89
182	1131	A	31	X	5	277.40	–1.01	276.39
182	1131	A	31	X	6	278.90	–1.01	277.89
182	1131	A	32	X	1	280.90	–1.01	279.89
182	1131	A	32	X	2	282.40	–1.01	281.39
182	1131	A	32	X	3	283.90	–1.01	282.89
182	1131	A	32	X	4	284.90	–1.01	283.89
182	1131	A	33	X	1	290.40	–1.01	289.39
182	1131	A	33	X	2	291.90	–1.01	290.89
182	1131	A	33	X	3	293.40	–1.01	292.39
182	1131	A	33	X	4	294.90	–1.01	293.89
182	1131	A	33	X	5	296.40	–1.01	295.39
182	1131	A	33	X	6	297.90	–1.01	296.89
182	1131	A	34	X	1	299.90	–1.01	298.89
182	1131	A	34	X	2	301.40	–1.01	300.39
182	1131	A	34	X	3	302.90	–1.01	301.89
182	1131	A	34	X	4	304.40	–1.01	303.39
182	1131	A	34	X	5	305.90	–1.01	304.89
182	1131	A	34	X	6	307.40	–1.01	306.39
182	1131	A	34	X	7	308.90	–1.01	307.89
182	1131	A	35	X	1	309.50	–1.01	308.49
182	1131	A	35	X	2	311.00	–1.01	309.99
182	1131	A	35	X	3	312.50	–1.01	311.49
182	1131	A	36	X	1	319.10	–1.01	318.09
182	1131	A	36	X	2	320.60	–1.01	319.59
182	1131	A	36	X	3	322.10	–1.01	321.09
182	1131	A	36	X	4	323.60	–1.01	322.59
182	1131	A	37	X	1	328.70	–1.01	327.69
182	1131	A	37	X	2	330.20	–1.01	329.19
182	1131	A	37	X	3	331.70	–1.01	330.69
182	1131	A	38	X	1	338.30	–1.01	337.29
182	1131	A	38	X	2	339.80	–1.01	338.79
182	1131	A	38	X	3	341.30	–1.01	340.29
182	1131	A	38	X	4	342.80	–1.01	341.79
182	1131	A	38	X	5	344.30	–1.01	343.29
182	1131	A	38	X	6	345.80	–1.01	344.79
182	1131	A	38	X	7	346.80	–1.01	345.79
182	1131	A	39	X	2	349.50	–1.01	348.49
182	1131	A	40	X	1	357.60	–1.01	356.59
182	1131	A	40	X	2	359.10	–1.01	358.09
182	1131	A	40	X	3	360.60	–1.01	359.59
182	1131	A	41	X	1	367.20	–1.01	366.19
182	1131	A	41	X	2	368.70	–1.01	367.69
182	1131	A	41	X	3	370.20	–1.01	369.19
182	1131	A	41	X	4	371.70	–1.01	370.69
182	1131	A	41	X	5	373.20	–1.01	372.19
182	1131	A	42	X	2	378.30	–1.01	377.29
182	1131	A	42	X	3	379.80	–1.01	378.79
182	1131	A	42	X	4	381.30	–1.01	380.29

Table T3 (continued).

Leg	Site	Hole	Core	Type	Section	Depth (mbsf)	Offset (m)	Depth (mcd)
182	1131	A	42	X	5	382.80	–1.01	381.79
182	1131	A	43	X	2	387.90	–1.01	386.89
182	1131	A	43	X	3	389.40	–1.01	388.39
182	1131	A	45	X	1	405.50	–1.01	404.49
182	1131	A	45	X	2	407.00	–1.01	405.99
182	1131	A	45	X	3	408.50	–1.01	407.49
182	1131	A	45	X	4	410.00	–1.01	408.99
182	1131	A	45	X	5	411.50	–1.01	410.49
182	1131	A	45	X	6	413.00	–1.01	411.99
182	1131	A	45	X	7	414.00	–1.01	412.99
182	1131	A	47	X	2	426.20	–1.01	425.19
182	1131	A	47	X	3	427.70	–1.01	426.69
182	1131	A	47	X	4	429.20	–1.01	428.19
182	1131	A	48	X	2	435.80	–1.01	434.79
182	1131	A	48	X	3	437.30	–1.01	436.29
182	1131	A	49	X	1	444.00	–1.01	442.99
182	1131	A	49	X	2	445.50	–1.01	444.49
182	1131	A	49	X	3	447.00	–1.01	445.99
182	1131	A	49	X	4	448.50	–1.01	447.49
182	1131	A	49	X	5	450.00	–1.01	448.99
182	1131	A	50	X	1	453.60	–1.01	452.59
182	1131	A	50	X	2	455.10	–1.01	454.09
182	1131	A	50	X	3	456.60	–1.01	455.59
182	1131	A	50	X	4	458.10	–1.01	457.09
182	1131	A	50	X	5	459.60	–1.01	458.59
182	1131	A	50	X	6	461.10	–1.01	460.09
182	1131	A	50	X	7	462.60	–1.01	461.59
182	1131	A	51	X	1	463.20	–1.01	462.19
182	1131	A	51	X	2	464.70	–1.01	463.69
182	1131	A	51	X	3	466.20	–1.01	465.19
182	1131	A	51	X	4	467.70	–1.01	466.69
182	1131	A	53	X	1	482.50	–1.01	481.49
182	1131	A	53	X	2	484.00	–1.01	482.99
182	1131	A	53	X	3	485.50	–1.01	484.49
182	1131	A	53	X	4	487.00	–1.01	485.99
182	1131	A	53	X	5	488.50	–1.01	487.49
182	1131	A	54	X	1	492.10	–1.01	491.09
182	1131	A	54	X	2	493.60	–1.01	492.59
182	1131	A	54	X	3	495.10	–1.01	494.09
182	1131	A	54	X	4	496.60	–1.01	495.59
182	1131	A	54	X	5	498.10	–1.01	497.09
182	1131	A	54	X	6	499.60	–1.01	498.59
182	1131	A	55	X	1	501.70	–1.01	500.69
182	1131	A	55	X	2	503.20	–1.01	502.19
182	1131	A	55	X	3	504.70	–1.01	503.69
182	1131	A	56	X	1	511.30	–1.01	510.29
182	1131	A	57	X	1	520.90	–1.01	519.89
182	1131	A	58	X	1	530.60	–1.01	529.59
182	1131	B	1	H	1	0.00	0.00	0.00
182	1131	B	1	H	2	1.50	0.00	1.50
182	1131	B	1	H	3	3.00	0.00	3.00
182	1131	B	1	H	4	4.50	0.00	4.50
182	1131	B	1	H	5	6.00	0.00	6.00
182	1131	B	1	H	6	7.50	0.00	7.50
182	1131	B	2	H	1	8.40	1.22	9.62
182	1131	B	2	H	2	9.90	1.22	11.12
182	1131	B	2	H	3	11.40	1.22	12.62
182	1131	B	2	H	4	12.90	1.22	14.12
182	1131	B	2	H	5	14.40	1.22	15.62
182	1131	B	2	H	6	15.90	1.22	17.12
182	1131	B	2	H	7	17.10	1.22	18.32
182	1131	B	3	H	1	17.90	1.37	19.27
182	1131	B	3	H	2	19.40	1.37	20.77
182	1131	B	3	H	3	20.90	1.37	22.27
182	1131	B	3	H	4	22.40	1.37	23.77
182	1131	B	3	H	5	23.90	1.37	25.27
182	1131	B	3	H	6	25.40	1.37	26.77
182	1131	B	3	H	7	26.90	1.37	28.27
182	1131	B	4	H	1	27.40	0.24	27.64

Table T3 (continued).

Leg	Site	Hole	Core	Type	Section	Depth (mbsf)	Offset (m)	Depth (mcd)
182	1131	B	4	H	2	28.90	0.24	29.14
182	1131	B	4	H	3	30.40	0.24	30.64
182	1131	B	4	H	4	31.90	0.24	32.14
182	1131	B	4	H	5	33.40	0.24	33.64
182	1131	B	4	H	6	34.90	0.24	35.14
182	1131	B	5	H	1	36.90	0.34	37.24
182	1131	B	5	H	2	38.40	0.34	38.74
182	1131	B	5	H	3	39.90	0.34	40.24
182	1131	B	5	H	4	41.40	0.34	41.74
182	1131	B	5	H	5	42.90	0.34	43.24
182	1131	B	5	H	6	44.40	0.34	44.74
182	1131	B	5	H	7	45.90	0.34	46.24
182	1131	B	6	H	1	46.40	1.44	47.84
182	1131	B	6	H	2	47.90	1.44	49.34
182	1131	B	6	H	3	49.40	1.44	50.84
182	1131	B	6	H	4	50.90	1.44	52.34
182	1131	B	7	H	1	55.90	2.00	57.90
182	1131	B	7	H	2	57.40	2.00	59.40
182	1131	B	7	H	3	58.90	2.00	60.90
182	1131	B	7	H	4	60.40	2.00	62.40
182	1131	B	7	H	5	61.90	2.00	63.90
182	1131	B	7	H	6	63.40	2.00	65.40
182	1131	B	7	H	7	64.90	2.00	66.90
182	1131	B	8	X	1	65.40	2.48	67.88
182	1131	B	8	X	2	66.90	2.48	69.38
182	1131	B	8	X	3	68.40	2.48	70.88
182	1131	B	9	X	1	69.10	2.24	71.34
182	1131	B	9	X	2	70.60	2.24	72.84
182	1131	B	9	X	3	72.10	2.24	74.34
182	1131	B	9	X	4	73.60	2.24	75.84
182	1131	B	9	X	5	75.10	2.24	77.34
182	1131	B	10	X	1	78.10	0.79	78.89
182	1131	B	10	X	2	79.60	0.79	80.39
182	1131	B	10	X	3	81.10	0.79	81.89
182	1131	B	10	X	4	82.60	0.79	83.39
182	1131	B	10	X	5	84.10	0.79	84.89
182	1131	B	11	X	1	87.40	–0.11	87.29
182	1131	B	11	X	2	88.90	–0.11	88.79
182	1131	B	11	X	3	90.40	–0.11	90.29
182	1131	B	11	X	4	91.90	–0.11	91.79
182	1131	B	12	X	1	96.40	–0.57	95.83
182	1131	B	12	X	2	97.90	–0.57	97.33
182	1131	B	12	X	3	99.40	–0.57	98.83
182	1131	B	12	X	4	100.90	–0.57	100.33
182	1131	B	12	X	5	102.40	–0.57	101.83
182	1131	B	12	X	6	103.90	–0.57	103.33

Notes: Depths measured at top of each section. This table is also available in **ASCII format.**

Table T4. Splice tie points, Site 1131.

Site	Hole	Core	Type	Section	Interval (cm)	Depth (mbsf)	Depth (mcd)		Site	Hole	Core	Type	Section	Interval (cm)	Depth (mbsf)	Depth (mcd)
1131	B	1	H	6	43	7.93	7.93	Tie to	1131	A	2	H	2	57	5.53	7.93
1131	A	2	H	3	123	7.63	10.03	Tie to	1131	B	2	H	1	40	8.81	10.03
1131	B	2	H	6	11	16.01	17.23	Tie to	1131	A	3	H	2	84.5	15.32	17.23
1131	A	3	H	6	40	20.80	22.71	Tie to	1131	B	3	H	3	44	21.34	22.71
1131	B	3	H	6	27	25.67	27.04	Tie to	1131	A	4	H	2	11	24.01	27.04
1131	A	4	H	4	48	27.38	30.41	Tie to	1131	B	4	H	2	126.5	30.17	30.41
1131	B	4	H	6	60	35.50	35.74	Tie to	1131	A	5	H	1	88	32.78	35.74
1131	A	5	H	5	24	38.14	41.10	Tie to	1131	B	5	H	3	85	40.76	41.10
1131	B	5	H	7	52	46.42	46.76	Append to	1131	B	6	H	1	0	46.40	47.84
1131	B	6	H	4	88	51.78	53.22	Append to	1131	A	7	H	1	0	50.90	53.86
1131	A	7	H	5	128	58.18	61.14	Tie to	1131	B	7	H	3	24	59.14	61.14
1131	B	7	H	6	91	64.31	66.31	Tie to	1131	A	8	X	3	63	64.07	66.31
1131	A	8	X	5	80	66.70	68.94	Append to	1131	A	9	X	1	0	67.60	70.80
1131	A	9	X	5	64	73.74	76.94	Append to	1131	A	10	X	1	0	76.60	77.18
1131	A	10	X	3	107	80.67	81.25	Tie to	1131	B	10	X	2	83.5	80.46	81.25
1131	B	10	X	5	104	85.14	85.93	Tie to	1131	A	11	X	1	104	86.44	85.93
1131	A	11	X	6	88	93.78	93.27									

Note: This table is also available in **ASCII format.**

Table T5. Composition of vacutainer gases, Hole 1131A.

Core, section	Depth (mbsf)	CO_2 (ppmv)	H_2S (ppmv)	C_1 (ppmv)	C_2 (ppmv)	C_3 (ppmv)	*i*-C_4 (ppmv)	*n*-C_4 (ppmv)	*i*-C_5 (ppmv)	*n*-C_5 (ppmv)	C_1/C_2
182-1131A-											
38X-5	344.80	784,949	125,568	81,267	286	51	17	11	14		284
40X-2	359.60	711,194	156,608	71,225	275	52	21		15	36	259
42X-4	381.80		118,177	61,093	247	49	18	9	14	26	247
43X-2	388.40	682,464	107,651	77,429	342	75	32	19	26	13	227

Note: Blank = not detected.

Table T6. Composition of headspace gas in sediment, Hole 1131A.

Core, section	Depth (mbsf)	CO_2 (ppmv)	H_2S (ppmv)	C_1 (ppmv)	C_2 (ppmv)	C_3 (ppmv)	C_4 (ppmv)	*i*-C_5 (ppmv)	*n*-C_5 (ppmv)	C_1/C_2
182-1131A-										
1H-2	1.50	NA	NA	2			NA	NA	NA	
2H-4	7.90	NA	NA	2			NA	NA	NA	
3H-4	17.40	NA	NA	16			NA	NA	NA	
4H-4	26.90	11,046	86	32	1					40
5H-4	36.40	13,606	3,435	128	3					49
6H-4	45.90	23,433	7,938	134	2					70
7H-4	55.40	21,389	8,681	243	2					128
8X-4	64.90	56,993	26,818	1,526	8					198
9X-4	72.10	71,682	35,116	3,263	13	3				257
10X-4	81.10	55,610	18,965	3,111	10	3				302
11X-4	89.90	72,572	27,796	4,752	13	4				363
12X-4	99.50	43,642	18,020	2,104	6	2				383
13X-4	109.10	69,216	28,673	4,778	11	3				442
14X-4	118.10	64,789	28,919	5,007	11	3				447
15X-4	127.10	78,977	41,216	7,677	17	5				449
16X-4	136.40	175,069	59,681	9,873	24	8				418
18X-3	153.60	66,663	12,604	5,877	13	4				456
19X-4	164.50	90,341	17,743	7,572	17	6				435
20X-4	173.80	89,231	10,887	6,358	14	5				448
21X-4	183.10	60,627	8,643	4,622	10	3				462
22X-4	192.70	97,873	16,900	8,631	20	6				438
23X-4	202.10	116,682	18,566	11,458	25	7				451
24X-4	211.10	115,646	17,633	10,329	24	7				423
25X-4	220.10	86,000	11,627	6,953	15	5				476
26X-4	229.50	131,571	3,734	7,368	19	7				388
27X-4	239.00	99,640	9,270	4,639	12	5				390
28X-4	248.00	106,718	14,618	6,634	15	5				434
30X-2	263.50	184,781	13,566	9,253	23	7				411
31X-4	275.90	135,094	19,225	8,243	21	6				387
32X-4	284.90	133,769	1,338	7,043	22	9				319
33X-4	294.90	141,318	35,332	7,005	19	6				363
34X-4	304.40	170,805	21,456	5,758	17	6				349
35X-3	312.50	162,103	26,055	5,285	17	7				315
36X-3	322.10	140,940	23,546	3,747	13	6				295
37X-3	331.70	97,752	9,583	2,171	8	4				271
38X-5	344.30	113,066	35,151	4,252	14	5				302
39X-2	349.50	61,069	526	1,760	7	4				241
40X-2	359.10	143,825	37,109	4,310	17	6			9	255
41X-4	371.70	104,933	12,993	2,630	12	5				221
42X-4	381.30	92,317	23,028	3,204	13	5				247
43X-3	389.40	130,898	33,745	4,497	22	8				205
44X-CC	395.90	76,480		1,993	14	8		8		147
45X-4	410.00		5,166	1,682	10	4			31	172
46X-CC	415.10	62,541	3,026	2,006	11	5				186
47X-4	429.20	75,795	14,746	2,675	16	6			7	170
48X-2	435.80	52,931	12,715	1,868	11	4				178
49X-4	448.50	84,592	12,945	2,280	15	6		5		155
50X-4	458.10	92,527	4,015	1,718	14	7		8		126
51X-4	467.70	106,092	7,678	2,408	17	6				143
52X-1	472.80	86,986	420	1,921	14	3				136
53X-4	487.00	95,004	12,475	1,392	12	5		6		120
54X-4	496.60	63,396	8,189	1,826	15	5				126
55X-3	504.70	58,949	6,759	1,300	11	4				118
56X-1	511.30	51,436	117	875	8	4				104
57X-1	520.90	44,001		709	8	1				91
58X-1	530.60	65,573		1,022	10	4		5		100
59X-CC	540.20	44,851		757	8					96
64X-CC	588.00	4,069		114	2					76
65X-CC	597.60	4,723		45						

Note: NA = not analyzed, blank = not detected.

Table T7. Calcium carbonate ($CaCO_3$), organic carbon (C_{org}), nitrogen (N), and sulfur (S) data, Hole 1131A. (See table note. Continued on next page.)

Core, section, interval (cm)	Depth (mbsf)	$CaCO_3$ (wt%)	C_{org} (wt%)	N (wt%)	S (wt%)
182-1131A-					
1H-1, 60-61	0.60	87.1	0.43	0.09	
2H-1, 60-61	4.00	88.1	0.24	0.08	
2H-3, 60-61	7.00	92.3	0.38	0.06	0.21
2H-5, 60-61	10.10	91.9	0.30	0.06	0.34
3H-1, 60-61	13.50	91.7	0.38	0.06	
3H-3, 60-61	16.50	91.6	0.19	0.06	0.26
3H-5, 60-61	19.50	92.3	0.20	0.06	
4H-1, 60-61	23.00	92.6	0.15	0.06	
4H-3, 60-61	26.00	91.9	0.12	0.05	
4H-5, 60-61	29.00	92.4	0.00	0.04	
5H-3, 60-61	35.50	91.5	0.10	0.04	
5H-5, 60-61	38.50	90.9	0.06	0.04	
6H-1, 60-61	42.00	90.5	0.11	0.05	
6H-3, 60-61	45.00	88.2	0.23	0.05	
6H-5, 60-61	48.00	91.6	0.18	0.05	
7H-1, 60-61	51.50	92.7	0.01	0.00	
7H-3, 60-61	54.50	92.0	0.03	0.04	
7H-5, 60-61	57.50	90.1	0.13	0.04	
8X-1, 60-61	61.00	89.8	0.29	0.00	
8X-3, 60-61	64.00	90.3	0.10	0.05	
8X-5, 60-61	66.50	89.5	0.04	0.05	
9X-1, 60-61	68.20	92.6	0.13	0.00	
9X-3, 60-61	71.20	93.1	0.15	0.00	
9X-5, 60-61	73.70	94.0	0.00	0.00	
10X-1, 60-61	77.20	93.5	0.00	0.00	
10X-3, 60-61	80.20	92.0	0.08	0.00	
10X-5, 60-61	83.20	89.6	0.25	0.04	
11X-1, 60-61	86.00	88.4	0.22	0.05	
11X-3, 60-61	89.00	85.7	0.35	0.00	
11X-5, 60-61	92.00	93.9	0.11	0.00	
12X-1, 59-60	95.59	93.9	0.10	0.00	
12X-3, 59-60	98.59	92.6	0.09	0.00	
12X-6, 59-60	103.09	93.3	0.04	0.04	
13X-1, 59-60	105.19	92.1	0.28	0.00	
13X-3, 59-60	108.19	92.8	0.00	0.00	
13X-5, 59-60	111.19	92.7	NA	NA	NA
14X-1, 60-61	114.20	91.4	NA	NA	NA
14X-3, 60-61	117.20	88.2	0.27	0.04	
14X-5, 60-61	120.20	89.1	NA	NA	NA
15X-1, 60-61	123.20	88.6	NA	NA	NA
15X-3, 60-61	126.20	86.6	0.56	0.06	
15X-5, 60-61	129.20	90.1	NA	NA	NA
16X-1, 60-61	132.50	89.6	NA	NA	NA
16X-3, 60-61	135.50	88.7	0.67	0.05	
16X-5, 60-61	138.50	92.3	NA	NA	NA
17X-1, 60-61	141.90	90.9	NA	NA	NA
17X-3, 60-61	144.90	90.9	0.45	0.00	
17X-5, 60-61	147.90	90.5	NA	NA	NA
18X-1, 60-61	151.20	91.6	NA	NA	NA
18X-3, 60-61	154.20	91.7	0.44	0.05	
18X-5, 59-60	156.69	91.4	NA	NA	NA
19X-1, 60-61	160.60	90.9	NA	NA	NA
19X-3, 60-61	163.60	90.1	0.54	0.05	
19X-5, 60-61	166.60	91.7	NA	NA	NA
20X-1, 60-61	169.90	91.3	NA	NA	NA
20X-3, 60-61	172.90	93.3	0.56	0.00	
20X-5, 60-61	175.90	92.5	NA	NA	NA
21X-1, 60-61	179.20	91.2	NA	NA	NA
21X-3, 60-61	182.20	92.3	0.63	0.05	
21X-5, 60-61	185.20	93.1	NA	NA	NA
22X-1, 60-61	188.80	91.4	NA	NA	NA
22X-3, 60-61	191.80	90.9	0.56	0.05	
23X-1, 60-61	198.20	91.9	NA	NA	NA
23X-3, 60-61	201.20	85.0	0.37	0.00	
23X-5, 59-60	204.19	91.6	NA	NA	NA
24X-1, 59-60	207.19	93.2	NA	NA	NA

Table T7 (continued).

Core, section, interval (cm)	Depth (mbsf)	$CaCO_3$ (wt%)	C_{org} (wt%)	N (wt%)	S (wt%)
24X-3, 60-61	210.20	93.3	0.52	0.05	
24X-5, 58-59	213.18	91.4	NA	NA	NA
25X-1, 60-61	216.20	89.4	NA	NA	NA
25X-3, 60-61	219.20	91.4	0.32	0.04	
26X-1, 60-61	225.60	86.0	NA	NA	NA
26X-3, 60-61	228.60	85.2	0.78	0.06	
26X-5, 60-61	231.60	95.8	NA	NA	NA
27X-1, 60-61	235.10	94.2	NA	NA	NA
27X-3, 60-61	238.10	94.2	0.40	0.03	
28X-1, 60-61	244.10	89.5	NA	NA	NA
28X-3, 60-61	247.10	86.7	0.81	0.00	
28X-5, 60-61	250.10	93.4	NA	NA	NA
30X-1, 60-61	262.60	93.3	0.36	0.03	
31X-1, 60-61	272.00	90.2	NA	NA	NA
31X-3, 60-61	275.00	89.4	0.39	0.04	
31X-5, 60-61	278.00	89.1	NA	NA	NA
32X-1, 60-61	281.50	87.8	NA	NA	NA
32X-3, 60-61	284.50	91.3	0.51	0.00	
33X-1, 60-61	291.00	92.0	NA	NA	NA
33X-3, 60-61	294.00	91.3	0.40	0.05	
33X-5, 60-61	297.00	90.0	NA	NA	NA
34X-1, 60-61	300.50	88.1	NA	NA	NA
34X-3, 60-61	303.50	89.4	0.55	0.05	
34X-5, 60-61	306.50	89.2	NA	NA	NA
35X-1, 60-61	310.10	88.9	NA	NA	NA
35X-3, 60-61	313.10	87.5	0.78	0.06	
36X-1, 60-61	319.70	90.8	NA	NA	NA
36X-3, 60-61	322.70	90.0	0.60	0.06	
37X-1, 60-61	329.30	89.3	NA	NA	NA
37X-3, 60-61	332.30	91.9	0.62	0.04	
38X-1, 60-61	338.90	87.7	NA	NA	NA
38X-3, 60-61	341.90	90.1	0.46	0.04	
38X-5, 60-61	344.90	90.3	NA	NA	NA
39X-1, 60-61	348.6 0	85.1	0.59	0.07	
40X-1, 60-61	358.20	91.7	NA	NA	NA
40X-3, 60-61	361.20	92.2	0.51	0.05	
41X-1, 60-61	367.80	90.5	NA	NA	NA
41X-3, 60-61	370.80	84.6	0.71	0.06	
41X-5, 60-61	373.80	91.3	NA	NA	NA
42X-1, 60-61	377.40	92.4	NA	NA	NA
42X-3, 60-61	380.40	88.3	0.99	0.07	
43X-3, 60-61	390.00	89.7	0.63	0.05	
45X-1, 60-61	406.10	89.2	NA	NA	NA
45X-3, 60-61	409.10	88.3	0.58	0.05	
45X-5, 60-61	412.10	88.8	NA	NA	NA
47X-1, 60-61	425.30	89.6	NA	NA	NA
47X-3, 60-61	428.30	92.1	0.44	0.04	
48X-1, 60-61	434.90	92.3	NA	NA	NA
48X-3, 59-60	437.89	88.1	0.67	0.06	
49X-1, 60-61	444.60	89.7	NA	NA	NA
49X-3, 60-61	447.60	91.1	0.54	0.05	
49X-5, 60-61	450.60	89.2	NA	NA	NA
50X-1, 60-61	454.20	89.2	NA	NA	NA
50X-3, 60-61	457.20	90.5	0.67	0.05	
50X-5, 60-61	460.20	90.1	NA	NA	NA
51X-1, 61-62	463.81	83.6	NA	NA	NA
51X-3, 61-62	466.81	85.5	0.65	0.05	
53X-1, 63-64	483.13	92.4	NA	NA	NA
53X-3, 47-48	485.97	89.5	0.53	0.04	
53X-5, 60-61	489.10	88.5	NA	NA	NA
54X-1, 60-61	492.70	88.2	NA	NA	NA
54X-3, 60-61	495.70	82.6	0.66	0.06	
54X-5, 60-61	498.70	90.9	NA	NA	NA
55X-1, 60-61	502.30	89.5	NA	NA	NA
55X-3, 60-61	505.30	87.9	0.35	0.00	
56X-1, 59-60	511.89	87.1	0.96	0.05	
57X-1, 59-61	521.49	89.3	0.75	0.05	
58X-1, 60-62	531.20	79.5	0.73	0.05	

Note: NA = not analyzed, blank = not detected.

Table T8. Interstitial water geochemistry, Site 1131.

Core, section, interval (cm)	Depth (mbsf)	pH	ppH	Alkalinity (mM)	Salinity	Cl^- (mM)	SO_4^{2-} (mM)	Na^+ (mM)	K^+ (mM)	Mg^{2+} (mM)	Ca^{2+} (mM)	Sr^{2+} (µM)	Li^+ (µM)	$H_4SiO_4^0$ (µM)	NH_4^+ (mM)	Fe^{2+} (µM)
182-1131A-																
1H-1, 145-150	1.45	7.52	7.80	4.27	35.0	565	29.7	469	11.3	56.1	11.9	90	38	321	0.4	3
2H-3, 145-150	7.85	7.39	7.60	3.15	35.0	572	29.1	470	11.4	55.6	10.8	90	38	171	0.4	6
3H-3, 145-150	17.35	7.12	7.08	10.62	36.0	600	29.2	489	11.5	54.1	9.3	133	43	323	2.4	3
4H-3, 140-150	26.80	6.98	6.95	25.87	38.0	619	29.9	523	12.1	46.2	6.5	221	54	523	5.7	4
5H-3, 140-150	36.30	6.83	6.86	33.46	40.0	637	32.1	563	12.7	39.4	5.3	265	62	768	8.3	6
6H-3, 140-150	45.80	6.74	6.80	41.02	42.0	666	34.0	618	13.2	34.3	4.9	269	65	758	11.0	5
7H-3, 140-150	55.30	6.78	6.70	62.68	44.0	694	37.5	677	14.5	21.4	4.1	247	71	725	14.3	0
8X-3, 140-150	64.80	6.84	6.75	78.17	47.0	708	41.1	733	14.6	16.8	2.8	212	72	763	15.0	0
9X-3, 140-150	72.00	6.95	6.76	89.78	48.0	722	40.7	763	15.0	14.0	2.8	216	72	775	17.0	0
10X-3, 140-150	81.00	6.81	6.76	101.17	50.0	752	40.8	794	15.4	12.8	2.5	207	65	861	18.0	0
11X-3, 140-150	89.80	6.76	6.74	104.02	52.0	785	40.3	824	15.7	11.9	2.5	212	83	757	20.9	0
12X-3, 140-150	99.40	6.79	6.73	111.46	54.0	819	39.6	858	16.0	11.2	2.4	216	70	774	20.6	0
13X-3, 140-150	108.90	6.80	6.73	122.09	56.0	852	38.5	902	16.6	10.1	2.3	252	75	789	20.9	0
14X-3, 140-150	118.40	6.73	6.71	126.37	58.0	906	36.8	928	16.8	9.8	2.2	238	72	809	22.6	0
16X-3, 140-150	136.30	6.77	NM	137.05	62.0	954	37.0	979	17.5	11.4	2.7	151	73	667	25.1	0
18X-3, 140-150	155.00	6.71	NM	134.88	67.0	1,011	31.5	1,019	18.1	10.2	2.3	278	81	822	25.0	0
20X-3, 140-150	173.70	6.80	NM	135.02	72.0	1,058	28.8	1,083	20.7	11.2	2.4	260	99	879	27.4	0
22X-3, 140-150	192.60	6.65	NM	130.16	69.0	1,086	23.7	1,109	19.8	10.7	2.5	382	95	870	26.7	0
24X-3, 140-150	211.00	6.68	NM	118.66	70.0	1,143	20.4	1,120	19.9	12.4	2.7	387	114	912	27.0	0
26X-3, 140-150	229.40	6.51	NM	116.47	72.0	1,135	17.6	1,152	20.2	13.9	2.9	433	135	738	26.5	0
28X-3, 140-150	247.50	6.47	NM	95.86	70.5	1,207	15.9	1,118	19.7	16.0	3.6	602	157	838	25.8	0
31X-3, 140-150	275.80	6.39	NM	95.47	76.0	1,246	14.7	1,216	21.3	17.4	3.8	832	209	1,000	28.6	0
33X-3, 140-150	294.80	6.33	NM	77.84	76.0	1,295	17.7	1,199	21.1	24.1	5.2	1107	257	918	24.9	0
35X-2, 140-150	312.40	6.18	NM	77.78	80.0	1,281	20.8	1,224	21.3	31.1	7.0	902	239	788	24.9	0
37X-2, 140-150	331.60	6.20	NM	59.20	78.0	1,383	23.8	1,193	21.1	39.3	8.8	797	234	799	23.9	0
39X-1, 140-150	349.40	6.23	NM	63.23	85.0	1,331	25.5	1,282	22.4	44.0	9.0	867	327	873	23.3	0
41X-3, 140-150	371.60	6.32	NM	49.82	83.0	1,437	28.9	1,252	22.4	51.0	11.8	650	259	1,001	22.8	3
43X-2, 140-150	389.30	6.05	NM	55.15	86.0	1,449	33.2	1,317	23.9	59.6	16.4	607	271	1,137	20.5	0
45X-3, 140-150	409.90	5.97	NM	52.19	88.0	1,513	37.0	1,291	23.2	69.4	19.7	540	262	986	21.2	0
47X-3, 140-150	429.10	5.95	NM	52.17	92.0	1,531	39.3	1,358	24.5	73.8	24.8	521	306	1,045	21.4	0
49X-3, 140-150	448.40	5.91	NM	48.68	94.0	1,527	42.7	1,352	24.9	82.4	31.1	484	332	1,054	18.9	0
51X-3, 140-150	467.40	5.93	NM	36.73	93.0	1,574	44.8	1,344	24.5	87.5	30.7	489	338	993	17.2	0
53X-3, 140-150	486.90	5.90	NM	31.17	94.0	1,499	47.7	1,366	24.7	92.5	34.5	484	336	1,018	15.4	2
55X-2, 140-150	504.60	5.93	NM	29.32	92.0	0	48.1	469	11.3	56.1	36.8	493	306	1,018	11.7	3

Note: NM = not measured.

Table T9. Summary of X-ray diffraction analysis, Site 1131. (See table notes. Continued on next page.)

Leg	Site	Hole	Core	Type	Section	Top (cm)	Bottom (cm)	Depth (mbsf)	Aragonite (wt%)	Quartz (wt%)	LMC (wt%)	HMC (wt%)	Dolomite (wt%)
182	1131	A	1	H	1	60	61	0.60	20	3	19	58	0
182	1131	A	1	H	3	60	61	0.60	20	1	31	49	0
182	1131	A	2	H	5	60	61	4.00	13	0	12	75	0
182	1131	A	2	H	1	60	61	4.00	16	1	19	64	0
182	1131	A	2	H	3	60	61	7.00	18	1	21	60	1
182	1131	A	2	H	5	60	61	10.05	13	0	22	65	0
182	1131	A	3	H	1	60	61	13.50	17	0	25	58	1
182	1131	A	3	H	3	60	61	16.50	13	0	22	65	0
182	1131	A	3	H	5	60	61	19.50	17	0	25	58	0
182	1131	A	4	H	1	60	61	23.00	16	0	31	53	0
182	1131	A	4	H	3	60	61	26.00	17	0	24	58	1
182	1131	A	4	H	5	60	61	29.00	22	1	29	49	0
182	1131	A	5	H	3	60	61	35.50	17	2	43	37	1
182	1131	A	5	H	5	60	61	38.50	21	1	53	24	1
182	1131	A	6	H	1	61	62	42.00	16	3	45	36	1
182	1131	A	6	H	3	61	62	45.00	15	0	43	41	2
182	1131	A	6	H	5	61	62	48.00	16	3	39	39	2
182	1131	A	7	H	1	60	61	51.50	20	1	22	53	3
182	1131	A	7	H	3	60	61	54.50	17	0	26	52	4
182	1131	A	7	H	5	60	61	57.50	7	5	36	48	4
182	1131	A	8	H	5	60	61	61.00	23	1	41	30	6
182	1131	A	8	H	3	60	61	64.00	19	1	47	29	5
182	1131	A	8	H	5	60	61	66.50	21	1	58	15	5
182	1131	A	9	H	1	60	61	68.20	19	0	70	0	11
182	1131	A	9	H	3	60	61	71.20	16	0	77	0	7
182	1131	A	9	H	5	61	62	73.70	17	1	75	0	6
182	1131	A	10	H	1	60	61	77.20	15	0	78	0	8
182	1131	A	10	H	3	60	61	80.20	15	1	77	0	8
182	1131	A	10	H	5	60	61	83.20	12	1	79	0	8
182	1131	A	11	H	1	60	61	86.00	14	1	76	0	9
182	1131	A	11	H	3	60	61	89.00	13	2	76	0	8
182	1131	A	11	H	5	60	61	92.00	18	1	66	0	15
182	1131	A	12	H	1	60	61	95.59	17	1	65	0	18
182	1131	A	12	H	3	60	61	98.59	18	2	69	0	12
182	1131	A	12	H	5	60	61	103.09	17	5	69	0	9
182	1131	A	13	H	1	60	61	105.19	15	1	73	0	11
182	1131	A	13	H	3	60	61	108.19	14	0	71	0	15
182	1131	A	13	H	5	60	61	111.19	15	0	76	0	9
182	1131	A	14	H	1	60	61	114.20	14	0	78	0	8
182	1131	A	14	H	3	60	61	117.20	9	1	77	0	13
182	1131	A	14	H	5	60	61	120.20	7	0	86	0	7
182	1131	A	15	H	1	60	61	123.20	6	10	74	0	10
182	1131	A	15	H	3	60	61	126.20	8	1	85	0	6
182	1131	A	15	H	5	60	61	129.20	12	4	73	0	10
182	1131	A	16	H	1	60	61	132.50	17	1	73	0	9
182	1131	A	16	H	3	60	61	135.50	18	2	45	32	4
182	1131	A	16	H	5	60	61	138.50	14	1	69	0	17
182	1131	A	17	H	1	60	61	141.90	13	0	81	0	6
182	1131	A	17	H	3	60	61	144.90	11	0	78	0	11
182	1131	A	17	X	5	60	61	147.90	13	1	78	0	8
182	1131	A	18	X	1	60	62	151.20	14	0	76	0	9
182	1131	A	18	X	3	60	62	154.20	13	0	74	0	13
182	1131	A	18	X	5	60	62	156.69	13	1	73	0	13
182	1131	A	19	X	1	60	61	160.60	13	1	73	0	14
182	1131	A	19	X	3	60	61	163.60	16	0	78	0	6
182	1131	A	19	X	5	60	61	166.60	21	1	69	0	9
182	1131	A	20	X	1	60	61	169.90	23	1	71	0	5
182	1131	A	20	X	3	60	61	172.90	15	1	71	0	14
182	1131	A	20	X	5	60	61	175.90	15	0	73	0	12
182	1131	A	21	X	1	60	61	179.20	20	0	70	0	10
182	1131	A	21	X	3	60	61	182.20	19	1	70	0	10
182	1131	A	21	X	5	60	61	185.20	14	1	76	0	9
182	1131	A	22	X	1	60	61	188.80	16	0	70	0	14
182	1131	A	22	X	3	60	61	191.80	16	1	71	0	13
182	1131	A	23	X	1	60	61	198.20	8	0	76	0	16
182	1131	A	23	X	3	60	61	201.20	9	1	74	0	16
182	1131	A	23	X	5	60	61	204.19	11	1	75	0	13
182	1131	A	24	X	1	60	61	207.19	17	4	70	0	10

Table T9 (continued).

Leg	Site	Hole	Core	Type	Section	Top (cm)	Bottom (cm)	Depth (mbsf)	Aragonite (wt%)	Quartz (wt%)	LMC (wt%)	HMC (wt%)	Dolomite (wt%)
182	1131	A	24	X	3	60	61	210.20	16	1	67	0	16
182	1131	A	24	X	5	60	61	213.18	14	5	65	0	16
182	1131	A	25	X	1	60	61	216.20	17	0	71	0	12
182	1131	A	25	X	3	60	61	219.20	12	1	74	0	13
182	1131	A	26	X	1	60	61	225.60	9	1	75	0	15
182	1131	A	26	X	3	60	61	228.60	19	4	71	0	5
182	1131	A	26		5	60	61	231.60	5	0	66	0	28
182	1131	A	27	X	1	60	61	235.10	16	1	73	0	9
182	1131	A	27	X	3	60	61	238.10	9	1	78	0	13
182	1131	A	28	X	1	60	61	244.10	12	1	73	0	14
182	1131	A	28		3	60	61	247.10	8	0	85	0	7
182	1131	A	28	X	5	62	63	250.10	13	0	70	0	17
182	1131	A	30	X	1	60	61	262.60	6	0	83	0	10
182	1131	A	31	X	1	60	61	272.00	7	1	78	0	13
182	1131	A	31	X	3	60	61	275.00	8	1	76	0	15
182	1131	A	31	X	5	60	61	278.00	8	4	75	0	14
182	1131	A	32	X	1	60	61	281.50	16	2	66	14	2
182	1131	A	32	X	3	60	61	284.50	13	12	57	16	2
182	1131	A	33	X	1	60	61	291.00	10	1	74	0	16
182	1131	A	33	X	3	60	61	294.00	7	0	73	0	20
182	1131	A	33	X	5	60	61	297.00	8	1	83	0	8
182	1131	A	34	X	1	62	63	300.50	10	1	80	0	9
182	1131	A	34	X	3	60	61	303.50	6	2	82	0	11
182	1131	A	34	X	5	60	61	306.50	3	1	69	0	27
182	1131	A	35	X	1	60	61	310.10	4	2	89	0	6
182	1131	A	35	X	3	60	61	313.10	22	1	37	39	1
182	1131	A	36	X	1	60	61	319.70	6	1	82	0	11
182	1131	A	36		3	60	61	322.70	14	1	80	0	4
182	1131	A	37		1	60	61	329.30	6	1	85	0	7
182	1131	A	37		3	60	61	332.30	3	1	80	0	16
182	1131	A	38	X	1	60	61	338.90	2	1	86	0	10
182	1131	A	38	X	3	60	61	341.90	1	0	78	0	21
182	1131	A	38	X	5	60	61	344.90	1	2	89	0	8
182	1131	A	39	X	1	60	61	348.60	15	2	76	0	7
182	1131	A	40	X	1	60	61	358.20	1	0	84	0	15
182	1131	A	40	X	3	60	61	361.20	2	0	86	0	12
182	1131	A	41	X	1	60	61	367.80	2	0	84	0	14
182	1131	A	41	X	3	60	61	370.80	3	1	89	0	7
182	1131	A	41	X	5	60	61	373.80	1	1	83	0	15
182	1131	A	42	X	1	60	61	377.40	5	1	90	0	5
182	1131	A	42	X	3	60	61	380.40	4	1	75	0	20
182	1131	A	43	X	3	60	61	390.00	2	0	88	0	10
182	1131	A	45	X	1	60	61	406.10	7	1	85	0	7
182	1131	A	45	X	3	60	61	409.10	5	1	87	0	8
182	1131	A	45	X	5	60	61	412.10	3	3	83	0	11
182	1131	A	47	X	1	60	61	425.30	2	1	83	0	13
182	1131	A	47	X	3	60	61	428.30	1	0	85	0	14
182	1131	A	48	X	1	60	61	434.90	2	1	86	0	11
182	1131	A	48	X	3	60	61	437.89	5	6	81	0	9
182	1131	A	49	X	1	60	61	444.60	4	1	87	0	8
182	1131	A	49	X	3	60	61	447.60	3	2	78	0	16
182	1131	A	49	X	5	60	61	450.60	2	1	89	0	8
182	1131	A	50	X	1	60	61	454.20	5	1	86	0	8
182	1131	A	50	X	3	60	61	457.20	5	1	86	0	9
182	1131	A	50	X	5	60	61	460.20	5	5	77	0	12
182	1131	A	51	X	1	61	62	463.81	9	1	86	0	3
182	1131	A	51	X	3	61	62	466.81	4	2	86	0	8
182	1131	A	53	X	1	63	64	483.13	5	1	91	0	4
182	1131	A	53	X	3	47	48	485.97	5	2	83	0	10
182	1131	A	53	X	5	60	61	489.10	2	2	83	0	12
182	1131	A	54	X	1	60	61	492.70	10	2	84	0	4
182	1131	A	54	X	3	60	61	495.70	6	2	84	0	8
182	1131	A	54	X	5	60	61	498.70	6	0	78	0	15
182	1131	A	55	X	1	60	61	502.30	7	1	83	0	8
182	1131	A	55	X	3	60	61	505.30	2	0	95	0	3
182	1131	A	56	X	1	59	60	511.89	5	1	91	0	4
182	1131	A	57	X	1	59	61	521.49	5	0	93	0	1
182	1131	A	58	X	1	60	62	531.20	8	2	86	0	4

Notes: LMC = low-Mg calcite, HMC = high-Mg calcite. This table is also available in **ASCII format.**

Table T10. *P*-wave velocity measurements from the multisensor track, Site 1131.

Leg	Site	Hole	Core	Type	Section	Interval (cm)	Depth (mbsf)	V_p (km/s)
182	1131	A	1	H	1	3.0	0.03	4.6221
182	1131	A	1	H	1	7.0	0.07	3.8639
182	1131	A	1	H	1	11.0	0.11	3.8544
182	1131	A	1	H	1	15.0	0.15	3.8521
182	1131	A	1	H	1	23.0	0.23	3.8544
182	1131	A	1	H	1	27.0	0.27	3.8319
182	1131	A	1	H	1	31.0	0.31	3.8386
182	1131	A	1	H	1	35.0	0.35	3.8454
182	1131	A	1	H	1	39.0	0.39	3.8274
182	1131	A	1	H	1	43.0	0.43	3.8053
182	1131	A	1	H	1	47.0	0.47	3.8274
182	1131	A	1	H	1	51.0	0.51	3.8230
182	1131	A	1	H	1	55.0	0.55	3.8141
182	1131	A	1	H	1	59.0	0.59	3.8242
182	1131	A	1	H	1	63.0	0.63	3.8220
182	1131	A	1	H	1	67.0	0.67	3.8141
182	1131	A	1	H	1	71.0	0.71	3.8043
182	1131	A	1	H	1	75.0	0.75	3.8021
182	1131	A	1	H	1	79.0	0.79	3.8087
182	1131	A	1	H	1	83.0	0.83	3.8009
182	1131	A	1	H	1	87.0	0.87	3.7965
182	1131	A	1	H	1	91.0	0.91	3.8119
182	1131	A	1	H	1	95.0	0.95	3.8053
182	1131	A	1	H	1	99.0	0.99	3.8141
182	1131	A	1	H	1	103.0	1.03	3.8185
182	1131	A	1	H	1	107.0	1.07	3.8053
182	1131	A	1	H	1	115.0	1.15	3.8176
182	1131	A	1	H	1	119.0	1.19	3.8242
182	1131	A	1	H	1	123.0	1.23	3.8198
182	1131	A	1	H	1	127.0	1.27	3.8109
182	1131	A	1	H	1	131.0	1.31	3.8287
182	1131	A	1	H	1	139.0	1.39	3.8392
182	1131	A	1	H	2	3.0	1.53	3.0140
182	1131	A	1	H	2	7.0	1.57	3.8706
182	1131	A	1	H	2	15.0	1.65	3.8501
182	1131	A	1	H	2	19.0	1.69	3.8344
182	1131	A	1	H	2	23.0	1.73	3.8488
182	1131	A	1	H	2	31.0	1.81	3.8309
182	1131	A	1	H	2	35.0	1.85	3.8287
182	1131	A	1	H	2	39.0	1.89	3.8242
182	1131	A	1	H	2	43.0	1.93	3.8344
182	1131	A	1	H	2	51.0	2.01	3.8344
182	1131	A	1	H	2	55.0	2.05	3.8100
182	1131	A	1	H	2	63.0	2.13	3.8299
182	1131	A	1	H	2	67.0	2.17	3.8100
182	1131	A	1	H	2	71.0	2.21	3.8122
182	1131	A	1	H	2	75.0	2.25	3.8232
182	1131	A	1	H	2	79.0	2.29	3.7968
182	1131	A	1	H	2	83.0	2.33	3.8122
182	1131	A	1	H	2	87.0	2.37	3.8131
182	1131	A	1	H	2	91.0	2.41	3.8210
182	1131	A	1	H	2	95.0	2.45	3.8321
182	1131	A	1	H	2	99.0	2.49	3.8331
182	1131	A	1	H	2	103.0	2.53	3.6870
182	1131	A	1	H	2	107.0	2.57	3.9106
182	1131	A	1	H	3	3.0	2.63	2.2448
182	1131	A	1	H	3	11.0	2.71	3.5064
182	1131	A	1	H	3	15.0	2.75	1.7434
182	1131	A	1	H	3	19.0	2.79	1.5099
182	1131	A	1	H	3	23.0	2.83	1.5195
182	1131	A	1	H	3	27.0	2.87	1.7727
182	1131	A	1	H	3	31.0	2.91	1.9163
182	1131	A	1	H	3	35.0	2.95	1.4372
182	1131	A	1	H	3	39.0	2.99	1.4384

Note: Only a portion of this table appears here. The complete table is available in **ASCII format.**

Table T11. Gamma-ray attenuation densiometry measurements from the multisensor track, Site 1131.

Leg	Site	Hole	Core	Type	Section	Interval (cm)	Depth (mbsf)	Density (g/cm^3)	Corrected density (g/cm^3)
182	1131	A	1	H	1	3.0	0.03	1.65	1.58
182	1131	A	1	H	1	7.0	0.07	1.63	1.56
182	1131	A	1	H	1	11.0	0.11	1.64	1.57
182	1131	A	1	H	1	15.0	0.15	1.64	1.57
182	1131	A	1	H	1	19.0	0.19	1.67	1.60
182	1131	A	1	H	1	23.0	0.23	1.66	1.60
182	1131	A	1	H	1	27.0	0.27	1.67	1.60
182	1131	A	1	H	1	31.0	0.31	1.66	1.59
182	1131	A	1	H	1	35.0	0.35	1.66	1.59
182	1131	A	1	H	1	39.0	0.39	1.65	1.58
182	1131	A	1	H	1	43.0	0.43	1.67	1.60
182	1131	A	1	H	1	47.0	0.47	1.67	1.60
182	1131	A	1	H	1	51.0	0.51	1.65	1.58
182	1131	A	1	H	1	55.0	0.55	1.66	1.60
182	1131	A	1	H	1	59.0	0.59	1.65	1.58
182	1131	A	1	H	1	63.0	0.63	1.66	1.59
182	1131	A	1	H	1	67.0	0.67	1.65	1.58
182	1131	A	1	H	1	71.0	0.71	1.65	1.58
182	1131	A	1	H	1	75.0	0.75	1.68	1.62
182	1131	A	1	H	1	79.0	0.79	1.65	1.58
182	1131	A	1	H	1	83.0	0.83	1.65	1.58
182	1131	A	1	H	1	87.0	0.87	1.64	1.58
182	1131	A	1	H	1	91.0	0.91	1.65	1.58
182	1131	A	1	H	1	95.0	0.95	1.66	1.59
182	1131	A	1	H	1	99.0	0.99	1.69	1.63
182	1131	A	1	H	1	103.0	1.03	1.69	1.62
182	1131	A	1	H	1	107.0	1.07	1.66	1.60
182	1131	A	1	H	1	111.0	1.11	1.67	1.60
182	1131	A	1	H	1	115.0	1.15	1.69	1.62
182	1131	A	1	H	1	119.0	1.19	1.67	1.60
182	1131	A	1	H	1	123.0	1.23	1.69	1.62
182	1131	A	1	H	1	127.0	1.27	1.68	1.61
182	1131	A	1	H	1	131.0	1.31	1.69	1.63
182	1131	A	1	H	1	135.0	1.35	1.69	1.62
182	1131	A	1	H	1	139.0	1.39	1.23	1.13
182	1131	A	1	H	2	3.0	1.53	1.68	1.61
182	1131	A	1	H	2	7.0	1.57	1.71	1.65
182	1131	A	1	H	2	11.0	1.61	1.70	1.63
182	1131	A	1	H	2	15.0	1.65	1.69	1.63
182	1131	A	1	H	2	19.0	1.69	1.68	1.61
182	1131	A	1	H	2	23.0	1.73	1.66	1.59
182	1131	A	1	H	2	27.0	1.77	1.66	1.59
182	1131	A	1	H	2	31.0	1.81	1.68	1.61
182	1131	A	1	H	2	35.0	1.85	1.69	1.62
182	1131	A	1	H	2	39.0	1.89	1.70	1.63
182	1131	A	1	H	2	43.0	1.93	1.71	1.65
182	1131	A	1	H	2	47.0	1.97	1.71	1.64
182	1131	A	1	H	2	51.0	2.01	1.68	1.62
182	1131	A	1	H	2	55.0	2.05	1.70	1.64
182	1131	A	1	H	2	59.0	2.09	1.71	1.65
182	1131	A	1	H	2	63.0	2.13	1.68	1.61
182	1131	A	1	H	2	67.0	2.17	1.69	1.62
182	1131	A	1	H	2	71.0	2.21	1.72	1.65
182	1131	A	1	H	2	75.0	2.25	1.70	1.64
182	1131	A	1	H	2	79.0	2.29	1.74	1.68
182	1131	A	1	H	2	83.0	2.33	1.71	1.65
182	1131	A	1	H	2	87.0	2.37	1.74	1.68
182	1131	A	1	H	2	91.0	2.41	1.71	1.64
182	1131	A	1	H	2	95.0	2.45	1.69	1.63
182	1131	A	1	H	2	99.0	2.49	1.71	1.64
182	1131	A	1	H	2	103.0	2.53	1.70	1.64
182	1131	A	1	H	2	107.0	2.57	1.69	1.63
182	1131	A	1	H	3	3.0	2.63	1.73	1.67

Note: Only a portion of this table appears here. The complete table is available in **ASCII format.**

Table T12. Magnetic susceptibility measurements from the multisensor track, Site 1131.

Leg	Site	Hole	Core	Type	Section	Interval (cm)	Depth (mbsf)	Magnetic susceptibility (10^{-6}; SI units)	Corrected susceptibility (10^{-6}; SI units)
182	1131	A	1	H	1	3.0	0.03	–0.8	–0.8
182	1131	A	1	H	1	11.0	0.11	–1.6	–1.6
182	1131	A	1	H	1	19.0	0.19	–2.0	–2.0
182	1131	A	1	H	1	27.0	0.27	–2.4	–2.4
182	1131	A	1	H	1	35.0	0.35	–2.7	–2.7
182	1131	A	1	H	1	43.0	0.43	–3.1	–3.1
182	1131	A	1	H	1	51.0	0.51	–3.0	–3.0
182	1131	A	1	H	1	59.0	0.59	–3.0	–3.0
182	1131	A	1	H	1	67.0	0.67	–2.6	–2.6
182	1131	A	1	H	1	75.0	0.75	–3.1	–3.1
182	1131	A	1	H	1	83.0	0.83	–3.0	–3.0
182	1131	A	1	H	1	91.0	0.91	–3.1	–3.1
182	1131	A	1	H	1	99.0	0.99	–2.9	–2.9
182	1131	A	1	H	1	107.0	1.07	–2.9	–2.9
182	1131	A	1	H	1	115.0	1.15	–3.1	–3.1
182	1131	A	1	H	1	123.0	1.23	–2.9	–2.9
182	1131	A	1	H	1	131.0	1.31	–3.3	–3.3
182	1131	A	1	H	1	139.0	1.39	–2.9	–2.9
182	1131	A	1	H	2	3.0	1.53	–0.7	–0.7
182	1131	A	1	H	2	11.0	1.61	–0.9	–0.9
182	1131	A	1	H	2	19.0	1.69	–0.8	–0.8
182	1131	A	1	H	2	27.0	1.77	–1.0	–1.0
182	1131	A	1	H	2	35.0	1.85	–1.1	–1.1
182	1131	A	1	H	2	43.0	1.93	–1.2	–1.2
182	1131	A	1	H	2	51.0	2.01	–2.2	–2.2
182	1131	A	1	H	2	59.0	2.09	–1.7	–1.7
182	1131	A	1	H	2	67.0	2.17	–1.3	–1.3
182	1131	A	1	H	2	75.0	2.25	–1.4	–1.4
182	1131	A	1	H	2	83.0	2.33	–1.6	–1.6
182	1131	A	1	H	2	91.0	2.41	–1.8	–1.8
182	1131	A	1	H	2	99.0	2.49	–1.5	–1.5
182	1131	A	1	H	2	107.0	2.57	–1.6	–1.6
182	1131	A	1	H	3	3.0	2.63	–0.9	–0.9
182	1131	A	1	H	3	11.0	2.71	–1.6	–1.6
182	1131	A	1	H	3	19.0	2.79	–1.6	–1.6
182	1131	A	1	H	3	27.0	2.87	–1.6	–1.6
182	1131	A	1	H	3	35.0	2.95	–1.4	–1.4
182	1131	A	1	H	3	43.0	3.03	–2.0	–2.0
182	1131	A	1	H	3	51.0	3.11	–1.8	–1.8
182	1131	A	2	H	1	3.0	3.43	–2.2	–2.2
182	1131	A	2	H	1	11.0	3.51	–2.5	–2.5
182	1131	A	2	H	1	19.0	3.59	–2.5	–2.5
182	1131	A	2	H	1	27.0	3.67	–2.1	–2.1
182	1131	A	2	H	1	35.0	3.75	–2.6	–2.6
182	1131	A	2	H	1	43.0	3.83	–2.7	–2.7
182	1131	A	2	H	1	51.0	3.91	–2.4	–2.4
182	1131	A	2	H	1	59.0	3.99	–2.6	–2.6
182	1131	A	2	H	1	67.0	4.07	–2.7	–2.7
182	1131	A	2	H	1	75.0	4.15	–2.6	–2.6
182	1131	A	2	H	1	83.0	4.23	–3.2	–3.2
182	1131	A	2	H	1	91.0	4.31	–2.8	–2.7
182	1131	A	2	H	1	99.0	4.39	–2.8	–2.7
182	1131	A	2	H	1	107.0	4.47	–2.8	–2.7
182	1131	A	2	H	1	115.0	4.55	–3.1	–3.0
182	1131	A	2	H	1	123.0	4.63	–3.4	–3.3
182	1131	A	2	H	1	131.0	4.71	–3.0	–2.9
182	1131	A	2	H	1	139.0	4.79	–3.7	–3.6
182	1131	A	2	H	2	3.0	4.93	–1.6	–1.6
182	1131	A	2	H	2	11.0	5.01	–2.4	–2.4
182	1131	A	2	H	2	19.0	5.09	0.1	0.1
182	1131	A	2	H	2	27.0	5.17	–2.8	–2.8
182	1131	A	2	H	2	35.0	5.25	–2.8	–2.8
182	1131	A	2	H	2	43.0	5.33	–2.8	–2.8

Note: Only a portion of this table appears here. The complete table is available in **ASCII format.**

Table T13. Natural gamma-ray measurements from the multisensor track, Site 1131.

Leg	Site	Hole	Core	Type	Section	Interval (cm)	Depth (mbsf)	NGR (cps)
182	1131	A	1	H	1	11.0	0.11	1.81
182	1131	A	1	H	1	27.0	0.27	0.69
182	1131	A	1	H	1	43.0	0.43	2.00
182	1131	A	1	H	1	59.0	0.59	1.50
182	1131	A	1	H	1	75.0	0.75	1.23
182	1131	A	1	H	1	91.0	0.91	0.54
182	1131	A	1	H	1	107.0	1.07	1.85
182	1131	A	1	H	1	123.0	1.23	1.69
182	1131	A	1	H	2	11.0	1.61	2.27
182	1131	A	1	H	2	27.0	1.77	1.31
182	1131	A	1	H	2	43.0	1.93	0.85
182	1131	A	1	H	2	59.0	2.09	0.50
182	1131	A	1	H	2	75.0	2.25	0.96
182	1131	A	1	H	2	91.0	2.41	1.35
182	1131	A	1	H	3	11.0	2.71	1.35
182	1131	A	1	H	3	27.0	2.87	2.19
182	1131	A	1	H	3	43.0	3.03	2.15
182	1131	A	2	H	1	11.0	3.51	2.73
182	1131	A	2	H	1	27.0	3.67	2.27
182	1131	A	2	H	1	43.0	3.83	2.81
182	1131	A	2	H	1	59.0	3.99	2.12
182	1131	A	2	H	1	75.0	4.15	2.89
182	1131	A	2	H	1	91.0	4.31	1.77
182	1131	A	2	H	1	107.0	4.47	3.58
182	1131	A	2	H	1	123.0	4.63	3.42
182	1131	A	2	H	2	11.0	5.01	2.46
182	1131	A	2	H	2	27.0	5.17	4.04
182	1131	A	2	H	2	43.0	5.33	2.08
182	1131	A	2	H	2	59.0	5.49	2.77
182	1131	A	2	H	2	75.0	5.65	0.62
182	1131	A	2	H	2	91.0	5.81	1.96
182	1131	A	2	H	2	107.0	5.97	1.85
182	1131	A	2	H	2	123.0	6.13	2.27
182	1131	A	2	H	2	139.0	6.29	4.35
182	1131	A	2	H	3	11.0	6.51	3.15
182	1131	A	2	H	3	27.0	6.67	2.77
182	1131	A	2	H	3	43.0	6.83	2.19
182	1131	A	2	H	3	59.0	6.99	4.23
182	1131	A	2	H	3	75.0	7.15	3.58
182	1131	A	2	H	3	91.0	7.31	4.31
182	1131	A	2	H	3	107.0	7.47	2.81
182	1131	A	2	H	3	123.0	7.63	3.69
182	1131	A	2	H	4	11.0	8.01	4.92
182	1131	A	2	H	4	27.0	8.17	5.00
182	1131	A	2	H	4	43.0	8.33	5.85
182	1131	A	2	H	4	59.0	8.49	3.46
182	1131	A	2	H	4	75.0	8.65	2.96
182	1131	A	2	H	4	91.0	8.81	2.69
182	1131	A	2	H	4	107.0	8.97	4.65
182	1131	A	2	H	4	123.0	9.13	4.65
182	1131	A	2	H	4	139.0	9.29	2.58
182	1131	A	2	H	5	11.0	9.56	4.54
182	1131	A	2	H	5	27.0	9.72	1.96
182	1131	A	2	H	5	43.0	9.88	3.42
182	1131	A	2	H	5	59.0	10.04	3.96
182	1131	A	2	H	5	75.0	10.20	4.77
182	1131	A	2	H	5	91.0	10.36	5.46
182	1131	A	2	H	5	107.0	10.52	3.08
182	1131	A	2	H	5	123.0	10.68	3.23
182	1131	A	2	H	6	11.0	11.03	3.69
182	1131	A	2	H	6	27.0	11.19	6.04
182	1131	A	2	H	6	43.0	11.35	4.77
182	1131	A	2	H	6	59.0	11.51	2.96
182	1131	A	2	H	6	75.0	11.67	4.27

Notes: NGR = natural gamma radiation. Only a portion of this table appears here. The complete table is available in **ASCII format.**

Table T14. Thermal conductivity measurements, Site 1131.

Leg	Site	Hole	Core	Type	Section	Interval (cm)	Depth (mbsf)	Thermal conductivity (W/[m·K])
182	1131	A	1	H	3	34.0	2.94	0.878
182	1131	A	2	H	3	75.0	7.15	0.881
182	1131	A	3	H	3	75.0	16.65	0.939
182	1131	A	4	H	3	75.0	26.15	0.927
182	1131	A	4	H	7	34.0	31.74	0.978
182	1131	A	5	H	1	91.0	32.81	0.957
182	1131	A	5	H	3	56.0	35.46	0.909
182	1131	A	6	H	3	75.0	45.15	0.841
182	1131	A	8	X	3	75.0	64.15	0.908
182	1131	A	7	H	3	69.0	54.59	1.212
182	1131	A	9	X	3	75.0	71.35	1.034
182	1131	A	10	X	3	60.0	80.20	0.996
182	1131	A	11	X	3	75.0	89.15	0.980
182	1131	A	12	X	3	75.0	98.75	0.944
182	1131	A	13	X	3	75.0	108.35	0.975
182	1131	A	14	X	3	70.0	117.30	1.012
182	1131	A	15	X	3	87.0	126.47	0.986
182	1131	A	16	X	3	80.0	135.70	0.978
182	1131	A	17	X	3	69.0	144.99	0.955
182	1131	A	18	X	3	66.0	154.26	0.939
182	1131	A	19	X	3	88.0	163.88	0.938
182	1131	A	20	X	3	80.0	173.10	0.994
182	1131	A	21	X	3	79.0	182.39	1.022
182	1131	A	22	X	3	87.0	192.07	1.034
182	1131	A	23	X	3	70.0	201.30	0.960
182	1131	A	24	X	3	75.0	210.35	1.028
182	1131	A	25	X	3	60.0	219.20	0.994
182	1131	A	26	X	3	75.0	228.75	0.891
182	1131	A	27	X	3	50.0	238.00	0.934
182	1131	A	28	X	3	75.0	247.25	1.007
182	1131	A	31	X	3	60.0	275.00	0.983
182	1131	A	32	X	3	75.0	284.65	0.993
182	1131	A	33	X	3	75.0	294.15	0.867
182	1131	A	34	X	3	75.0	303.65	0.799
182	1131	A	35	X	3	75.0	313.25	0.998
182	1131	A	36	X	3	75.0	322.85	1.041
182	1131	A	38	X	3	51.0	341.81	0.927
182	1131	A	39	X	2	75.0	350.25	1.101
182	1131	A	40	X	3	68.0	361.28	1.021
182	1131	A	41	X	3	75.0	370.95	0.959
182	1131	B	1	H	3	80.0	3.80	0.836
182	1131	B	2	H	3	75.0	12.15	0.959
182	1131	B	3	H	3	75.0	21.65	0.942
182	1131	B	4	H	3	75.0	31.15	0.938
182	1131	B	5	H	4	75.0	42.15	0.917
182	1131	B	6	H	3	75.0	50.15	0.847
182	1131	B	7	H	3	75.0	59.65	0.979
182	1131	B	8	X	3	63.0	69.03	0.876
182	1131	B	9	X	3	66.0	72.76	1.028
182	1131	B	10	X	3	88.0	81.98	1.045
182	1131	B	11	X	3	75.0	91.15	1.019
182	1131	B	12	X	3	75.0	100.15	1.029

Note: This table is also available in **ASCII format.**

Table T15. In situ formation temperature estimates, Site 1131.

Leg, core, section	Depth (mbsf)	Mudline temperature (°C)	Formation temperature (°C)	Fitting error (°C)
182-1131A-4H	0	13.55		
	32.00		13.72	0.005
182-1131B-6H	0	11.98		
	51.10		14.18	0.016
			14.25	0.013
182-1131A-13X	0	<13.95		
	0	14.10		
	114.25		17.00	0.005
			16.58	0.040

Notes: Average mudline temperature = 1.92°C. Additional estimate of seafloor temperature using an expendable bathythermograph = 10.34–10.30. This table is also available in **ASCII format.**

Table T16. Discrete *P*-wave velocity measurements using PWS1, PWS2, and PWS3, Site 1131.

Leg	Site	Hole	Core	Type	Section	Interval (cm)	Depth (mbsf)	PWS 1, 2, or 3	V_p (km/s)
182	1131	A	1	H	1	18.3	0.18	1	1.6143
182	1131	A	1	H	1	76.0	0.76	1	1.6005
182	1131	A	1	H	1	123.7	1.24	1	1.5943
182	1131	A	1	H	2	11.4	1.61	1	1.5574
182	1131	A	1	H	2	56.4	2.06	1	1.5633
182	1131	A	1	H	2	98.2	2.48	1	1.5918
182	1131	A	1	H	3	30.2	2.90	1	1.5903
182	1131	A	2	H	1	13.4	3.53	1	1.6036
182	1131	A	2	H	1	63.2	4.03	1	1.6030
182	1131	A	2	H	1	122.4	4.62	1	1.6169
182	1131	A	2	H	2	12.0	5.02	1	1.5569
182	1131	A	2	H	2	67.5	5.58	1	1.6229
182	1131	A	2	H	2	131.3	6.21	1	1.6287
182	1131	A	2	H	3	46.8	6.87	1	1.5878
182	1131	A	2	H	3	96.8	7.37	1	1.5726
182	1131	A	2	H	3	133.7	7.74	1	1.5649
182	1131	A	2	H	4	16.9	8.07	1	1.6235
182	1131	A	2	H	4	79.9	8.70	1	1.6242
182	1131	A	2	H	4	138.5	9.29	1	1.6300
182	1131	A	2	H	5	45.7	9.91	1	1.5835
182	1131	A	2	H	5	114.3	10.59	1	1.5732
182	1131	A	2	H	6	39.3	11.31	1	1.6147
182	1131	A	3	H	1	64.6	13.55	1	1.5469
182	1131	A	3	H	1	113.4	14.03	1	1.6200
182	1131	A	3	H	2	136.9	15.77	1	1.6342
182	1131	A	3	H	5	40.7	19.31	1	1.6058
182	1131	A	3	H	5	98.5	19.89	1	1.6014
182	1131	A	4	H	2	25.5	24.16	1	1.6007
182	1131	A	4	H	2	97.0	24.87	1	1.6120
182	1131	A	4	H	3	64.7	26.05	1	1.6073
182	1131	A	4	H	4	67.5	27.58	1	1.6058
182	1131	A	1	H	1	97.2	0.97	2	1.5427
182	1131	A	1	H	2	32.6	1.83	2	1.5959
182	1131	A	1	H	2	77.7	2.28	2	1.6172
182	1131	A	1	H	3	9.7	2.70	2	1.5525
182	1131	A	1	H	3	43.6	3.04	2	1.5573
182	1131	A	2	H	1	42.7	3.83	2	1.6027
182	1131	A	2	H	1	99.5	4.40	2	1.5392
182	1131	A	2	H	2	49.5	5.40	2	7.4117
182	1131	A	2	H	2	49.5	5.40	2	1.5724
182	1131	A	2	H	2	104.1	5.94	2	1.6464
182	1131	A	2	H	3	19.7	6.60	2	1.5561
182	1131	A	2	H	3	73.4	7.13	2	1.5226
182	1131	A	2	H	3	110.4	7.50	2	1.5204
182	1131	A	2	H	4	50.2	8.40	2	1.6053
182	1131	A	2	H	4	114.3	9.04	2	1.6027
182	1131	A	2	H	5	20.6	9.66	2	1.5537
182	1131	A	2	H	5	71.8	10.17	2	1.5294
182	1131	A	2	H	5	135.0	10.80	2	1.5751
182	1131	A	2	H	6	13.7	11.06	2	1.6616
182	1131	A	2	H	6	68.7	11.61	2	1.5215
182	1131	A	3	H	1	88.4	13.78	2	1.5352
182	1131	A	3	H	1	130.5	14.21	2	1.5226
182	1131	A	3	H	1	138.6	14.29	2	1.5317
182	1131	A	3	H	2	19.8	14.60	2	1.5386
182	1131	A	3	H	2	68.6	15.09	2	1.5679
182	1131	A	3	H	2	111.0	15.51	2	1.5799
182	1131	A	3	H	3	14.6	16.05	2	1.5661
182	1131	A	3	H	3	53.1	16.43	2	1.6267
182	1131	A	3	H	3	89.3	16.79	2	1.5842
182	1131	A	3	H	3	130.3	17.20	2	1.6252
182	1131	A	3	H	4	8.0	17.48	2	1.5673
182	1131	A	3	H	4	45.3	17.85	2	1.5842
182	1131	A	3	H	4	88.0	18.28	2	1.5733

Note: Only a portion of this table appears here. The complete table is available in **ASCII format.**

Table T17. Index properties measurements, Site 1131.

Leg	Site	Hole	Core	Type	Section	Top (cm)	Bottom (cm)	Depth (mbsf)	Bulk water content (%)	Dry water content (%)	Bulk density (g/cm³)	Dry density (g/cm³)	Grain density (g/cm³)	Porosity (%)	Void ratio
182	1131	A	1	H	3	34.0	36.0	2.94	39.9	66.5	1.50	0.90	2.17	58.5	1.41
182	1131	A	2	H	1	64.0	66.0	4.04	37.7	60.5	1.49	0.93	2.05	54.8	1.21
182	1131	A	2	H	2	64.0	66.0	5.54	44.1	79.0	1.44	0.81	2.13	62.2	1.64
182	1131	A	2	H	3	64.0	66.0	7.04	38.4	62.2	1.45	0.90	1.96	54.4	1.19
182	1131	A	2	H	4	64.0	66.0	8.54	38.6	62.9	1.35	0.83	1.69	50.9	1.04
182	1131	A	2	H	5	64.0	66.0	10.09	43.0	75.5	1.36	0.78	1.81	57.1	1.33
182	1131	A	2	H	6	64.0	66.0	11.56	36.6	57.7	1.44	0.91	1.88	51.4	1.06
182	1131	A	3	H	1	65.0	67.0	13.55	37.3	59.4	1.46	0.92	1.95	53.1	1.13
182	1131	A	3	H	2	65.0	67.0	15.05	41.0	69.6	1.50	0.89	2.22	60.1	1.51
182	1131	A	3	H	3	65.0	67.0	16.55	36.5	57.5	1.49	0.95	2.02	53.1	1.13
182	1131	A	3	H	4	65.0	67.0	18.05	35.8	55.9	1.56	1.00	2.21	54.7	1.21
182	1131	A	3	H	5	65.0	67.0	19.55	34.0	51.6	1.47	0.97	1.91	49.0	0.96
182	1131	A	3	H	6	65.0	67.0	21.05	35.2	54.3	1.49	0.96	1.97	51.1	1.05
182	1131	A	3	H	7	31.0	33.0	22.21	36.5	57.5	1.56	0.99	2.22	55.5	1.25
182	1131	A	4	H	1	65.0	67.0	23.05	37.6	60.3	1.44	0.90	1.92	53.0	1.13
182	1131	A	4	H	2	65.0	67.0	24.55	33.9	51.4	1.52	1.00	2.02	50.4	1.02
182	1131	A	4	H	3	65.0	67.0	26.05	36.3	57.1	1.51	0.96	2.06	53.5	1.15
182	1131	A	4	H	4	65.0	67.0	27.55	36.4	57.3	1.49	0.95	2.02	53.1	1.13
182	1131	A	4	H	5	65.0	67.0	29.05	35.4	54.7	1.55	1.00	2.15	53.5	1.15
182	1131	A	4	H	6	65.0	67.0	30.55	33.0	49.4	1.63	1.09	2.31	52.7	1.11
182	1131	A	4	H	7	59.0	61.0	31.99	31.1	45.2	1.54	1.06	1.99	46.7	0.88
182	1131	A	5	H	2	65.0	67.0	34.05	31.8	46.6	1.64	1.12	2.29	51.0	1.04
182	1131	A	5	H	3	65.0	67.0	35.55	35.1	54.2	1.49	0.97	1.98	51.2	1.05
182	1131	A	5	H	4	65.0	67.0	37.05	36.2	56.8	1.53	0.97	2.12	54.0	1.18
182	1131	A	5	H	5	65.0	67.0	38.55	34.5	52.7	1.61	1.05	2.30	54.2	1.19
182	1131	A	5	H	6	65.0	67.0	40.05	36.3	57.0	1.43	0.91	1.85	50.8	1.03
182	1131	A	6	H	1	65.0	67.0	42.05	35.4	54.8	1.52	0.98	2.07	52.5	1.11
182	1131	A	6	H	2	65.0	67.0	43.55	36.4	57.3	1.57	1.00	2.25	55.8	1.26
182	1131	A	6	H	3	65.0	67.0	45.05	37.1	59.1	1.45	0.91	1.91	52.4	1.10
182	1131	A	6	H	4	65.0	67.0	46.55	35.7	55.5	1.58	1.02	2.26	55.1	1.23
182	1131	A	6	H	5	65.0	67.0	48.05	33.4	50.1	1.54	1.03	2.07	50.3	1.01
182	1131	A	6	H	6	65.0	67.0	49.55	30.7	44.2	1.55	1.08	2.02	46.5	0.87
182	1131	A	6	H	7	59.0	61.0	50.99	34.2	51.9	1.55	1.02	2.10	51.6	1.07
182	1131	A	7	H	1	65.0	67.0	51.55	31.3	45.5	1.61	1.11	2.19	49.3	0.97
182	1131	A	7	H	2	65.0	67.0	53.05	37.2	59.2	1.43	0.90	1.88	52.0	1.09
182	1131	A	7	H	3	65.0	67.0	54.55	36.8	58.1	1.43	0.90	1.85	51.2	1.05
182	1131	A	7	H	4	65.0	67.0	56.05	35.5	55.0	1.55	1.00	2.15	53.5	1.15
182	1131	A	7	H	5	65.0	67.0	57.55	34.6	53.0	1.51	0.98	2.01	50.9	1.04
182	1131	A	7	H	6	65.0	67.0	59.05	35.9	56.0	1.50	0.96	2.01	52.4	1.10
182	1131	A	8	X	1	65.0	67.0	61.05	33.4	50.1	1.58	1.05	2.17	51.5	1.06
182	1131	A	8	X	2	65.0	67.0	62.55	37.1	58.9	1.49	0.94	2.04	54.0	1.18
182	1131	A	8	X	3	65.0	67.0	64.05	37.0	58.8	1.52	0.96	2.14	55.1	1.23
182	1131	A	8	X	4	65.0	67.0	65.55	35.6	55.3	1.58	1.02	2.25	54.9	1.22
182	1131	A	8	X	5	65.0	67.0	66.55	33.4	50.2	1.54	1.02	2.05	50.1	1.00
182	1131	A	9	X	1	65.0	67.0	68.25	33.3	49.9	1.56	1.04	2.11	50.7	1.03
182	1131	A	9	X	2	65.0	67.0	69.75	34.5	52.6	1.58	1.04	2.22	53.3	1.14
182	1131	A	9	X	3	65.0	67.0	71.25	33.7	50.9	1.51	1.00	1.99	49.7	0.99
182	1131	A	9	X	4	65.0	67.0	72.75	33.8	51.0	1.57	1.04	2.16	51.9	1.08
182	1131	A	10	X	1	65.0	67.0	77.25	35.2	54.2	1.51	0.98	2.02	51.7	1.07
182	1131	A	10	X	2	65.0	67.0	78.75	35.1	54.0	1.52	0.99	2.06	52.1	1.09
182	1131	A	10	X	3	65.0	67.0	80.25	36.6	57.6	1.56	0.99	2.25	55.8	1.26
182	1131	A	10	X	4	65.0	67.0	81.75	34.2	51.9	1.51	0.99	2.00	50.3	1.01
182	1131	A	10	X	5	65.0	67.0	83.25	34.5	52.7	1.67	1.09	2.48	56.1	1.28
182	1131	A	11	X	1	65.0	67.0	86.05	41.6	71.3	1.35	0.79	1.76	55.0	1.22
182	1131	A	11	X	2	65.0	67.0	87.55	35.0	53.9	1.47	0.96	1.92	50.3	1.01
182	1131	A	11	X	3	65.0	67.0	89.05	35.8	55.8	1.56	1.00	2.21	54.6	1.21
182	1131	A	11	X	4	65.0	67.0	90.55	32.8	48.9	1.58	1.06	2.16	50.7	1.03
182	1131	A	11	X	5	65.0	67.0	92.05	29.7	42.2	1.61	1.13	2.12	46.6	0.87
182	1131	A	12	X	1	69.0	71.0	95.69	31.0	45.0	1.56	1.08	2.05	47.3	0.90
182	1131	A	12	X	2	69.0	71.0	97.19	30.8	44.5	1.60	1.11	2.13	48.0	0.93
182	1131	A	12	X	3	69.0	71.0	98.69	29.6	42.1	1.65	1.16	2.22	47.7	0.91
182	1131	A	12	X	4	69.0	71.0	100.19	29.2	41.2	1.59	1.13	2.06	45.3	0.83
182	1131	A	12	X	5	69.0	71.0	101.69	33.8	51.0	1.58	1.04	2.18	52.0	1.09
182	1131	A	12	X	6	69.0	71.0	103.19	30.8	44.4	1.66	1.15	2.29	49.8	0.99
182	1131	A	13	X	1	39.0	41.0	104.99	31.2	45.3	1.54	1.06	2.00	46.9	0.88

Notes: Only a portion of this table appears here. The complete table is available in **ASCII format.**

Table T18. Undrained shear strength measurements, Site 1131.

Leg	Site	Hole	Core	Type	Section	Interval (cm)	Depth (mbsf)	Maximum shear strength (kPa)	Peak (kPa)
182	1131	A	1	H	2	87.9	2.38	2.79	3.40
182	1131	A	1	H	3	39.9	3.00	6.75	8.23
182	1131	A	2	H	1	120.1	4.60	1.44	1.76
182	1131	A	2	H	2	109.4	5.99	3.78	4.61
182	1131	A	2	H	3	120.7	7.61	6.75	8.23
182	1131	A	2	H	4	128.7	9.19	5.49	6.70
182	1131	A	2	H	5	130.0	10.75	7.83	9.55
182	1131	A	2	H	6	38.5	11.31	6.39	7.79
182	1131	A	3	H	1	126.4	14.16	7.92	9.66
182	1131	A	3	H	2	124.5	15.65	6.03	7.35
182	1131	A	3	H	3	114.7	17.05	6.75	8.23
182	1131	A	3	H	4	118.4	18.58	5.22	6.37
182	1131	A	3	H	5	122.0	20.12	7.47	9.11
182	1131	A	3	H	6	124.3	21.64	3.96	4.83
182	1131	A	4	H	1	123.9	23.64	5.58	6.81
182	1131	A	4	H	2	123.0	25.13	4.77	5.82
182	1131	A	4	H	3	127.5	26.67	2.88	3.51
182	1131	A	4	H	4	124.8	28.15	9.99	12.18
182	1131	A	4	H	5	121.9	29.62	4.41	5.38
182	1131	A	4	H	7	132.1	-1.00	9.63	11.75
182	1131	A	5	H	1	135.9	33.26	8.82	10.76
182	1131	A	5	H	2	122.0	34.62	5.58	6.81
182	1131	A	5	H	3	115.9	36.06	11.70	14.27
182	1131	A	5	H	4	120.8	37.61	6.48	7.90
182	1131	A	5	H	5	121.5	39.12	6.93	8.45
182	1131	A	6	H	1	129.7	42.70	10.35	12.62
182	1131	A	6	H	2	118.4	44.08	2.43	2.96
182	1131	A	6	H	3	111.2	45.51	7.65	9.33
182	1131	A	6	H	4	133.6	47.24	4.77	5.82
182	1131	A	6	H	5	137.4	48.77	17.46	21.30
182	1131	A	6	H	6	87.7	49.78	17.46	21.30
182	1131	A	7	H	1	78.1	51.68	10.89	13.28
182	1131	A	7	H	4	120.1	56.60	8.28	10.10
182	1131	A	7	H	5	127.0	58.17	6.48	7.90
182	1131	A	7	H	5	127.0	58.17	6.48	7.90
182	1131	A	7	H	6	114.1	59.54	3.69	4.50
182	1131	A	8	X	1	130.4	61.70	4.77	5.82
182	1131	A	8	X	2	124.2	63.14	7.02	8.56
182	1131	A	8	X	3	114.4	64.54	7.29	8.89
182	1131	A	8	X	4	90.3	65.80	9.18	11.20
182	1131	A	9	X	1	135.9	68.96	4.59	5.60
182	1131	A	9	X	2	109.7	70.20	13.86	16.90
182	1131	A	9	X	3	122.4	71.82	19.89	24.26
182	1131	A	9	X	4	85.4	72.95	14.40	17.56
182	1131	A	10	X	1	107.1	77.67	6.57	8.01
182	1131	A	10	X	2	127.2	79.37	5.31	6.48
182	1131	A	10	X	3	121.5	80.82	7.74	9.44
182	1131	A	10	X	4	117.9	82.28	35.82	43.69
182	1131	A	10	X	5	118.8	83.79	20.79	25.36
182	1131	A	11	X	2	130.2	88.20	15.30	18.66
182	1131	A	11	X	3	96.1	89.36	5.58	6.81
182	1131	A	11	X	4	119.3	91.09	12.15	14.82
182	1131	A	11	X	5	117.3	92.57	9.63	11.75
182	1131	A	12	X	1	117.7	96.18	21.96	26.78
182	1131	A	12	X	2	130.4	97.80	6.30	7.68
182	1131	A	12	X	3	95.4	98.95	15.12	18.44
182	1131	A	12	X	4	122.5	100.72	9.72	11.86
182	1131	A	12	X	5	100.5	102.00	10.71	13.06
182	1131	A	12	X	6	77.7	103.28	33.84	41.27
182	1131	A	13	X	1	115.8	105.76	5.22	6.37
182	1131	A	13	X	2	121.3	107.31	7.56	9.22
182	1131	A	13	X	3	109.5	108.69	4.59	5.60
182	1131	A	13	X	4	132.9	110.43	12.96	15.81
182	1131	A	13	X	5	72.4	111.32	21.24	25.91

Note: Only a portion of this table appears here. The complete table is available in **ASCII format.**

Table T19. Summary of tool strings, intervals logged, and logging speeds, Hole 1131A.

Tool string	First pass	
	Interval (mbsf)	Speed (m/hr)
Triple combo/LDEO-TAP	0-927 (main)	275
FMS/sonic	0-921.5 (main)	275

Note: Triple combo = triple combination logging tool, LDEO-TAP = Lamont-Doherty Earth Observatory high-resolution temperature/acceleration/pressure tool, FMS = Formation MicroScanner.